ANL-ARC-218

Development of the ANL Plant Dynamics Code and Control Strategies for the Supercritical Carbon Dioxide Brayton Cycle and Code Validation with Data from the Sandia Small-Scale Supercritical Carbon Dioxide Brayton Cycle Test Loop

Nuclear Engineering Division

About Argonne National Laboratory

Argonne is a U.S. Department of Energy laboratory managed by UChicago Argonne, LLC under contract DE-AC02-06CH11357. The Laboratory's main facility is outside Chicago, at 9700 South Cass Avenue, Argonne, Illinois 60439. For information about Argonne, see http://www.anl.gov.

Availability of This Report

This report is available, at no cost, at http://www.osti.gov/bridge. It is also available on paper to the U.S. Department of Energy and its contractors, for a processing fee, from:

U.S. Department of Energy
Office of Scientific and Technical Information
P.O. Box 62
Oak Ridge, TN 37831-0062
phone (865) 576-8401
fax (865) 576-5728
reports@adonis.osti.gov

Disclaimer

This report was prepared as an account of work sponsored by an agency of the United States Government. Neither the United States Government nor any agency thereof, nor UChicago Argonne, LLC, nor any of their employees or officers, makes any warranty, express or implied, or assumes any legal liability or responsibility for the accuracy, completeness, or usefulness of any information, apparatus, product, or process disclosed, or represents that its use would not infringe privately owned rights. Reference herein to any specific commercial product, process, or service by trade name, trademark, manufacturer, or otherwise, does not necessarily constitute or imply its endorsement, recommendation, or favoring by the United States Government or any agency thereof. The views and opinions of document authors expressed herein do not necessarily state or reflect those of the United States Government or any agency thereof, Argonne National Laboratory, or UChicago Argonne, LLC.

ANL-ARC-218

Development of the ANL Plant Dynamics Code and Control Strategies for the Supercritical Carbon Dioxide Brayton Cycle and Code Validation with Data from the Sandia Small-Scale Supercritical Carbon Dioxide Brayton Cycle Test Loop

Anton Moisseytsev and James J. Sienicki
Nuclear Engineering Division
Argonne National Laboratory

September 29, 2011

ABSTRACT

Significant progress has been made in the ongoing development of the Argonne National Laboratory (ANL) Plant Dynamics Code (PDC), the ongoing investigation and development of control strategies, and the analysis of system transient behavior for supercritical carbon dioxide (S-CO_2) Brayton cycles.

Several code modifications have been introduced during FY2011 to extend the range of applicability of the PDC and to improve its calculational stability and speed. A new and innovative approach was developed to couple the Plant Dynamics Code for S-CO_2 cycle calculations with SAS4A/SASSYS-1 Liquid Metal Reactor Code System calculations for the transient system level behavior on the reactor side of a Sodium-Cooled Fast Reactor (SFR) or Lead-Cooled Fast Reactor (LFR). The new code system allows use of the full capabilities of both codes such that whole-plant transients can now be simulated without additional user interaction. Several other code modifications, including the introduction of compressor surge control, a new approach for determining the solution time step for efficient computational speed, an updated treatment of S-CO_2 cycle flow mergers and splits, a modified enthalpy equation to improve the treatment of negative flow, and a revised solution of the reactor heat exchanger (RHX) equations coupling the S-CO_2 cycle to the reactor, were introduced to the PDC in FY2011. All of these modifications have improved the code computational stability and computational speed, while not significantly affecting the results of transient calculations.

The improved PDC was used to continue the investigation of S-CO_2 cycle control and transient behavior. The coupled PDC-SAS4A/SASSYS-1 code capability was used to study the dynamic characteristics of a S-CO_2 cycle coupled to a SFR plant. Cycle control was investigated in terms of the ability of the cycle to respond to a linear reduction in the electrical grid demand from 100% to 0% at a rate of 5%/minute. It was determined that utilization of turbine throttling control below 50% load improves the cycle efficiency significantly. Consequently, the cycle control strategy has been updated to include turbine throttle valve control. The new control strategy still relies on inventory control in the 50%-90% load range and turbine bypass for fine and fast generator output adjustments, but it now also includes turbine throttling control in the 0%-50% load range. In an attempt to investigate the feasibility of using the S-CO_2 cycle for normal decay heat removal from the reactor, the cycle control study was extended beyond the investigation of normal load following. It was shown that such operation is possible with the extension of the inventory and the turbine throttling controls. However, the cycle operation in this range is calculated to be so inefficient that energy would need to be supplied from the electrical grid assuming that the generator could be capable of being operated in a motoring mode with an input electrical energy from the grid having a magnitude of about 20% of the nominal plant output electrical power level in order to maintain circulation of the CO_2 in the cycle. The work on investigation of cycle operation at low power level will be continued in the future.

In addition to the cycle control study, the coupled PDC-SAS4A/SASSYS-1 code system was also used to simulate thermal transients in the sodium-to-CO_2 heat exchanger. Several possible conditions with the potential to introduce significant changes to the heat exchanger temperatures were identified and simulated. The conditions range from reactor scram and primary sodium pump failure or intermediate sodium pump failure on the reactor side to pipe breaks and valve malfunctions on the S-CO_2 side. It was found that the maximum possible rate of the heat exchanger wall temperature change for the particular heat exchanger design assumed is limited to ±7 °C/s for less than 10 seconds.

Modeling in the Plant Dynamics Code has been compared with available data from the Sandia National Laboratories (SNL) small-scale S-CO_2 Brayton cycle demonstration that is being assembled in a phased approach currently at Barber-Nichols Inc. and at SNL in the future. The available data was obtained with an earlier configuration of the S-CO_2 loop involving only a single-turbo-alternator-compressor (TAC) instead of two TACs, a single low temperature recuperator (LTR) instead of both a LTR and a high temperature recuperator (HTR), and fewer than the later to be installed full set of electric heaters. Due to the absence of the full heating capability as well as the lack of a high temperature recuperator providing additional recuperation, the temperature conditions obtained with the loop are too low for the loop conditions to be prototypical of the S-CO_2 cycle. In particular, the data includes conditions in which two-phase flow is present whereas the complete demonstration to be assembled in the future would nominally operate in the supercritical regime. The experiments attempted to simulate steady-state conditions but in reality were not held in an unvarying state long enough to achieve a true steady state. Good agreement is obtained between the Printed Circuit Heat Exchanger™ (PCHE™) model in the code and the temperature data for the low temperature recuperator and cooler which are both PCHEs. However, comparison with pressure drop data is difficult because the differences between the measured absolute pressures upstream and downstream of the recuperator and cooler contain large uncertainties because of the small differences obtained relative to the absolute values (i.e., the differential pressure across each heat exchanger was not directly measured). The development of a radial flow turbine model needed for the radial flow turbine component of the TAC initiated several years ago at ANL was completed and the model was implemented in the Plant Dynamics Code. The radial turbine model prediction for the turbine outlet pressure agrees well with the measured value but the outlet temperatures disagree due to the presence of significant heat losses downstream of the turbine final stage in the experiment loop. Comparison of the radial compressor model with the compressor data is difficult due to significant inaccuracies in the measured pressures particularly at the compressor inlet as well as significant windage and other parasitic losses in the compressor. Nonetheless, reasonably good agreement is obtained for conditions around the loop when a value is inferred for the heat loss downstream of the turbine such that a loop energy balance can be established. However, the resulting heat loss is a steady state value and it is not currently known how the heat loss would vary under various transient scenarios. Consequently, it was not possible to attempt to model the transient behavior of the loop and compare with transient data. Development of a Plant Dynamics Code capability to calculate transients

for various configurations of the loop during its phased assembly is a high priority for future work.

Table of Contents

ABSTRACT i

List of Figures vi

List of Tables vii

1 Introduction 9

2 ANL Plant Dynamics Code Improvements 11

2.1 Coupling with SAS4A/SASSYS-1 Code 11
2.1.1 Coupling Approach 11
2.1.2 Accuracy of the Coupling Scheme 14
2.1.3 Comparison with Previous Calculations 15
2.2 Compressor Surge Control 17
2.3 Alternative Time Step Control 21
2.4 Negative Flow Treatment and Enthalpy Change Equations 22
2.5 Simplified Treatment of Flow Splitters and Mixers 23
2.6 Revised Solution for RHX 24
2.7 Error Corrections 25

3 Dynamics Studies of the S-CO_2 Cycle with the Plant Dynamics Code 26

3.1 S-CO_2 Cycle Control Update for Low Grid Demand 26
3.2 Operation at Low Power Level 40
3.3 Thermal Transients for the Sodium-to-CO_2 HX 47

4 Modeling of the Sandia S-CO_2 Loop with the Plant Dynamics Code 57

4.1 Experimental Data 57
4.2 Individual Component Models 62
4.2.1 Recuperator 62
4.2.2 Cooler 64
4.2.3 Heaters 65
4.2.4 Compressor 66
4.2.5 Turbine 68
4.2.6 Piping 71
4.3 Modeling of the Entire Loop 71
4.3.1 Structure 71
4.3.2 Additional Code Development and Solution Algorithm 72
4.3.3 Results for Entire Loop Simulation 78
4.4 Dynamic Simulation 82

5 Summary and Future Work 84

Acknowledgements 88

References 89

Appendix A
Input Files for SNL S-CO_2 Loop Modeling with the Plant Dynamics Code.....91

Appendix B
Output Files from the Plant Dynamics Code for SNL S-CO_2 Loop Modeling ...103

LIST OF FIGURES

Figure 2-1. PDC-SAS4A/SASSYS-1 Coupling Approach. 13
Figure 2-2. Sodium RHX Temperature Change Prediction Error. 14
Figure 2-3. Extrapolation Error at the Beginning of a Transient. 15
Figure 2-4. Coupled and Iterative Solutions from PDC/SAS4A/SASSYS-1 Calculations. 16
Figure 2-5. Compressor Surge Control. 17
Figure 2-6. Example of Compressor Surge Control Action. 20
Figure 2-7. New Approach for Enthalpy Equation. 22
Figure 3-1. Electrical Grid Load Following with Previous Control Strategy. 27
Figure 3-2. Electrical Grid Load Following with Updated Control Strategy. 35
Figure 3-3. Cycle Operation at Low Reactor Power. 42
Figure 3-4. Na-CO_2 HX Thermal Transient for 25 cm CO_2 Pipe Break. 49
Figure 3-5. Na-CO_2 HX Thermal Transient for 1 m CO_2 Pipe Break. 51
Figure 3-6. Na-CO_2 HX Thermal Transient for HX Bypass Valve Opening. 52
Figure 3-7. Na-CO_2 HX Thermal Transient for Idealized Loss-of-CO_2 Side Heat Removal. 53
Figure 3-8. Na-CO_2 HX Thermal Transient for Loss of Intermediate Sodium Pump. 55
Figure 3-9. Na-CO_2 HX Thermal Transient for Reactor Scram with Primary Sodium Pump Trip. 56
Figure 4-1. Projected Layout of the SNL S-CO_2 Loop. 57
Figure 4-2. Modeled SNL S-CO_2 Loop Configuration and Experimental Data at 3200 s. 59
Figure 4-3. Example of Experimental Data for Run 1041. 59
Figure 4-4. Experimental Conditions at 4500 s (a) and 6100 s (b). 61
Figure 4-5. Modeled Structure of the SNL S-CO_2 Loop in the PDC. 72
Figure 4-6. Equilibrium Flow Rate and Pressure Ratio in a Loop. 76
Figure 4-7. PDC Results (Top) of the Simulated SNL S-CO_2 Loop Experimental Conditions (Bottom). 81

LIST OF TABLES

Table 3-1. Updated S-CO_2 Cycle Control Strategy 34
Table 4-1. CO_2 Properties for Experimental Conditions around the Turbine..... 60
Table 4-2. Heat Exchanger Model Performance Prediction for LTR 63
Table 4-3. Heat Exchanger Model Performance Predictions for Cooler 65
Table 4-4. Selection of Hot Side Temperatures for Heater 66
Table 4-5. Selection of the Compressor-Inlet Conditions 67
Table 4-6. Comparison of the PDC Radial Turbine Model Prediction with Experimental Data and Design Conditions..... 70

1 Introduction

The ANL Plant Dynamics Code (PDC) [1] for the analysis of supercritical carbon dioxide (S-CO_2) Brayton cycle power converters has been under development at Argonne National Laboratory for several years. The Plant Dynamics Code has been used previously for control and transient analysis of the S-CO_2 cycle coupled to Lead-Cooled Fast Reactors (LFRs), such as SSTAR and STAR-LM, as well as Sodium-Cooled Reactors (SFRs), such as various Advanced Burner Reactor (ABR) preconceptual designs.

The present report serves as a project update report on PDC code development and continuing investigation of S-CO_2 cycle control and transient behavior as well as validation of modeling in the code. The report covers activities and analyses carried out during Fiscal year 2011 (FY2011).

Plant Dynamics Code development and improvement has continued. The focus has been on extending the code capabilities and improving its stability in applications involving various conditions. To extend the code range of applicability, a coupling approach with the SAS4A/SASSYS-1 Liquid Metal Reactor Code System was developed for the PDC. The SAS4A/SASSYS-1 code is a leading capability for transient and accident analysis of Liquid Metal Reactor (LMR) systems. When coupled to the PDC, the resulting combined analytical tool provides unique capabilities for very detailed analysis of a LMR with a S-CO_2 cycle energy conversion plant. Among other improvements to the PDC undertaken in FY2011 are the introduction of compressor surge control, an update to the negative flow treatment and enthalpy equations for flow mixers and splitters with CO_2, and improvements in the numerical solution scheme.

With the recent PDC improvements, the analysis of the S-CO_2 cycle control and transient behavior was continued. The focus of the control analysis work has been on studying the cycle behavior at low power and the transition to a viable reactor decay heat removal mode. The S-CO_2 cycle control strategy was updated to improve its efficiency at low electrical grid loads (<50%).

In addition, work was initiated on the validation of the PDC modeling based on experimental data from the Sandia National Laboratories (SNL) small-scale S-CO_2 Brayton cycle demonstration loop. The available experimental data was used to validate the steady-state performance predictions obtained with the PDC for various cycle components, such as turbomachinery and the heat exchangers, as well as the performance of the entire loop. To simulate the SNL S-CO_2 loop with the PDC, it has been necessary to develop a radial turbine performance model and to integrate it into the PDC.

The report presents the details of the work on the code improvements, control analysis, and SNL loop modeling and code validation in the following sections.

2 ANL Plant Dynamics Code Improvements

Several improvements to the ANL Plant Dynamics Code (PDC) have been made during FY2011. The most significant ones are described below in details. In addition, some minor errors (i.e., "bugs") were identified in the code and were fixed.

Even though direct comparative analyses have not been carried out, none of the modifications to the code are expected to significantly affect the results obtained previously with the code. The improvements simply extend the code capabilities or increase the computational speed and stability. The minor "bugs" fixed in the code are related to portions of the code not used in previous analysis (such as a treatment of multiple coolers, for example).

2.1 Coupling with SAS4A/SASSYS-1 Code

The Plant Dynamics Code (PDC) [1] has been used previously for control and transient analysis of the S-CO_2 cycle coupled to Lead-Cooled fast reactors (LFRs), including SSTAR and STAR-LM [2]. In order to extend the applicability of the PDC to reactor systems outside LFRs, an option was introduced to the PDC to directly define the reactor-side fluid conditions, including temperature, flow rate, and pressure, at the reactor heat exchanger (RHX) as time-dependent tables. In the case of a Sodium-Cooled Fast Reactor (SFR), the RHX would be an intermediate sodium-to-CO_2 heat exchanger [3]. The reactor-side fluid conditions need to be calculated by a separate reactor analysis code.

The SAS4A/SASSYS-1 Liquid Metal Reactor Code System [4] is the leading capability for modeling a SFR or LFR at the system level. The SAS4A/SASSYS-1 code couples reactor dynamics with thermal hydraulics calculations. The SAS4A/SASSYS-1 code incorporates very detailed reactivity feedback models along with comprehensive thermal hydraulic models for the primary, intermediate, and decay heat liquid metal loops. The SAS4A/SASSYS-1 code also supports the modeling of the balance-of-plant (BOP). However, this option is currently limited to steam cycles only.

In order to carry out simultaneous transient calculations of the entire plant incorporating a SFR with a S-CO_2 cycle BOP, a coupling between the PDC and SAS4A/SASSYS-1 codes is needed.

2.1.1 Coupling Approach

Simultaneous calculations using the PDC and SAS4A/SASSYS-1 codes were carried out previously for a SFR with a S-CO_2 cycle [3,5]. Those calculations included separately

running the two codes and iteratively updating the time-dependent input boundary conditions. Although a satisfactory convergence was obtained, running two codes this way required about 5 iterative runs of each code for a single transient. Although this was, in fact, a remarkably low number of iterations, a more efficient approach was sought.

To simplify the transient analysis of a SFR with a S-CO_2 cycle, a new coupling approach was developed. The main goal of the coupling is to implement data transfer between the two codes at each time step (rather than after the entire transient is calculated). The newly developed coupling approach utilizes the restart capability of SAS4A/SASSYS-1 to allow the code to be executed for some transient time, paused, and restarted later with modifications to the input files. That restart capability is used to basically implement SAS4A/SASSYS-1 calculations on a step-by-step basis, using an algorithm shown in Figure 2-1 and described below. The transient calculation is preceded by steady-state calculations in both the PDC and SAS4A/SASSYS-1.

The transient calculations at each time step start with a guess of an intermediate sodium RHX-outlet temperature. That guess is based on the extrapolation of the results at a previous time step (or steady-state values). The sodium RHX-outlet temperature is selected for such an extrapolation because it is expected that it would be a slow-changing variable due to the thermal inertia of the heat exchanger mass. Currently, no iterations are implemented to verify the extrapolated value; it is simply compared to the actual value calculated on the next time step. As it is demonstrated below, that simple extrapolation provides sufficient accuracy for the dynamics calculations.

The extrapolated RHX-outlet temperature is supplied to the SAS4A/SASSYS-1 restart input file. Then, the SAS4A/SASSYS-1 code is called to calculate the reactor side parameters for one time step. After that, SAS4A/SASSYS-1 output files are read and the data required for the PDC calculations – intermediate sodium flow rate and its temperature at RHX inlet – are provided as input data for PDC calculations. Since the S-CO_2 cycle time step is usually smaller than a reactor time step, the PDC code is run for one or several time steps until it reaches the same transient time as that of the SAS4A/SASSYS-1 code. The PDC calculates the S-CO_2 cycle parameters along with the sodium temperature at the RHX outlet. The latter value is used again to calculate the next guess for the SAS4A/SASSYS-1 calculations. That process continues until the specified maximum transient time is reached.

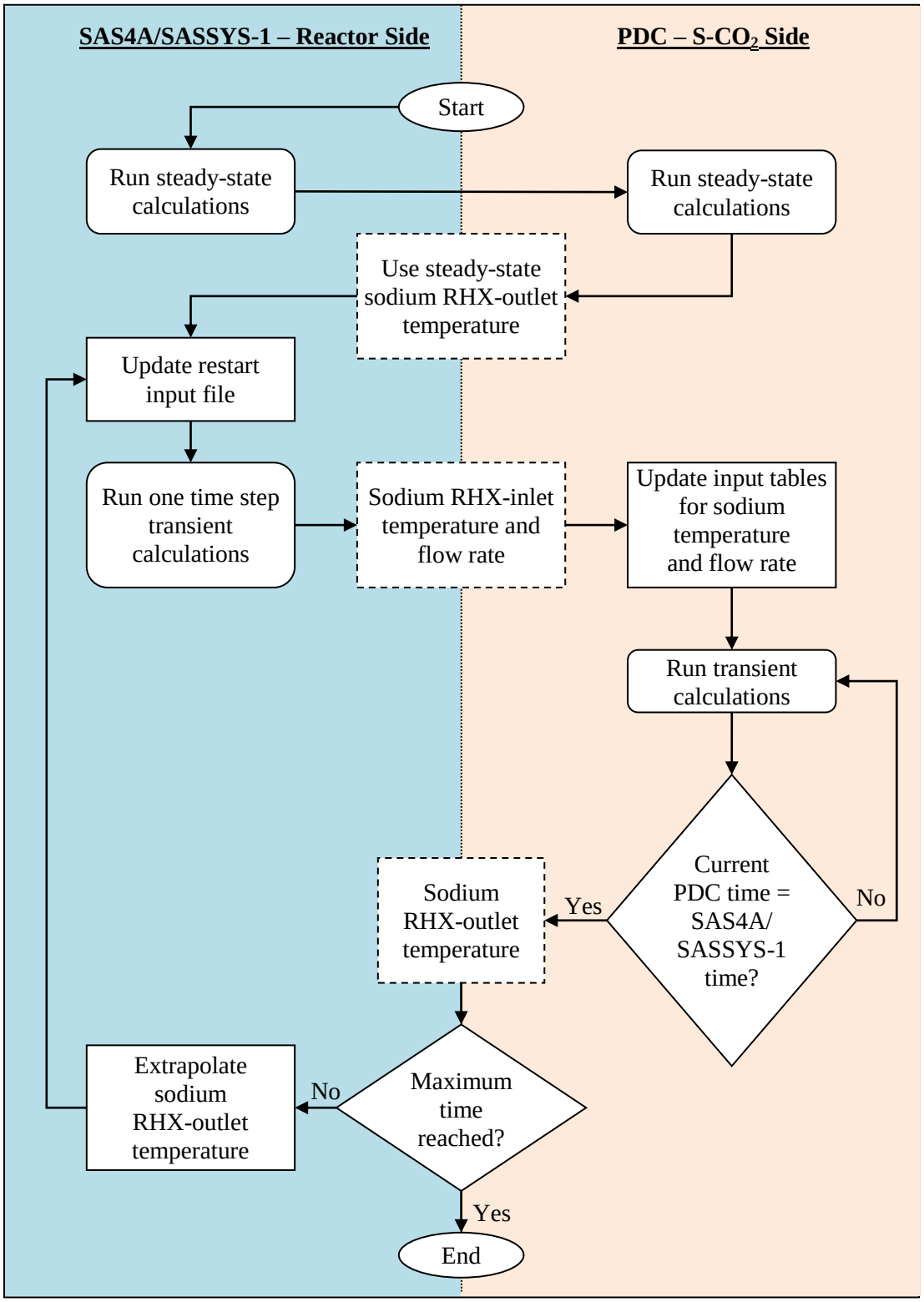

Figure 2-1. PDC-SAS4A/SASSYS-1 Coupling Approach.

2.1.2 Accuracy of the Coupling Scheme

As discussed above, the coupling scheme relies on the extrapolation of the sodium temperature change in RHX. Figure 2-2 shows an example of the calculated error in the prediction of the sodium temperature change in the RHX. The plotted value in Figure 2-2 is:

$$Prediction\ Error = \left|\frac{\Delta T_{actual} - \Delta T_{predicted}}{\Delta T_{actual}}\right|.$$

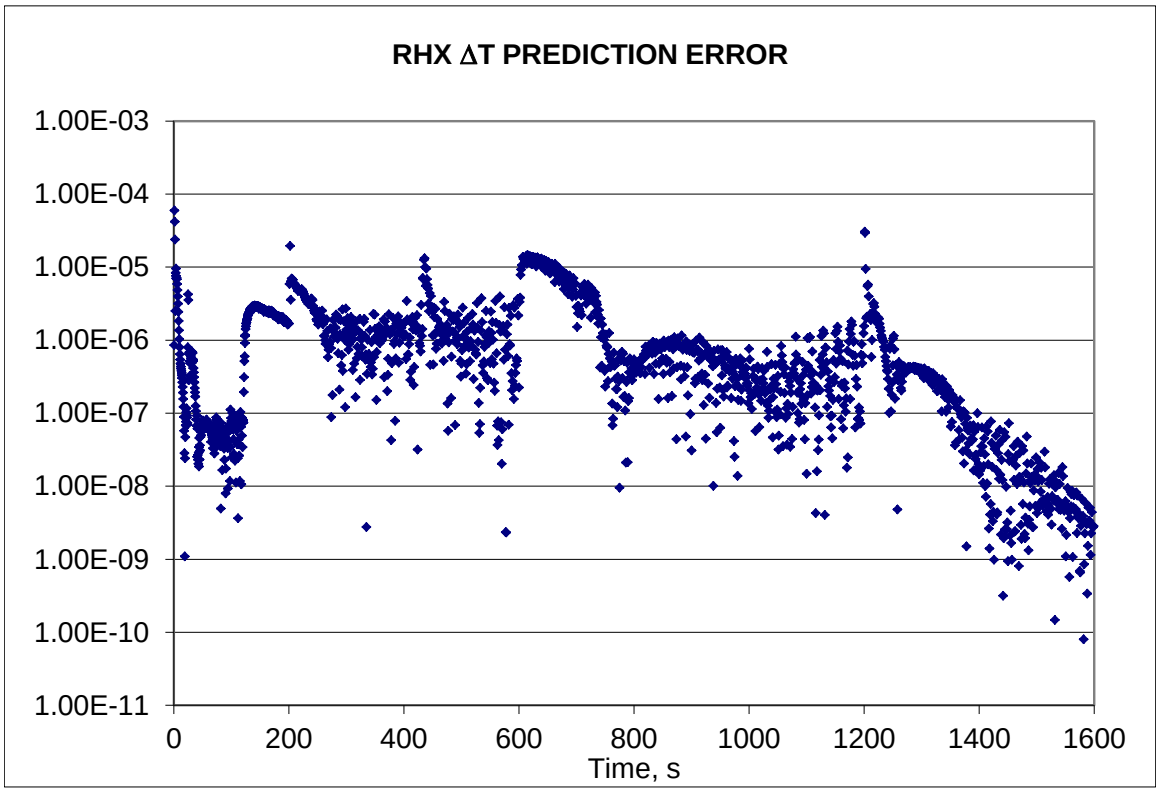

Figure 2-2. Sodium RHX Temperature Change Prediction Error.

The prediction error in Figure 2-2 is plotted as a function of time for a transient that simulated linear grid load reduction from 100 % to 0 % in 1200 s. The maximum error in the sodium temperature change is calculated at the very beginning of the transient. This is due to the fact that at those earlier times no transient information is available and the prediction could only be made based on the steady-state value, as schematically illustrated in Figure 2-3. Once the temperature change starts varying, the accuracy of the prediction increases significantly. The prediction error also increases when significant

changes are introduced to the system. For example, the error shows an increase at the start and stop of the inventory control action (between 200 and 600 s) and at the transition to steady-state operation at zero power at 1200 s. In any case, the prediction error does not exceed 10^{-4} and stays well below that value for most of the transient. Since the transient calculations on S-CO_2 side were done with the convergence criteria of 10^{-5}, the simple extrapolation described above provides sufficient accuracy for the dynamics calculations and no iterations are needed.

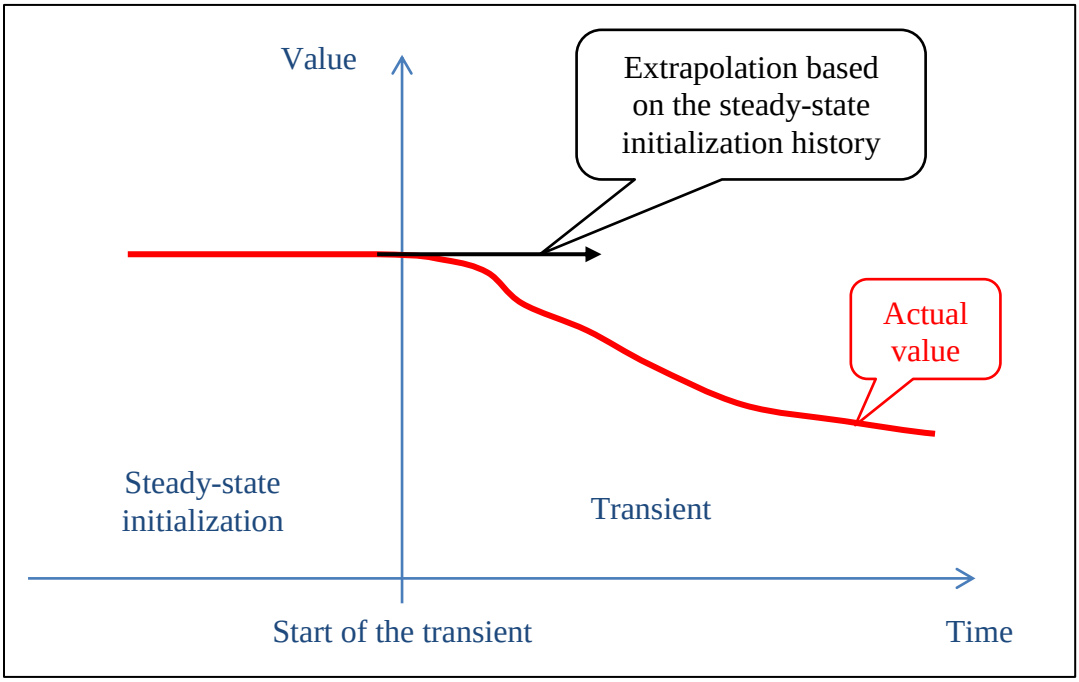

Figure 2-3. Extrapolation Error at the Beginning of a Transient.

2.1.3 Comparison with Previous Calculations

The calculations based on this coupled approach produce results very close to those obtained previously with the iterative coupling, as shown in Figure 2-4 for the sodium RHX-outlet temperature.

Figure 2-4 shows the solution obtained using the new coupling approach ("Coupled") in comparison with the solutions obtained previously under an iterative approach ("Iterations 1-4"). As expected, the iterative solution gradually approaches the coupled solution. After the second iteration, the results are very close. The results for Iterations 3 and 4 are almost identical, suggesting that four iterations are enough in this case. After the fourth iteration, the temperatures agree to within 1°C or less with the coupled solution.

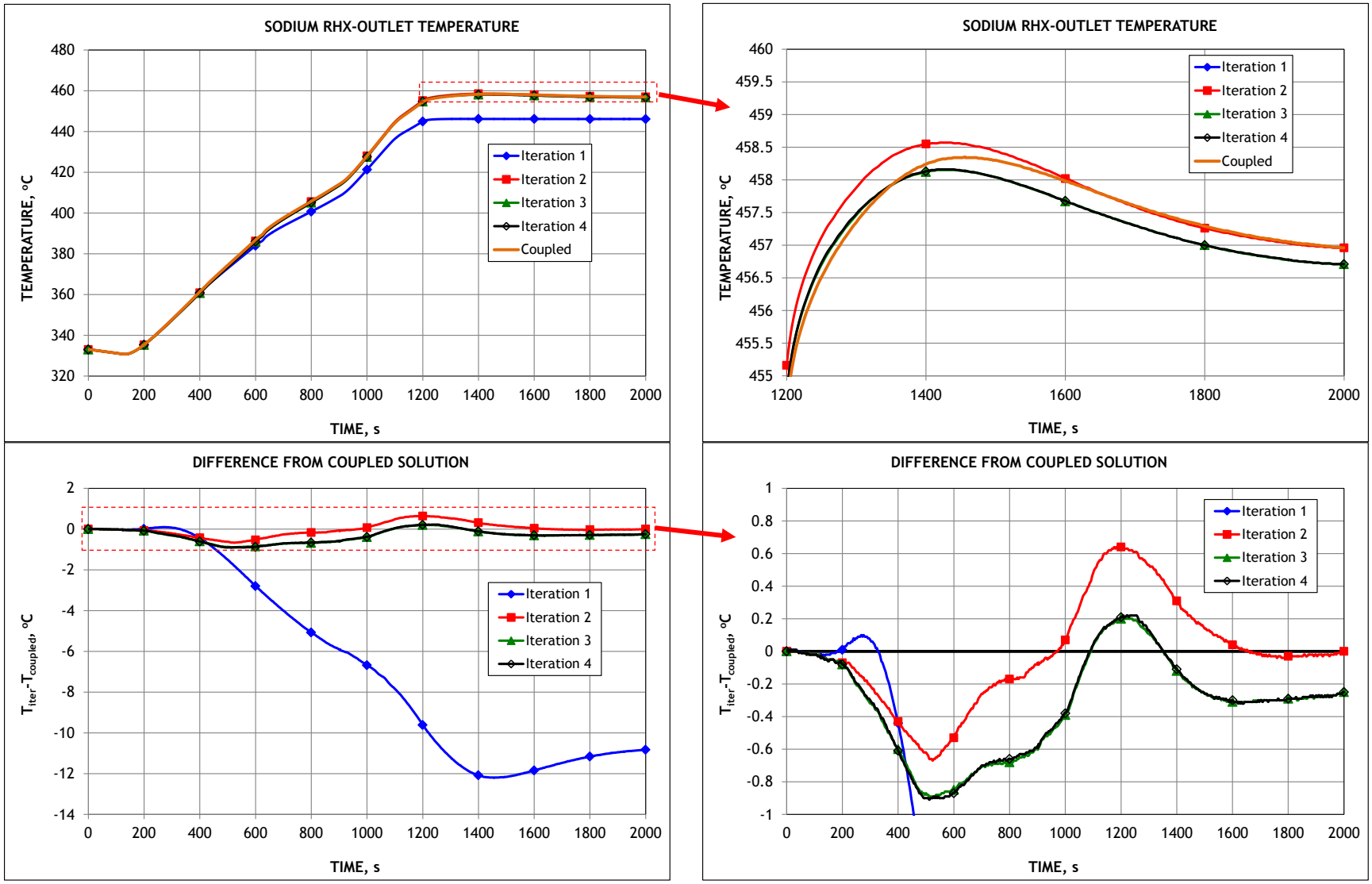

Figure 2-4. Coupled and Iterative Solutions from PDC/SAS4A/SASSYS-1 Calculations.

As demonstrated above, the coupled solution is very close to that obtained previously under the iterative approach. However, the results are obtained much faster now. It is estimated that reading/writing the files along with SAS4A/SASSYS-1 calculations only add about 10% to the calculation time of the PDC code alone (the calculation time is dominated by the PDC code due to much smaller time step on the S-CO_2 side). This is much faster than running five or so iterations of both codes. Moreover, this coupling approach implements automatic data transfer between the codes, such that no user input is needed during the transient simulation. Because of that, the transient results, such as those demonstrated in Section 3 of this report, are now obtained in 1-2 hours compared to 1-2 days with the previous coupling.

2.2 Compressor Surge Control

A compressor surge control option was added to the code. The surge control works by recirculating part of the flow from a compressor outlet back to its inlet. The surge (or stall) occurs when the compressor flow becomes too low. When flow is recirculated, the flow rate through the compressor increases such that the compressor operating point moves away from the onset of surge.

When compressor surge control is implemented, the control scheme monitors the stall/surge approach and increases or decreases the recirculated flow. Under normal conditions, and away from the surge, no flow recirculation is needed. The surge control also incorporates a cooler in the recirculation loop to avoid constant overheating of the compressor flow. Figure 2-5 shows the elements of compressor surge control.

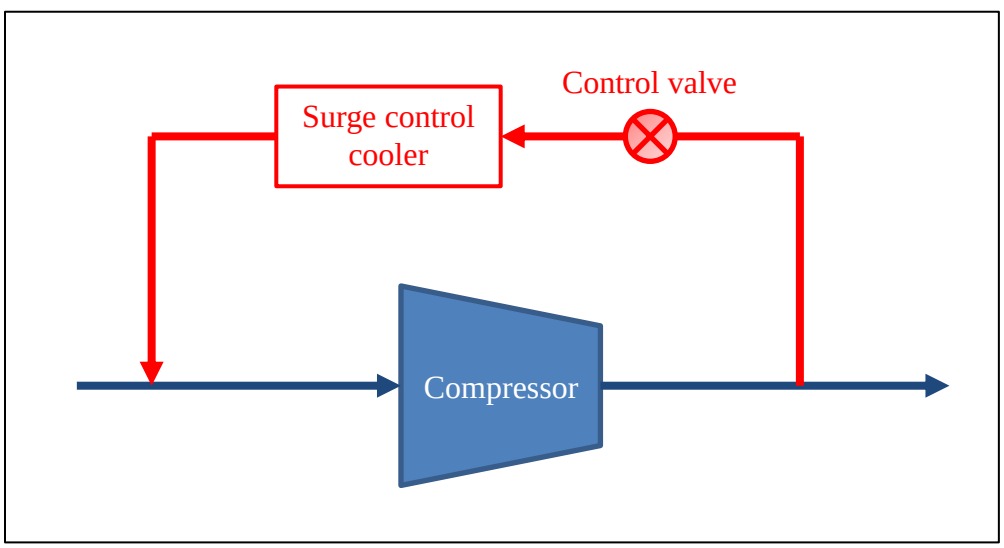

Figure 2-5. Compressor Surge Control.

An idealized automatic surge control was implemented in the PDC whereas the surge loop cooler brings the recirculated flow temperature exactly to that of the compressor inlet. Under this idealized approach, no effect on temperatures (enthalpies) is introduced by the surge control such that only flow (density) equations are affected by the surge flow. That is, when the surge recirculation flow exists, the derivative of the density at the outlet of the compressor is decreased by the surge flow and the derivative of the density at the compressor inlet is increased:

$$\frac{\partial \rho_{out}}{\partial t} = \cdots - \frac{1}{V_{out}} \dot{m}_{surge}$$

$$\frac{\partial \rho_{in}}{\partial t} = \cdots + \frac{1}{V_{in}} \dot{m}_{surge}$$

Note that the equations above reflect only changes to the derivatives from the surge control. There are other contributors to density equations, such as from regular compressor flow, which are omitted in the present report from the above equations for simplicity.

A simple proportional control was modeled for the compressors which monitors the approach to stall and increases/decreases the recirculating flow as necessary. The stall margin is calculated during the compressor map generation as a difference between the current flow rate and the surge flow rate, normalized to the compressor's steady-state flow. When the stall margin falls below the controlled value (e.g., 0.2), the surge control starts to increase the recirculating flow.

Figure 2-6 shows an example of the implementation of surge control. An example was selected specifically to cause the compressors to operate close to the surge point. The minimum surge margin was set to 0.2. As Figure 2-6 demonstrates, shortly after reaching that minimum value for Comp. 1, the control system starts to increase the recirculating flow. In this specific example, the calculated recirculated flow was about 1/3 of the total compressor flow (0.07 vs. 0.25, as normalized to the steady-state turbine flow). As can be seen from Figure 2-6, the control system enacts the recirculation flow for Comp. 1 only. Surge in Comp. 2 is avoided without any action of its surge control. This fact is due to parallel operation of the two compressors in the recompression S-CO_2 cycle. In this parallel configuration, the two compressors basically operate at the same pressure ratio. So, when the surge control on one compressor opens the recirculation valve, the flow rate in this control increases and the pressure ratio for this compressor decreases. That decrease in the pressure ratio is communicated to the second compressor such that the flow rate in it increases automatically, thus moving away from the low surge flow. Overall, the surge control system is effective in avoiding surge in both compressors. The surge margin is maintained close to the controlled value of 0.2 for both compressors. The

previous experience with the PDC has shown that without the surge control, the solution would probably be unstable in the proximity of surge.

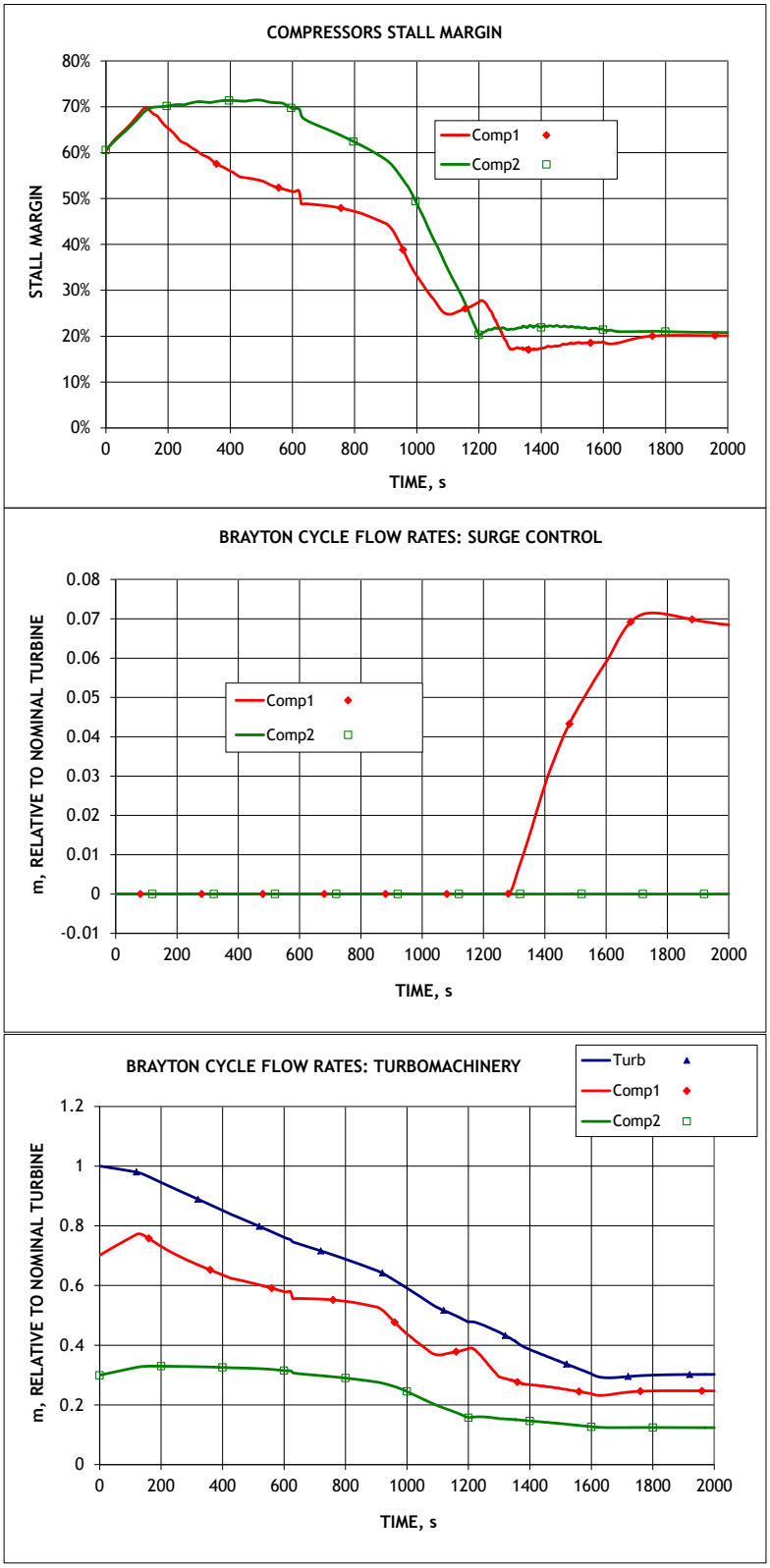

Figure 2-6. Example of Compressor Surge Control Action.

2.3 Alternative Time Step Control

An alternative time step control and convergence scheme was implemented in the PDC. Under the previous scheme, the time step was selected by performing calculations over the current time step with a specified number of sub-steps, then dividing the sub-step size by half, and repeating the calculations until such a division of the sub-step does not change the results at the end of the time step by more than the specified tolerance. That solution scheme required performing the same calculations at least two times to determine the number of time sub-steps.

A new solution scheme was developed under which the size of the time sub-step is selected based on the contribution of each term in the Taylor series expansion as follows:

$$\left| \frac{y_i^{(k)}}{y_i} \frac{h^k}{k!} \right| \le \varepsilon ,$$

where $y_i^{(k)}$ = k-th derivative of the calculated value y_i (such as a flow rate or temperature), h = the time sub-step.

In the solution scheme with Taylor series, several time-derivatives are calculated for each variable. These derivatives are all calculated at the same time. That is the first derivatives are calculated for all variables, then the second derivatives are calculated, and so on. In this new time step control approach, the equation above is applied to all calculated values and all calculated derivatives at each sub-step. For example, when the k-th derivatives are calculated, the time sub-step, h, is determined such that the k-th term in the series expansion is less than the specified accuracy, using the above equation. Then, the smallest value of h determined for all variables is selected as the current sub-step. Then all variables at the end of the selected time sub-step are calculated. After that, all derivatives are calculated again, and a new sub-step size is calculated, until the end of the main time step is reached.

The calculations have shown that the sub-step size determined by this approach is about the same as that from the previous scheme. However, the derivatives are calculated only once (in previous approach with halving the time sub-step, the derivatives were effectively calculated twice per sub-step). Thus, the new approach improves the computational time by as much as 50% without compromising the accuracy. In any case, the previous time-step control scheme is also retained in the code; the selection of which scheme to use was added as a code input parameter ("Convergence option" input in Dynamic_dat.txt file: 0 = halving time step, 1 = based on derivatives).

2.4 Negative Flow Treatment and Enthalpy Change Equations

The negative flow treatment in the PDC was updated by simplifying the equations for enthalpy change. Previously, the time derivative of the enthalpy at each node was calculated based on the flow at the node border (i.e., the inlet flow rate). The flow rates, however, are calculated inside each region, such that calculating the inlet flow involved addition of the flow rates from two adjoining regions, as demonstrated in Figure 2-7, "Previous approach" side. That addition became complicated in the case where one flow was negative. It also required additional work in determining the meaning of the inlet flow for the flow split and mixer locations in the cycle.

Under the new approach, the time derivative of the enthalpy at the node border is defined solely by the flow rate inside that node (i.e., region flow as opposed to the inlet flow), as shown in Figure 2-7, "New approach" side. Thus, no calculations of the inlet flow rate for a node are needed. Figure 2-7 shows the example when the flow is positive, i.e., from node i to node i+1. In the case of the negative flow, the right hand side of the enthalpy change equation in Figure 2-7 is added to the derivative of h_i (rather than h_{i+1}).

The new approach not only simplifies the equations by eliminating the need for calculating the inlet flow (especially for the locations of cycle component connections), but also improves the stability at negative flow conditions. With this modification, it is possible to calculate severe transients, such as very large pipe break.

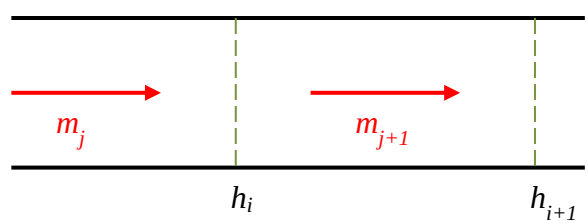

Previous approach

$$\dot{m}_i = \frac{\dot{m}_j + \dot{m}_{j+1}}{2}$$

$$\frac{\partial h_{i+1}}{\partial t} = \cdots + \dot{m}_i (h_i - h_{i+1})$$

New approach

$$\frac{\partial h_{i+1}}{\partial t} = \cdots + \dot{m}_{j+1} (h_i - h_{i+1})$$

Figure 2-7. New Approach for Enthalpy Equation.

2.5 Simplified Treatment of Flow Splitters and Mixers

Another implication of the simplified enthalpy equation described in previous section is a possibility of introducing a simplified treatment of flow split/merge points. Previously, an instantaneous mixing approach was used under which the derivatives of the "inlet" enthalpies were calculated as described in previous section, and the derivatives of the "outlet" enthalpies were determined under the assumption that the energy wouldn't accumulate between the "inlet" and "outlet" points. That approach required quite complicated considerations of which node is considered the "inlet" and which is the "outlet." The determination was based on the flow rates at the beginning of the time sub-step. In the cases where the flow rate changes violently during a time step (such as in the proximity to a pipe break or during the transition from steady-state equations to the dynamic equations at the first few dynamics steps), the determination of which flows should be considered "inlet" and "outlet' may not necessarily hold during the time sub-step. Under the most severe circumstances, when the flow rates would change from positive to negative during a sub-step, that instantaneous mixing assumption was believed to be a cause of instabilities in the solution of the dynamic equations.

To eliminate the instantaneous mixing assumption, a new treatment of flow mixing and splitting points was developed. The mixer or splitter locations are now considered to be a common volume. Under this approach, all nodes around a mixer or a splitter are assumed to be identical. That is, the temperatures, pressures, and enthalpies are all the same for "inlet" and "outlet" nodes. At the beginning of the dynamic calculations, all enthalpies are set to be equal to the outlet enthalpy. Then, in transient calculations, the derivatives of the enthalpy from each incoming flow, calculated using the "New approach" equations in Figure 2-7, are added up to determine the rate of change of that common enthalpy.

For example, for a mixer with two inlet flows, $i1$ and $i2$, and one outlet flow, $o1$, all enthalpies are set to be equal to the outlet enthalpy at the dynamics initialization step:

$$h_{i1} = h_{i2} = h_{o1}$$

During the dynamic calculations, the changes in enthalpy are calculated only for flows which enter the mixer. For example, if flows are still in the same direction as in steady-state, then the derivatives for h_{i1} and h_{i2} are calculated:

$$\frac{\partial h_{i1}}{\partial t} = \cdots + \dot{m}_{j1}(h_{i1-1} - h_{i1})$$

$$\frac{\partial h_{i2}}{\partial t} = \cdots + \dot{m}_{j2}(h_{i2-1} - h_{i2})$$

$$\frac{\partial h_{o1}}{\partial t} = \cdots + 0$$

where j_1 and j_2 correspond to the inlet flow nodes for nodes i_1 and i_2, respectively.

Note that the equations above only consider the treatment for the mixer itself. There could be other components in enthalpy equations, such as heat transfer, which are omitted from the above equations for simplicity and replaced with "…".

When all changes from the inlet flows are calculated, then the derivatives are added to insure the same properties for all nodes:

$$\frac{\partial h_{o1}}{\partial t} = \frac{\partial h_{i1}}{\partial t} + \frac{\partial h_{i2}}{\partial t} + \frac{\partial h_{o1}}{\partial t}$$

$$\frac{\partial h_{i1}}{\partial t} = \frac{\partial h_{o1}}{\partial t}$$

$$\frac{\partial h_{i2}}{\partial t} = \frac{\partial h_{o1}}{\partial t}$$

Since the enthalpies are set to be equal at the first time step and all the derivatives of the enthalpies are equalized at each time step, the enthalpies for all mixer ports will be equal at each time step. A similar approach is applied to the density equations as well as for the splitters.

The main advantage of this new approach is that no instantaneous mixing assumption is needed, removing the believed source of possible instabilities. The only drawback of the new approach is that the information on the incoming temperatures for the mixers and splitters is lost. For example, for the turbine bypass mixing location, the new approach does not allow tracking of the temperature coming in from the bypass line. The inlet temperature from the main line is very close to that at the turbine outlet. However, the bypass line usually involves a significant pressure drop through the bypass valve, such that the temperature downstream of the valve could be significantly different from that on the upstream side of the valve. It is noted, however, that the incoming temperatures are not used in the dynamics equations, which are based on the enthalpies. As described above, the enthalpy equations would still account for the difference between the enthalpies in the incoming flows in the new mixer treatment.

2.6 Revised Solution for RHX

Originally, the PDC was developed for the dynamic analysis of entire plant, including the reactor and energy conversion sides. Later, the reactor and energy conversion parts of

the PDC dynamic equations were separated in order to facilitate an analysis of various reactor systems. To implement such a separation, a special treatment is needed for the reactor heat exchanger (RHX) wall temperature change to provide coupling between the reactor and Brayton cycle parts. In particular, an assumption has to be made that the heat exchanger wall temperature is a slowly changing variable, such that only the first term in the Taylor series expansion, determined by the first derivative of the temperature, is sufficient.

After coupling the PDC to the SAS4A/SASSYS-1 code, the reactor side is no longer calculated by the PDC (the PDC now solves equations inside the RHX only). The reactor side coolant conditions at the RHX inlet are provided as input, either directly through the input files or indirectly from the results of SAS4A/SASSYS-1 calculations. Therefore, all heat exchanger equations can now be solved simultaneously, such that a special treatment to separate the reactor and Brayton cycle sides is no longer needed. Therefore, the equations for the reactor-side coolant inside the RHX and the RHX wall temperature are recombined with the Brayton cycle equations, eliminating the assumption on the RHX wall temperature change.

2.7 Error Corrections

As part of the ongoing collaboration between ANL and CEA, Cadarache (France) on the PDC under the Generation IV International Forum (GIF) framework, an independent check of the code was carried out by CEA personnel. As a result, several errors in the code were identified.

Among the errors ("bugs") which have not been identified by ANL already, the majority deal with parts of the code that were never used in analyses at ANL. For example, the compressor design subroutine has an option of using a vaneless diffuser. CEA found that in this option, the diffuser outlet enthalpy wasn't defined anywhere in the code. This issue was not identified earlier by ANL because in all compressor designs, considered so far, vaned diffusers were utilized.

Other similar issues include transferring the turbine and cooler data between the subroutines at some locations in the code. In some places, an entire array of design parameters was transferred to subroutines instead of the data for a particular turbine and cooler. However, in the transient simulations performed so far, only one turbine and one cooler were used, such that the array had the same meaning as just one parameter. CEA has confirmed that applying those changes to the code did not affect the results of transient simulations. Still, identifying those "bugs" was a very useful outcome of the ANL-CEA cooperation for future analyses.

3 Dynamics Studies of the S-CO_2 Cycle with the Plant Dynamics Code

3.1 S-CO_2 Cycle Control Update for Low Grid Demand

The investigation of the S-CO_2 cycle control strategy with the ANL Plant Dynamics Code (PDC) has been continued. In previous work, the cycle control strategy was developed to allow the electrical grid load following in the entire range, i.e. from 0% up to 100 % load. To confirm that the recent code modifications (described in Section 2) did not worsen the controllability of the cycle, the grid load following calculations were repeated. In this calculation, the electrical grid demand was changed linearly from 100% all the way to 0% at 5%/min rate (i.e., from 100% to 0% in 1,200 s) followed by operation at 0% generator power for 400 s to confirm the cycle stability. Similar to the previous calculations [5], autonomous reactor control was assumed whereby the reactor power isn't actively controlled and is changed due to the reactivity feedbacks only. The simulations are carried out for the same 1000 MWt cycle design as before. This time, the calculations include the direct coupling with the SAS4A/SASSYS-1 code as described in Section 2.1 as well as other PDC modifications described in the previous section (except that the compressor surge control was disabled in these calculations). The results of these confirmatory calculations are shown in Figure 3-1. Overall, the results are very close to those obtained before.

The results in Figure 3-1, as well as the previous control results, were obtained under the control strategy which assumed turbine bypass control at loads below the inventory control range, i.e., below 50% load. That control mechanism was implemented at low loads because it was the simplest and the fastest available control. In particular, the control logic for turbine bypass control in the PDC was organized in such a way that the final generator power adjustment is done by the action on the turbine bypass valve. Thus, in the absence of other actions, the turbine bypass control is applied automatically to adjust the generator output in order to match the grid demand. Second, the turbine bypass control is very fast – the action of increasing and decreasing of the bypass flow is almost instantaneous since it is based on pressure change rather than on temperatures (the change rate of the latter is always limited by the thermal inertia of the system). Lastly, the majority of the control strategy development for the S-CO_2 cycle was focused on cycle operability at higher grid loads since it is unusual to operate nuclear reactors at very low loads and the S-CO_2 cycle control analysis was entirely devoted to cycle applications for nuclear reactors. Therefore, the simplest and the most effective control strategy, – turbine bypass control, – was implemented at low loads.

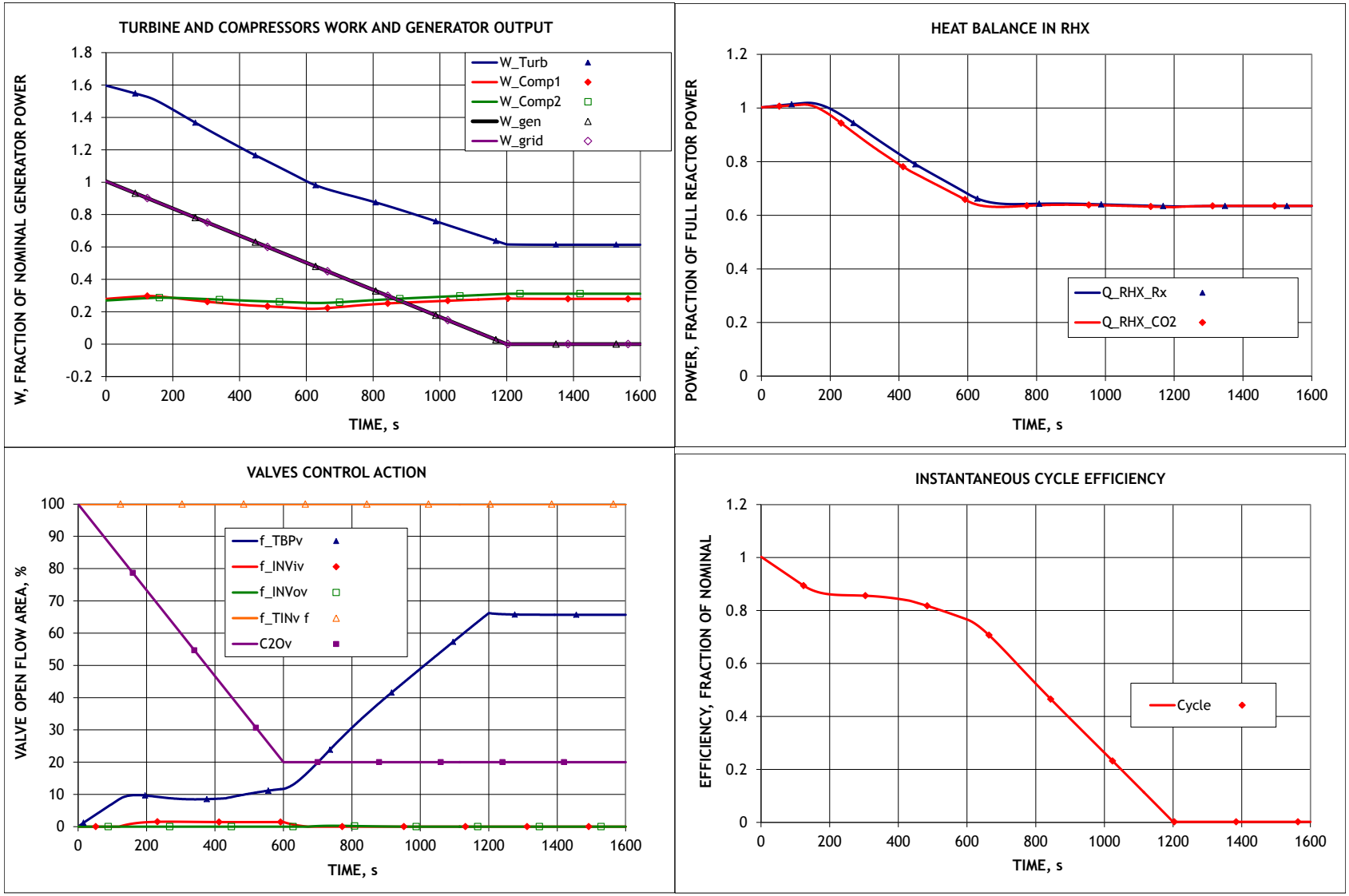

Figure 3-1. Electrical Grid Load Following with Previous Control Strategy.

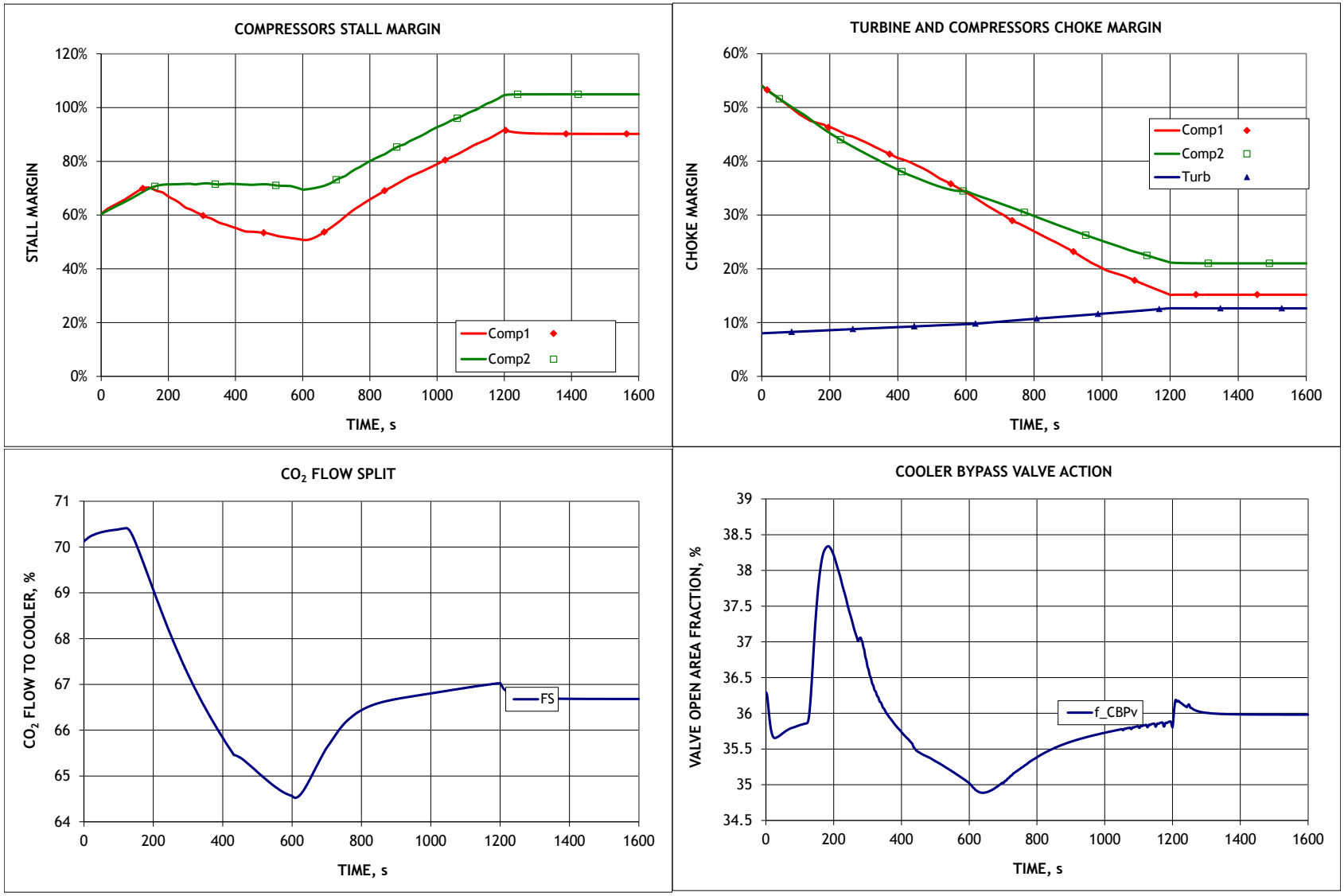

Figure 3-1. Electrical Grid Load Following with Previous Control Strategy. (Continued)

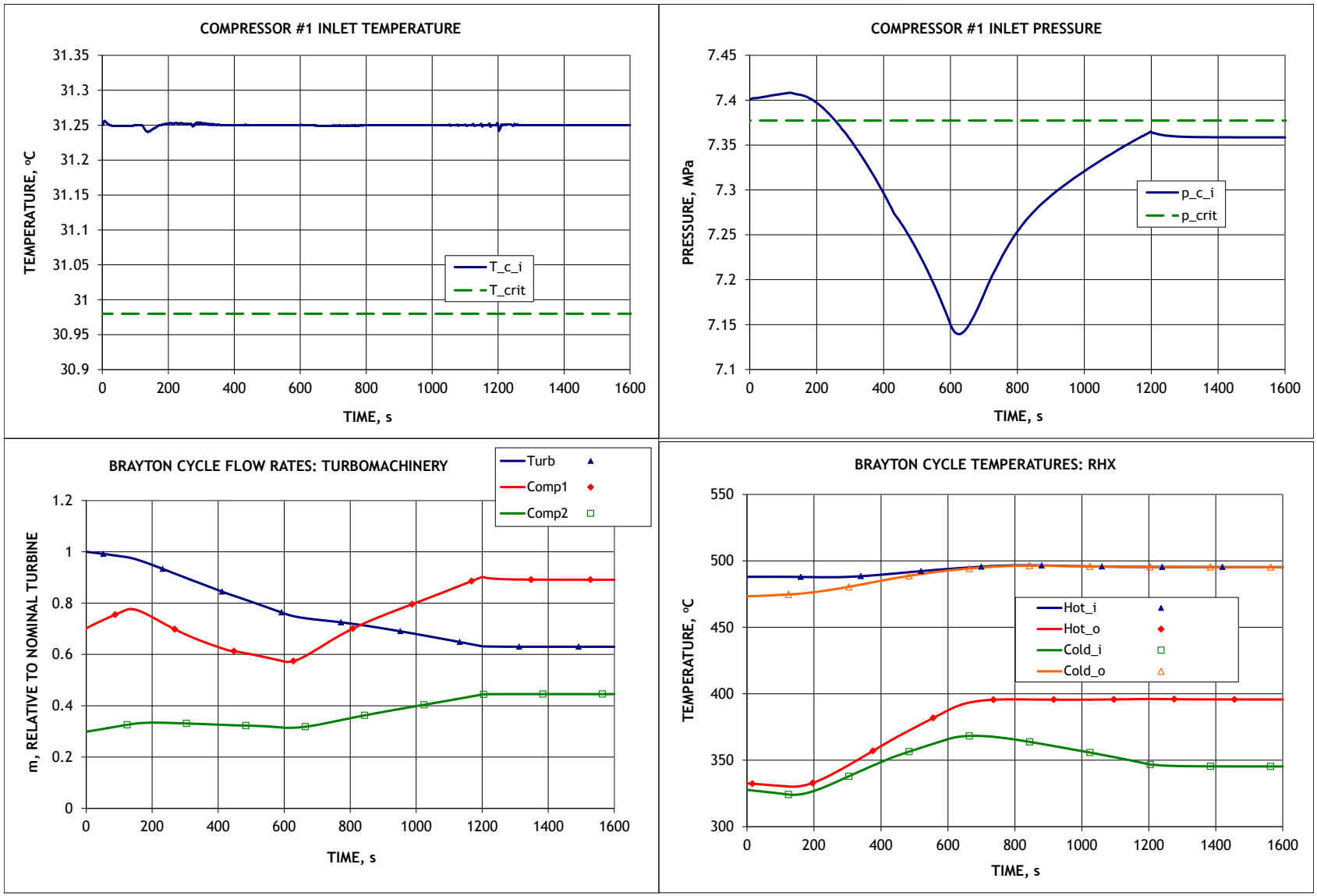

Figure 3-1. Electrical Grid Load Following with Previous Control Strategy. (Continued)

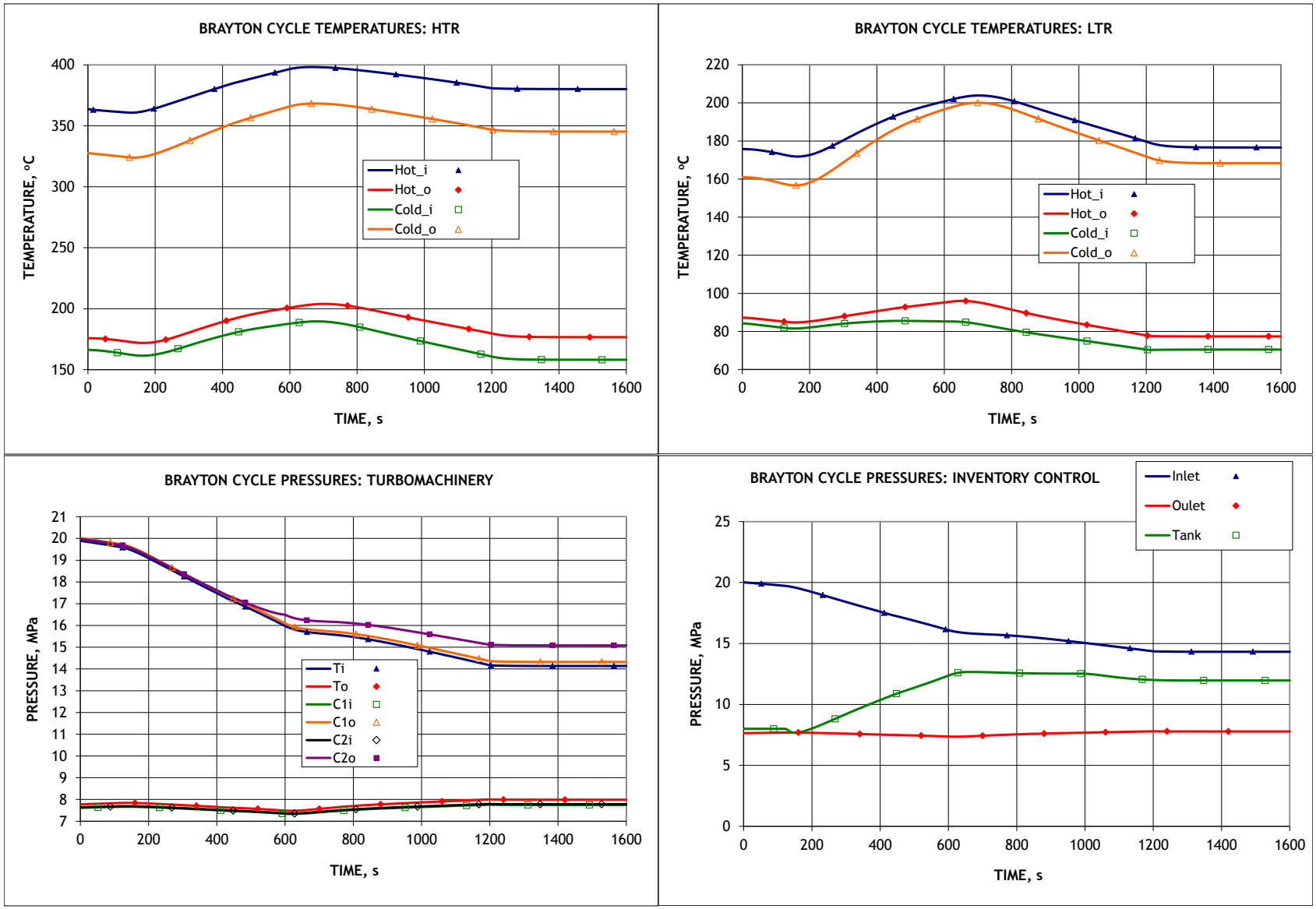

Figure 3-1. Electrical Grid Load Following with Previous Control Strategy. (Finished)

However, as the results in Figure 3-1 indicate, the turbine bypass is not the most efficient control in terms of plant thermal efficiency. In fact, it is *the least* efficient control mechanism. The energy balance in the RHX plot shows that the heat removal rate by the cycle from the reactor sides changes only between about 200 s and 600 s, or between 80% and 50% load, that is in the range of the inventory control action, with some thermal delay. Above 90% load and below 50% load, i.e., when only the turbine bypass control is implemented, the heat removal rate in the RHX (as wells as the reactor power) does not change. That is, the same power is supplied to the cycle despite the reducing generator output. In other words, the same amount of energy going into cycle is used less and less efficiently with a larger and larger portion of it going into parasitic losses, such as increased compressor work and/or increased heat removal in the cooler. This observation is confirmed by the cycle efficiency plot which shows an almost exactly linear decline in efficiency outside the 200-600 s range.

Aside from the inefficiency itself, such operation at low load has another negative consequence. As the results in Figure 3-1 demonstrate, the reactor power (which is very close to the RHX heat removal rate) is about 60% of the full rated value by the end of the transient. Since the transient simulated the reduction in load all the way to 0%, the similar path would be followed in a case of planned reactor separation from the grid. In that procedure, the next step on the reactor control would be shutting down the reactor power with subsequent operation at the decay heat level. That decay heat level is initially about 6% of full power and slowly declines with time. To safely remove the decay heat from the reactor, some sort of decay heat removal system should be implemented in any nuclear reactor. Ideally, the same energy conversion system, S-CO_2 cycle in this case, could be used for the decay heat removal mode. However, as the results obtained so far suggest, such operation of the S-CO_2 cycle would be problematic, at least with the current cycle control approach. When the reactor is ready to be disconnected from the grid under the current cycle control scheme, the reactor power is about 60% and reducing the reactor power to 6% decay level would introduce a heat imbalance in the RHX which in similar calculations has previously led to overcooling and possible freezing of the intermediate coolant (sodium in this system). Even if a separate dedicated decay heat removal system, other than S-CO_2 cycle, is implemented, still a transition is to be made from 60% reactor power to 6% power. Because of the significant difference in the power levels, it would be difficult to ensure reactor coolability during such transition.

For the reasons discussed above, it was decided to continue investigation of the S-CO_2 cycle control strategy in order to increase the plant efficiency at lower levels and to achieve a better transition to the decay heat removal mode. In seeking both of these goals, the first step would be to find a cycle control strategy which would increase cycle efficiency at lower power level thus reducing the reactor power at the end of the load reduction transient. The ultimate goal for this search would be finding a control approach that would lead to operating a reactor system with a 6% or less power level by the time the grid demand reaches 0%.

Earlier S-CO_2 cycle control analysis based on the quasi-static approach suggested that

the highest cycle efficiency at reduced loads is achieved with inventory control. However, this control has limited range mostly due to the size (i.e., volume) of the inventory control tanks. In the current control approach, inventory control operates passively by the pressure difference between the cycle pressures and the inventory control tank/vessel pressure. This arrangement has an obvious advantage that no pumps are needed to add or remove the CO_2 inventory in the cycle. The possibility of increasing the inventory control range is discussed in the next section of this report. However, before the inventory control system is changed, other options were first investigated.

The results of the quasi-static control analysis suggested that in the absence of inventory control, the highest efficiency of the cycle at the reduced loads is achieved either by the turbine throttling or by implementing RHX bypass on the S-CO_2 side. The cycle efficiency was calculated to be about the same for these two options. The turbine throttling was selected for further analysis since it is expected to have lesser thermal impact on the RHX structures than the RHX bypass.

Turbine throttling control is achieved by the regulating action of a valve located at the turbine inlet (for these reasons, the control can also be called turbine inlet control). Partially closing the valve introduces a pressure drop upstream the turbine such that a smaller pressure difference is available in the turbine reducing the useful turbine work and the net generator output. Turbine inlet (throttling) control has already been implemented in the PDC. Similar to inventory control, a table of the controlled parameter versus the grid load is supplied in the input file. In the case of turbine inlet control, the controlled parameter is the desired pressure drop across the control valve. The automatic control logic is implemented in the PDC to maintain the required valve pressure drop by opening and closing the valve. Similar to inventory control, any difference between the idealized control and the control action resulting from use of the table will be adjusted by the turbine bypass control action. In idealized control, no action on the turbine bypass would be required. Practically, the values for the control table are selected such that the turbine bypass control action is minimal.

The results of transient simulations using coupled the PDC and SAS4A/SASSYS-1 codes for the same 5%/min load reduction transient for the case when turbine throttling control is involved are shown in Figure 3-2. The turbine throttling (inlet) valve action is shown as the valve open area fraction in the "f_TINv f" curve on the **VALVES CONTROL ACTION** plot. Initially, the valve is fully opened (open fraction = 100%) and starts to close after the grid demand is reduced below 50% (after 600 s). The valve control action is forced by the following input in the control table (BCcontrol_dat.txt input file for PDC):

Load, %	0	50	100
Valve Δp, MPa	4.65	0	0

The table is set up to eliminate any valve action between 50% and 100% load. Below 50% load, the valve pressure drop is linearly increasing to 4.65 MPa with decreasing

load. The value of 4.65 MPa is selected such that the turbine bypass valve stays around 10% open during the turbine throttling action (after 600 s).

Note that the turbine throttling action increases the pressure at the compressor outlet (while the pressure at the turbine inlet is decreasing). That increase in the compressor-outlet pressure does not impose any concern on the structural design since the turbine throttling action occurs at low loads *after* some CO_2 inventory is removed by means of the inventory control above 50% load. Therefore, the throttling action starts when the compressor-outlet pressure is significantly lower than the maximum pressure at design conditions (about 16 MPa versus 20 MPa maximum as indicated in Figure 3-2). So, the compressor-outlet pressure stays below 20 MPa even with the increase from the turbine throttling action.

That compressor-outlet pressure increase has another implication on the cycle control. Previously, the inventory control action was limited to the point when the compressor-outlet pressure reduced to the increasing inventory control tank pressure level. With the increase in the cycle pressures due to turbine throttling, the inventory control action can be extended somewhat beyond the previous limit. Since inventory control is always beneficial to the cycle efficiency, that possibility was taken advantage of in the simulation in Figure 3-2. Inventory control was operated between 90% and 50% loads and again between 25% and 10% loads.

The main effect of the turbine throttling control in Figure 3-2 is the increase in cycle efficiency below 50% load (compared to just turbine bypass control in Figure 3-1). Even though the cycle efficiency still *has to be* 0% at zero load, the cycle efficiency above 0% load increases. For example, the cycle efficiency at 25% load (900 s) is now about one-half of the design value (i.e., around 20%) compared to <0.4 times the design value (16 %) in the previous case. As a result, the heat removal rate in the RHX by the S-CO_2 cycle is now reduced to about 25% full power at the end of the transient, compared to ~60% before. Those results show clear benefits at lower loads of turbine throttle control compared to turbine bypass control. Thus, the recommended S-CO_2 cycle control strategy has been updated to include turbine throttling, as indicated in Table 3-1. Highlighted in red are the changes from previous results.

Similar to previous cases, the simulations in Figure 3-2 were carried out assuming autonomous reactor control. The results show that the internal reactivity feedbacks are strong enough to match the heat removal in the RHX – the reactor power approaches the same 25% full power level by the end of the transient – without the significant increase in reactor temperatures – the core-outlet temperature stays at or below the steady-state value.

Table 3-1. Updated S-CO_2 Cycle Control Strategy

Control Mechanism	Range
Inventory	50%-90% and 10%-25%
Turbine throttling	0%-50%
Turbine bypass	90%-100% and all other loads to assist inventory and turbine throttling controls
Cooler bypass	All loads to maintain minimum temperature
Cooling water flow rate	All loads to maintain operability of the cooler bypass
Compressor surge control	When needed to avoid surge

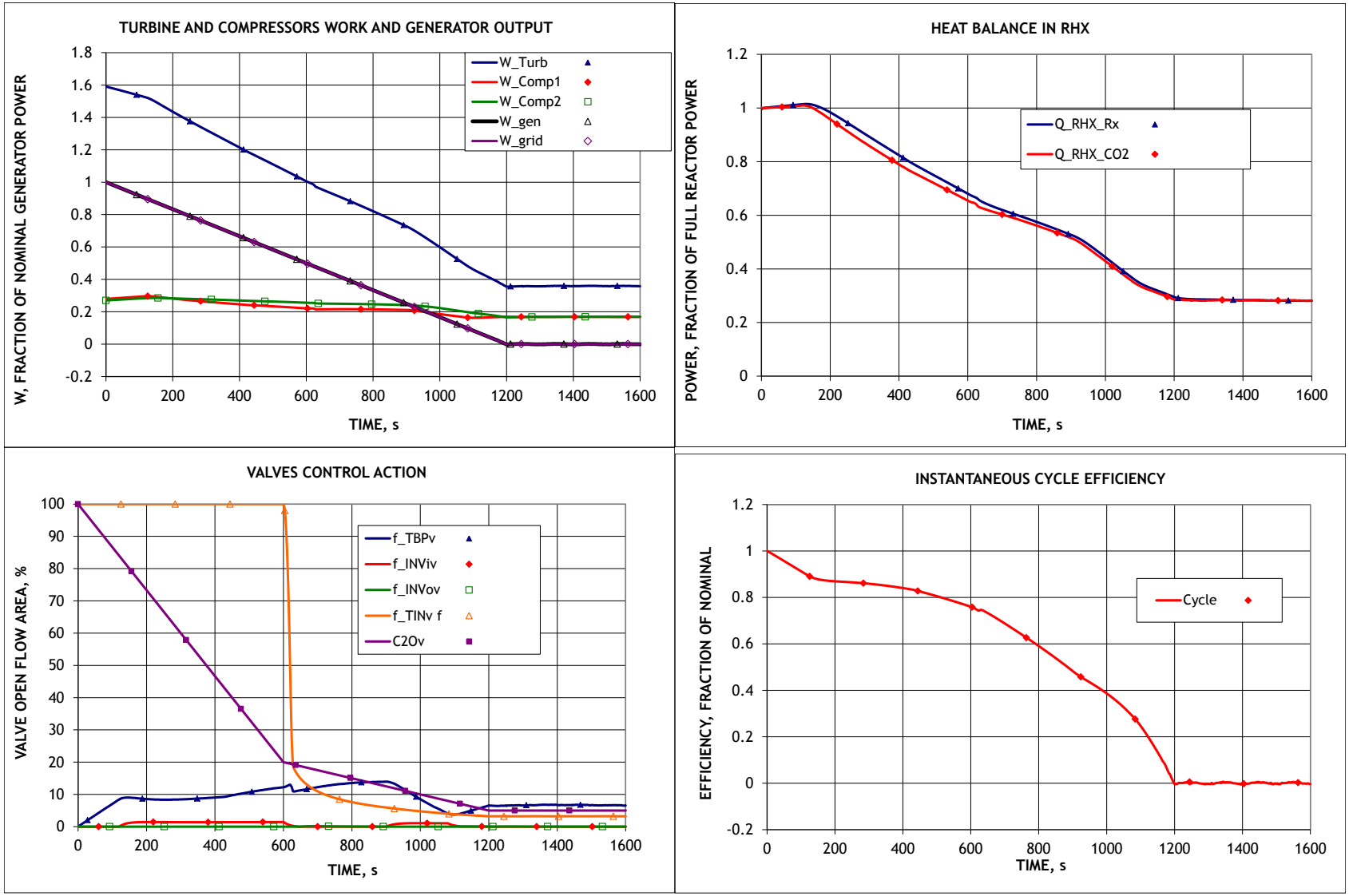

Figure 3-2. Electrical Grid Load Following with Updated Control Strategy.

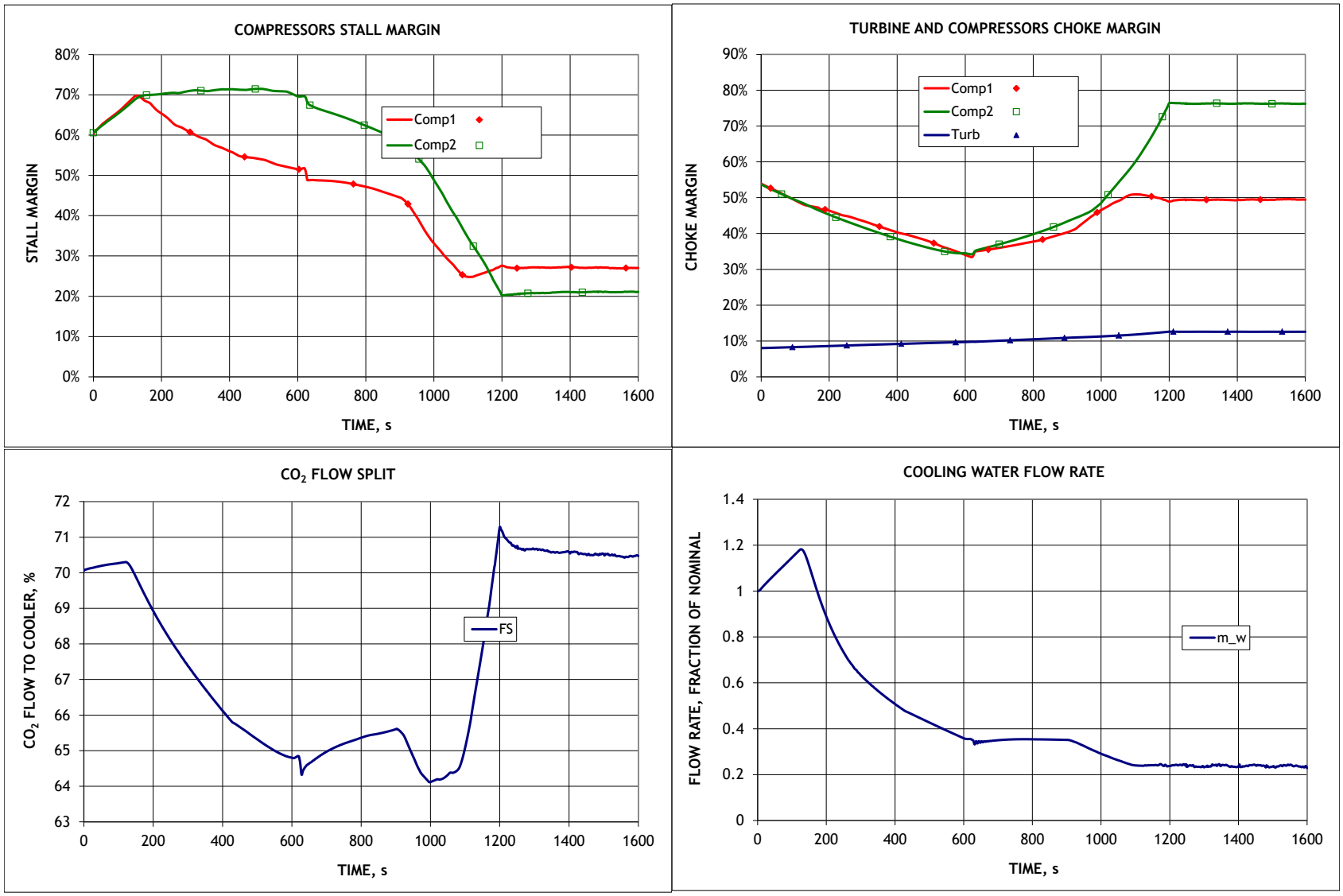

Figure 3-2. Electrical Grid Load Following with Updated Control Strategy. (Continued)

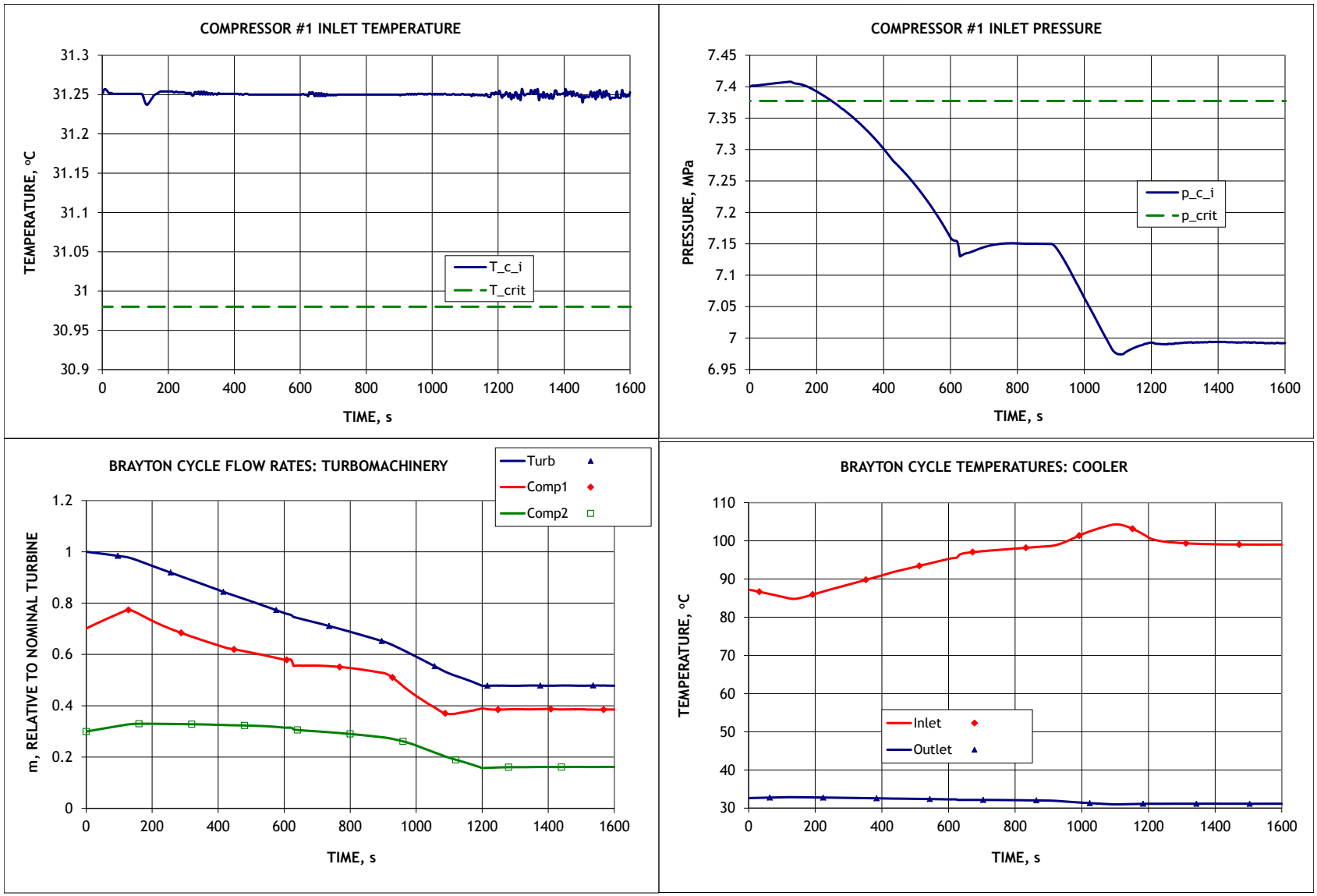

Figure 3-2. Electrical Grid Load Following with Updated Control Strategy. (Continued)

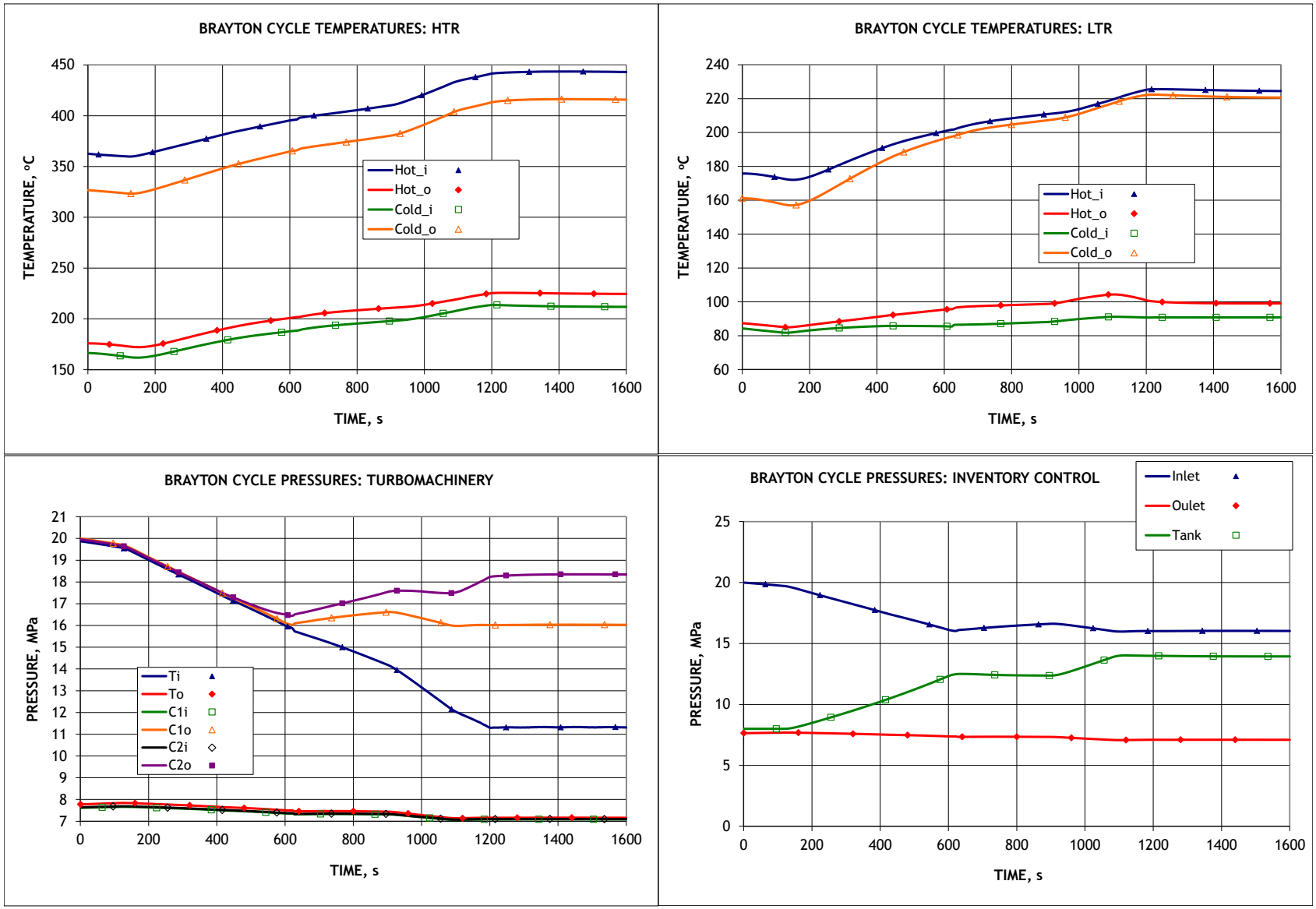

Figure 3-2. Electrical Grid Load Following with Updated Control Strategy. (Continued)

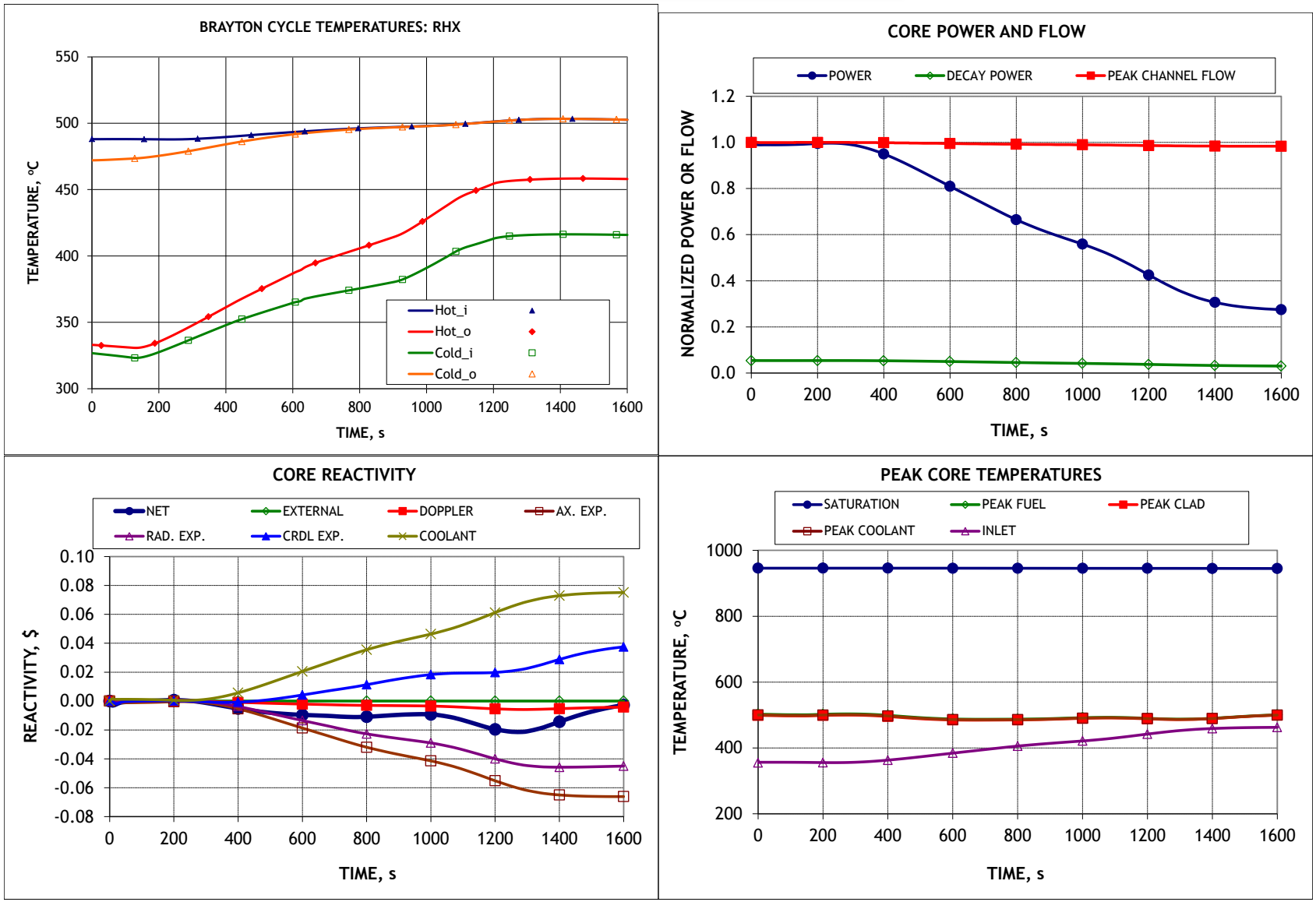

Figure 3-2. Electrical Grid Load Following with Updated Control Strategy. (Finished)

3.2 Operation at Low Power Level

The results presented above demonstrate that the higher system efficiency achieved with an updated control strategy means that the reactor power is now reduced to about 25% with autonomous reactor control. Even though it is much closer to the 6% initial decay heat level following scram, it is still too high, such that a transition to the decay heat removal mode may be complicated.

A possibility of further reducing the reactor power by operating the S-CO_2 cycle control beyond the scope needed for the generator control was investigated. In this simulation, the turbine throttling action was continued even after reaching zero generator output. Also, inventory control was allowed to operate beyond its normal range, for example, by using charging compressors and/or chillers or simply vacating the cycle. The goal of the study was to find the cycle control which would reduce the heat removal rate in the RHX to, ideally, 6% full power or less. Since the simulation would involve operating the S-CO_2 cycle controls beyond the actions needed for the grid load following, it is expected that the generator output will fall below the grid demand. That is, in the current simulation, where the grid demand goes to zero, the generator net output would be negative, i.e. the generator would need to be capable of working as a motor.

Figure 3-3 shows the results of a transient simulation in which the heat removal rate by the cycle in the RHX was reduced to 6%, i.e. to the initial decay heat level. To implement this simulation, the grid demand, after reducing from 100% to 0% at the same 5%/min rate as before, was reduced even further to -1% just to initiate additional control actions which are triggered by using negative values for loads in the input tables. The inventory control and turbine throttling control tables were extended to add more action at negative loads. To eliminate any restrictions from the inventory control tank pressure, the tank volume was artificially increased 100 times compared to the previous simulations such that the calculated tank pressure is almost constant even when CO_2 mass is added to the tank. The simulation time was extended to 2,000 s to find a stable solution.

Even though the goal of reducing the heat removal rate to 6% was achieved (the reactor power decreases to almost the decay heat level by 2,000 s), the cycle operation in this regime is very inefficient. As a result of additional control action, the net generator output drops below the grid demand after about 1,300 s. In this simulation, compressor surge control was needed. After about 1,300 the surge flow rate in Comp. 1 increases dramatically and reaches a level comparable or even exceeding the flow rate in the turbine. As a result, most of the power from the generator, which now operates in a motoring mode, comes to provide the recirculation of that surge protection flow. At the same time, additional action from the turbine throttling valve decreases the pressure at the turbine inlet to a level almost equal to the low pressure in the cycle. As a result, the turbine work is reduced to almost zero around 1,650 s. The net electrical power input

from the electrical grid to the generator drops to -20% of the nominal electrical power output. That is, for an equivalent 1000 MWe plant, the generator in motor mode would need an electrical power input of 200 MWe from the electrical grid for initial decay heat removal.

Overall, the results in Figure 3-3 demonstrate that a S-CO_2 cycle with current control approach can theoretically operate at the reactor decay heat level. Practically, however, that operation would be very inefficient. In particular, to circulate CO_2 around the cycle, a net electrical input of 20% full plant capacity would be needed.

It is important to note that the results in Figure 3-3 were obtained under the control strategy developed for normal load following. It is possible that there could be a control approach, designed specifically for decay heat removal operation, which would implement reasonable S-CO_2 cycle operation in this mode. The work on finding this control approach will be continued in the future. One possibility is to reduce the rotational speed of the turbine and compressors. In all previous simulations it was assumed that there is a synchronous connection of the generator to the grid such that the turbomachinery shaft rotational speed is fixed at the grid frequency. That assumption was extended in the current study to the situation of operation with zero grid demand. In reality, though, when the plant is disconnected from the grid, the shaft rotational speed is no longer dictated by the grid frequency. So, the shaft speed can be reduced to provide more effective compressor operation at low power and flow. That option has not been investigated yet because it would require generation of asynchronous maps for the turbine and two compressors for the PDC simulation.

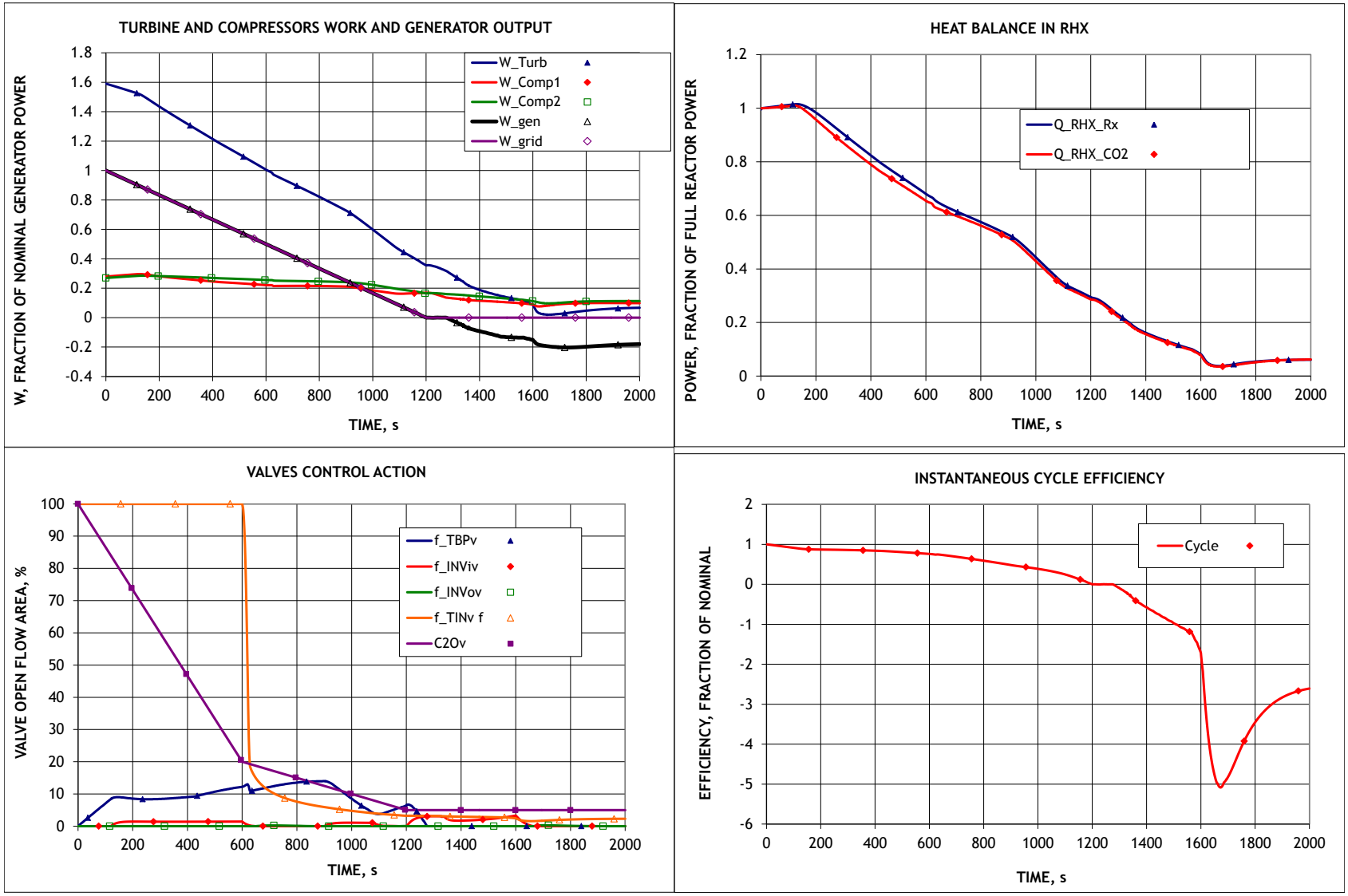

Figure 3-3. Cycle Operation at Low Reactor Power.

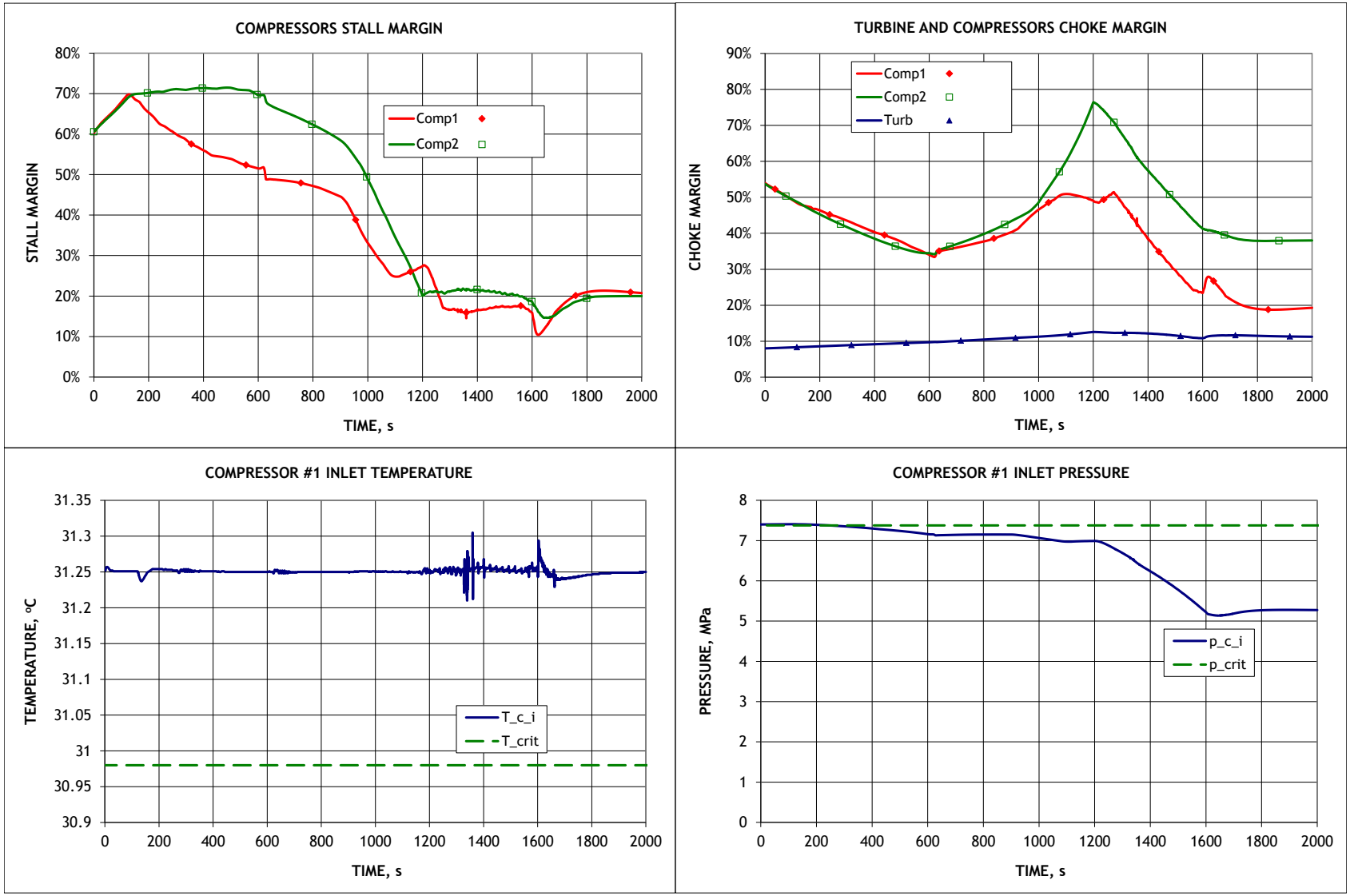

Figure 3-3. Cycle Operation at Low Reactor Power. (Continued)

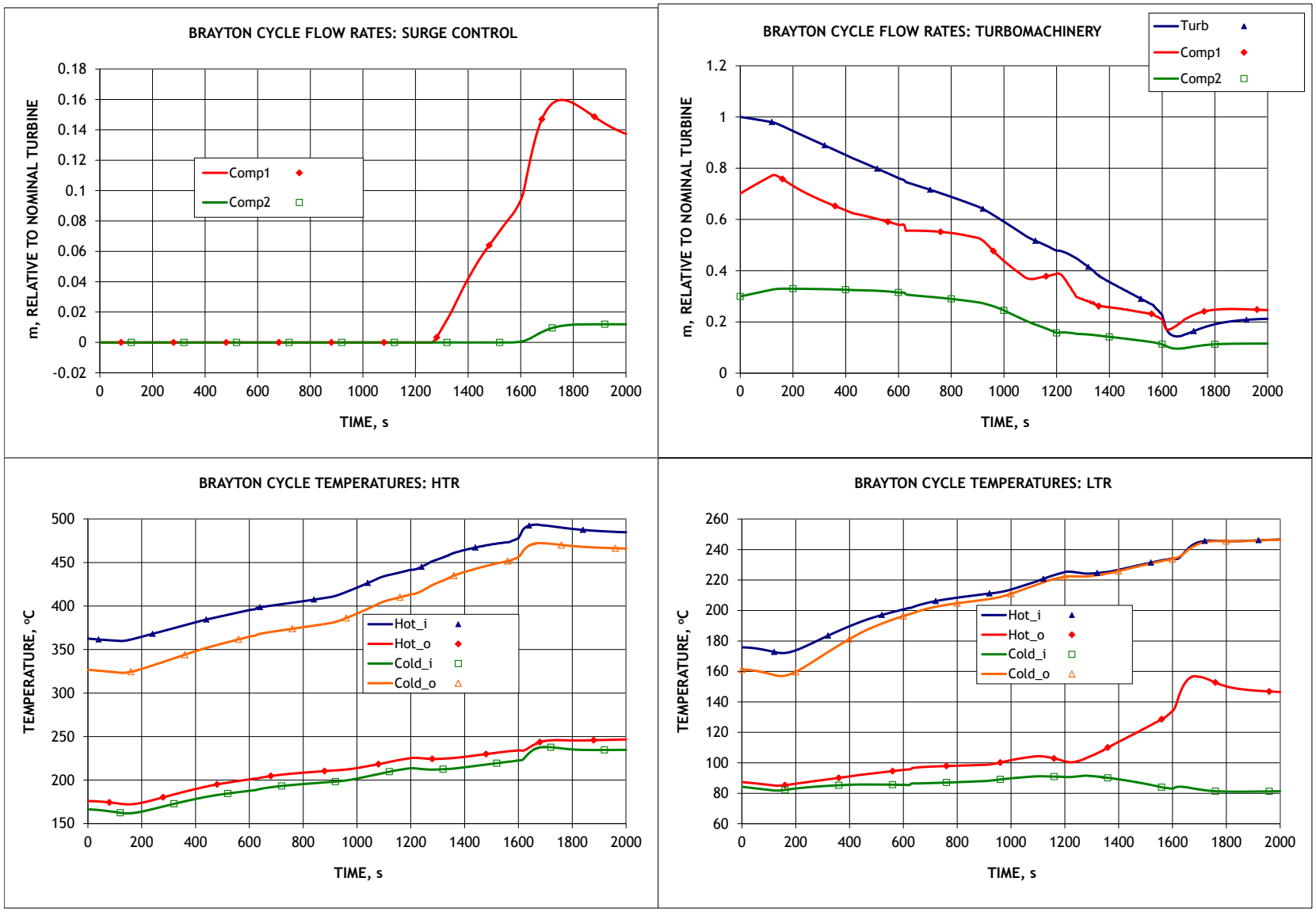

Figure 3-3. Cycle Operation at Low Reactor Power. (Continued)

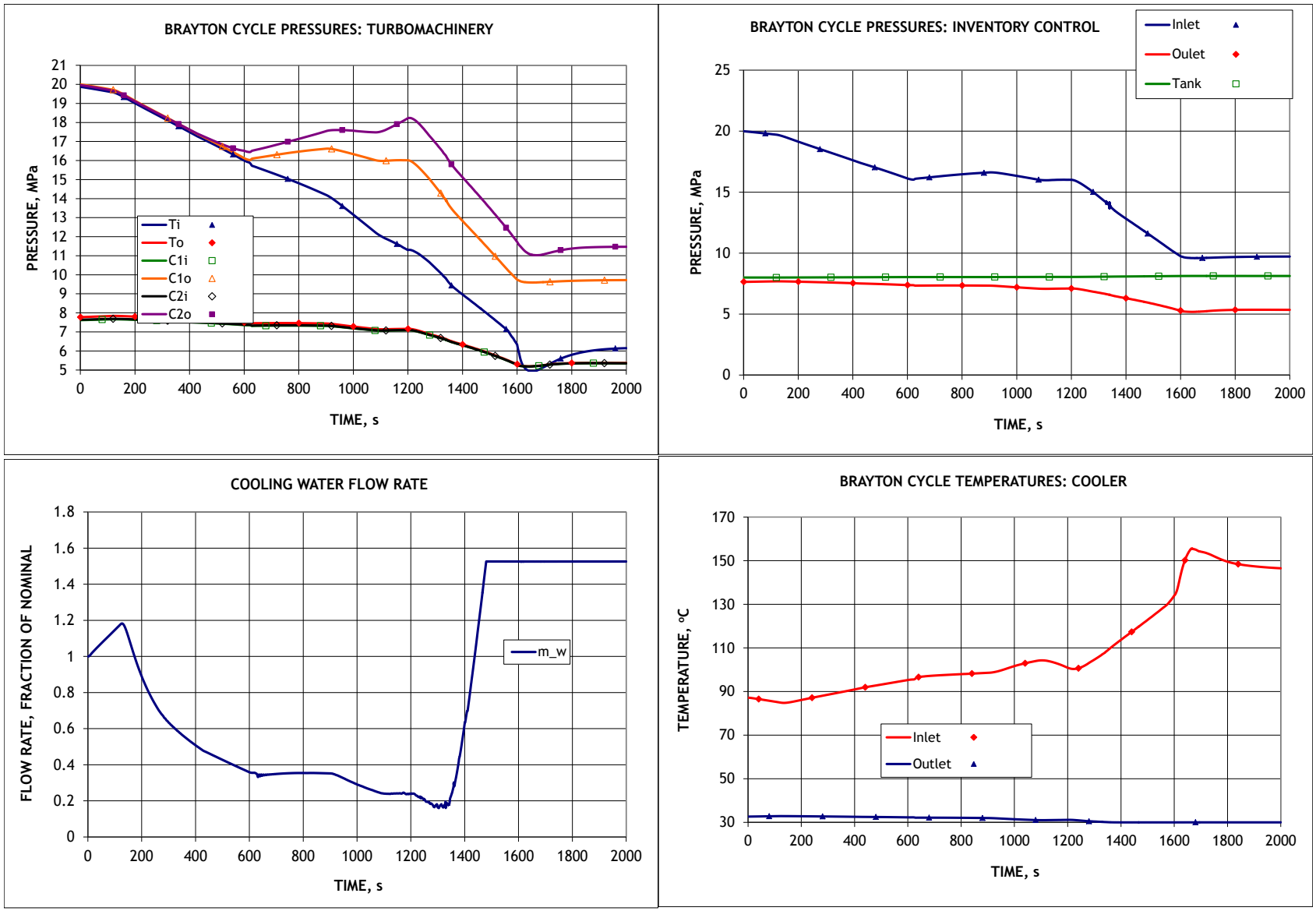

Figure 3-3. Cycle Operation at Low Reactor Power. (Continued)

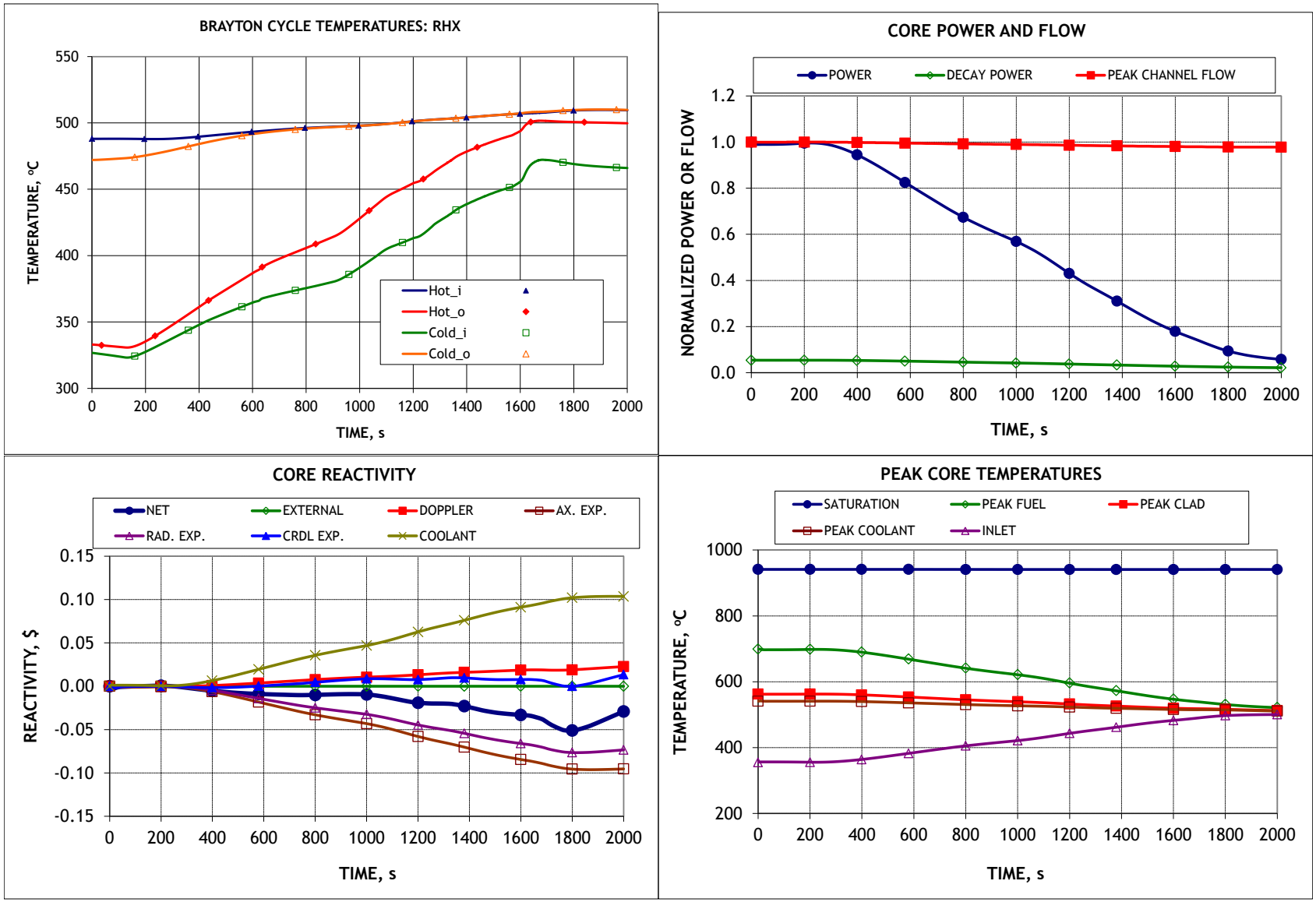

Figure 3-3. Cycle Operation at Low Reactor Power. (Finished)

3.3 Thermal Transients for the Sodium-to-CO_2 HX

Recent PDC modifications, including the coupling to the SAS4A/SASSYS-1 code, updated negative flow treatment, and the updated RHX solution allow the analysis of transients which couldn't be simulated previously. Those transients involve rapidly changing conditions around the heat exchangers. Such transients, which under severe rates of change can potentially result in thermal shock, are important in providing temperature rate of change information for heat exchanger design. This information has not been used in previous designs mostly because there was no analytical tool to provide such information. The coupled PDC-SAS4A/SASSYS-1 code offers such a capability.

Among all the heat exchangers in a plant, those that couple two sufficiently different systems are most likely to experience thermal shocking. In a system involving a sodium-cooled reactor with a S-CO_2 cycle, an example of such an interfacing heat exchanger would be an intermediate Na-to-CO_2 heat exchanger. There could be situations, either during normal operation or in accidents, when the conditions on one side would be different from those on another. An example of such situation would be a failure of an intermediate sodium pump while the S-CO_2 cycle continues to operate as normal. Such events could introduce significant thermal transients in the heat exchanger. These transients would be the most severe in the heat exchangers coupling two independent systems, such as a Na-CO_2 HX. For comparison, in case of the S-CO_2 cycle recuperators, the flow on both sides is provided by the same compressor, such that the flow on one side couldn't be stopped without affecting the flow on the other side.

For these reasons, for the first round of a thermal shock study, dynamics calculations of possible thermal transients for the Na-CO_2 heat exchanger using the combined PDC and SAS4A/SASSYS-1 codes were carried out. The focus is on finding accident conditions which provide the fastest rate of the heat exchanger wall temperature change. Two types of transients, "up transients" and "down transients," are investigated.

In up transients, the wall is heated up following the reduced heat removal capability by the CO_2 flow. That reduction in the heat removal rate can be caused by a decreased or completely lost CO_2 flow through the heat exchanger. The CO_2 flow can be affected, for example, in the case of a CO_2 pipe break at the HX inlet. The CO_2 pipe break event was simulated with a couple of break sizes. The results for the case of 25 cm equivalent diameter break are shown in Figure 3-4 (in the assumed design, there are four parallel CO_2 pipes leading to the HX each with a 1 m inner diameter). The first graph in Figure 3-4, as well as in all further figures in this section, shows the change of the wall temperature with time for several axial locations (5 axial nodes are assumed in this simulation). The second graph shows the time derivative of the wall temperature change at the same locations. As demonstrated in Figure 3-4, a pipe break on CO_2 side leads to a quick reduction in both the CO_2 pressure and its flow rate. As a result, the heat removal capability by the CO_2 side is reduced and the entire heat exchanger is heated up. The

maximum heatup rate for this transient is about +3.5 °C/s.

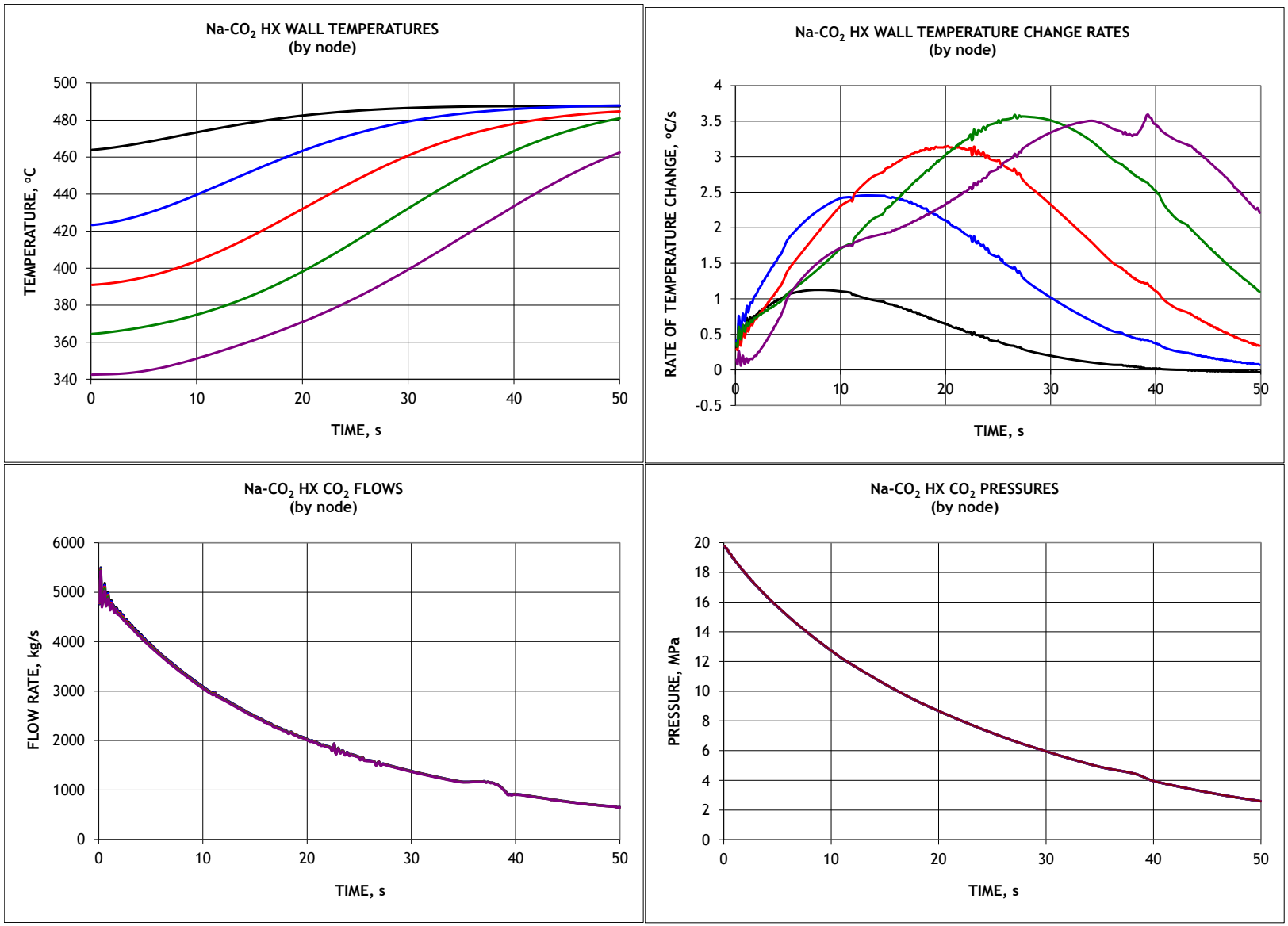

Figure 3-4. Na-CO_2 HX Thermal Transient for 25 cm CO_2 Pipe Break.

Another simulation was carried out with a larger pipe break. Figure 3-5 shows the results for a 1 m break (the size of one of the four pipes leading to the HX). The transient is much faster than the previous one. The maximum wall temperature change rate of about +14 °C/s is calculated for this large pipe break. However, that high rate lasts only a fraction of a second as the cycle is almost completely evacuated of CO_2 in less than 8 s. During this short time, the HX wall temperature changes by 20 °C at most. Also, the results of the CO_2 flow rate calculations show oscillating behavior which is most likely a result of the numerical solution scheme and/or specification of insufficient accuracy.

In addition to the pipe break, an event involving sudden HX bypass line valve opening was simulated. The results of this transient (Figure 3-6) are similar to the 25 cm pipe break case. The maximum rate of wall temperature change is +5 °C/s in this case. Note that there is a drop in the CO_2 side pressure which is caused by CO_2 cooling in the system as a result of most of the CO_2 flow bypassing the Na-CO_2 HX.

In addition to those CO_2 flow reduction transients, an idealized accident was simulated in which heat flow to the CO_2 side is artificially turned off at time t=0. This idealized loss of heat removal by the CO_2 side would bound most of the other up transients for the Na-CO_2 HX. The results for this transient, shown in Figure 3-7, indicate that the maximum rate is +7 °C/s; the rate remains above +5 °C/s for 5-10 seconds.

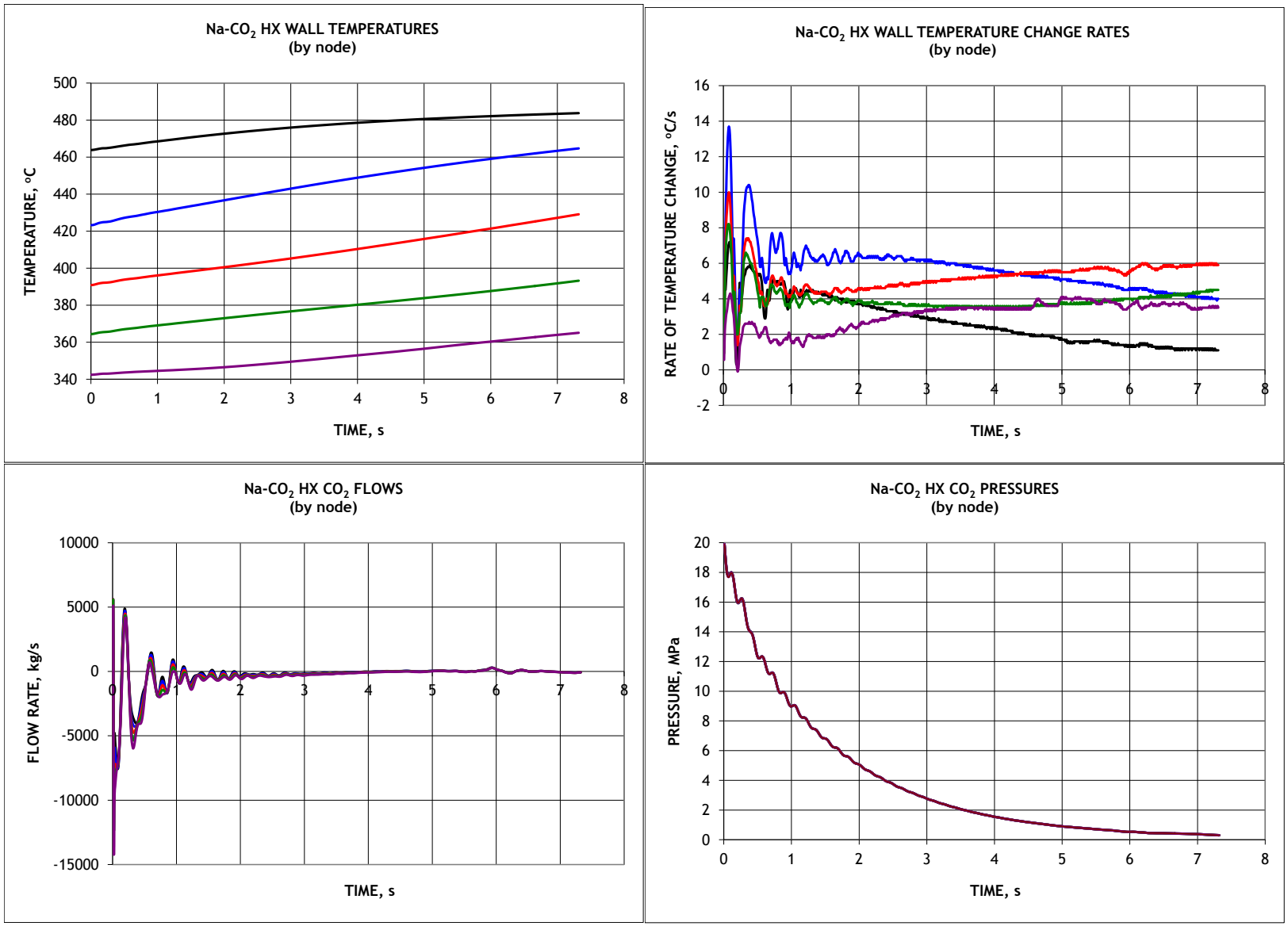

Figure 3-5. Na-CO_2 HX Thermal Transient for 1 m CO_2 Pipe Break.

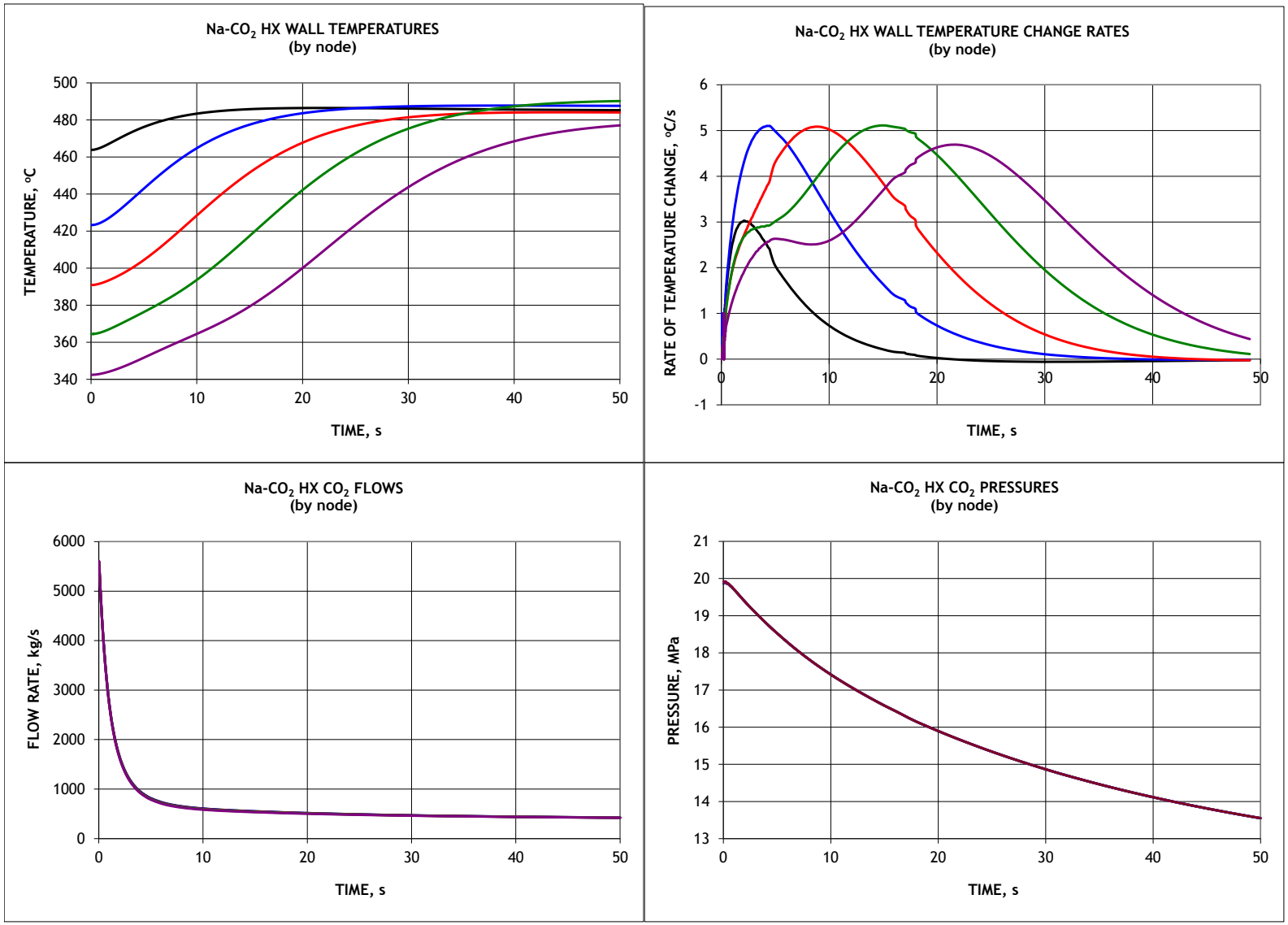

Figure 3-6. Na-CO_2 HX Thermal Transient for HX Bypass Valve Opening.

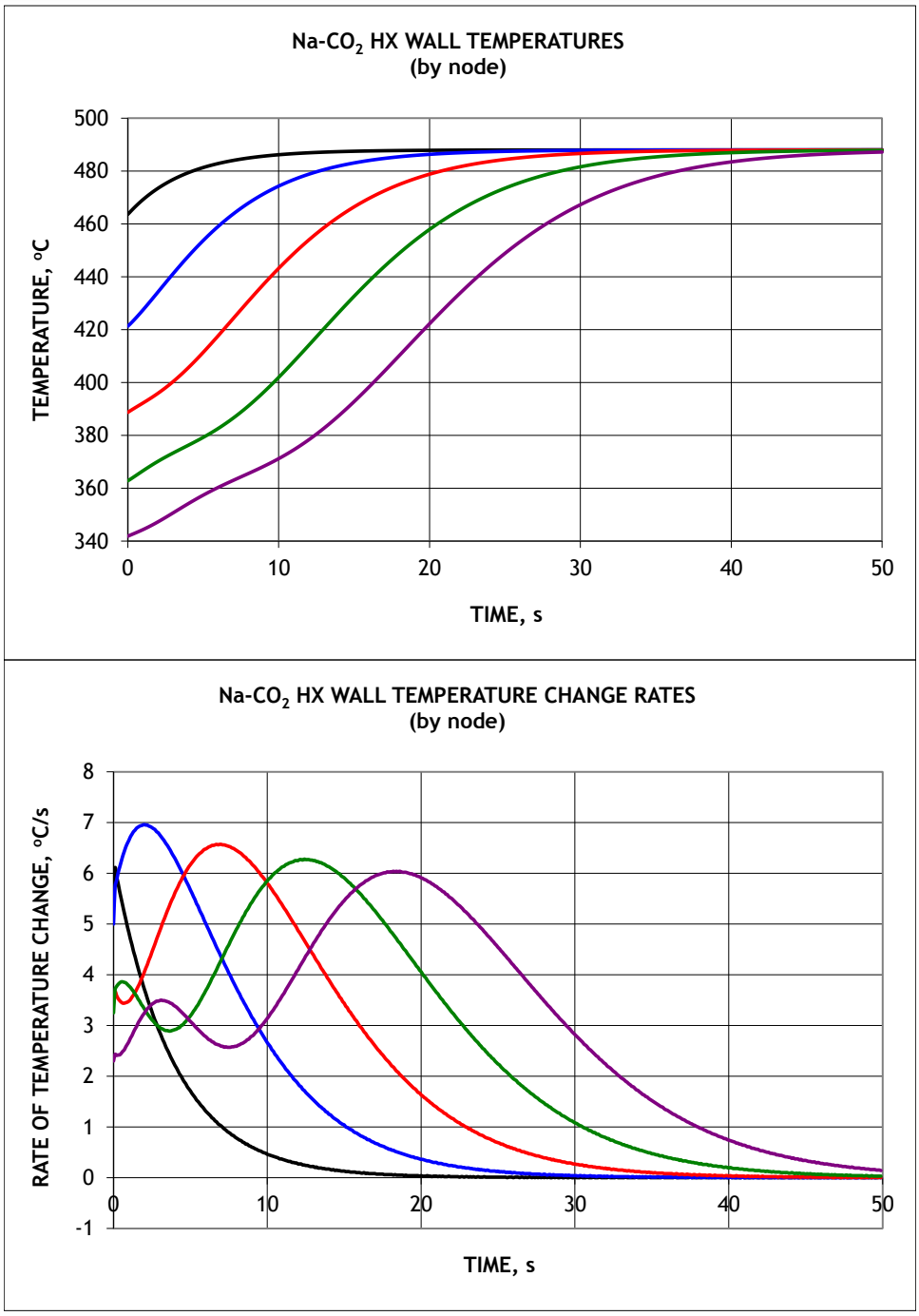

Figure 3-7. Na-CO_2 HX Thermal Transient for Idealized Loss-of-CO_2 Side Heat Removal.

For down transients, two events which would reduce the HX wall temperature were simulated. The first one was a sudden stopping of the intermediate sodium pumps. The results of this simulation are shown in Figure 3-8. The maximum wall temperature change is calculated to be about -7 °C/s and it remains more negative than -5 °C/s for about 8 s.

The second down transient was the loss of electric power to the primary sodium pumps with simultaneous reactor scram. In this event, there is a time delay for the "cold" front to reach the Na-CO_2 HX, as indicated in Figure 3-9. Also, the magnitude of the maximum rate of temperature change is much smaller than in the other down transient, at about -1.6 °C/s.

Overall, the simulation of thermal shock transients for the Na-CO_2 HX shows that the rate of the wall temperature change for more or less realistic conditions is limited by ±7 °C/s for 10 seconds. Considering that the analyzed conditions were selected to represent the most severe transients, this rate of temperature change is rather small. This is a direct consequence of using Printed Circuit Heat Exchangers for the Na-CO_2 HX with its large stainless steel mass. Nevertheless, this possible rate of wall temperature change must be taken into account in future heat exchanger designs.

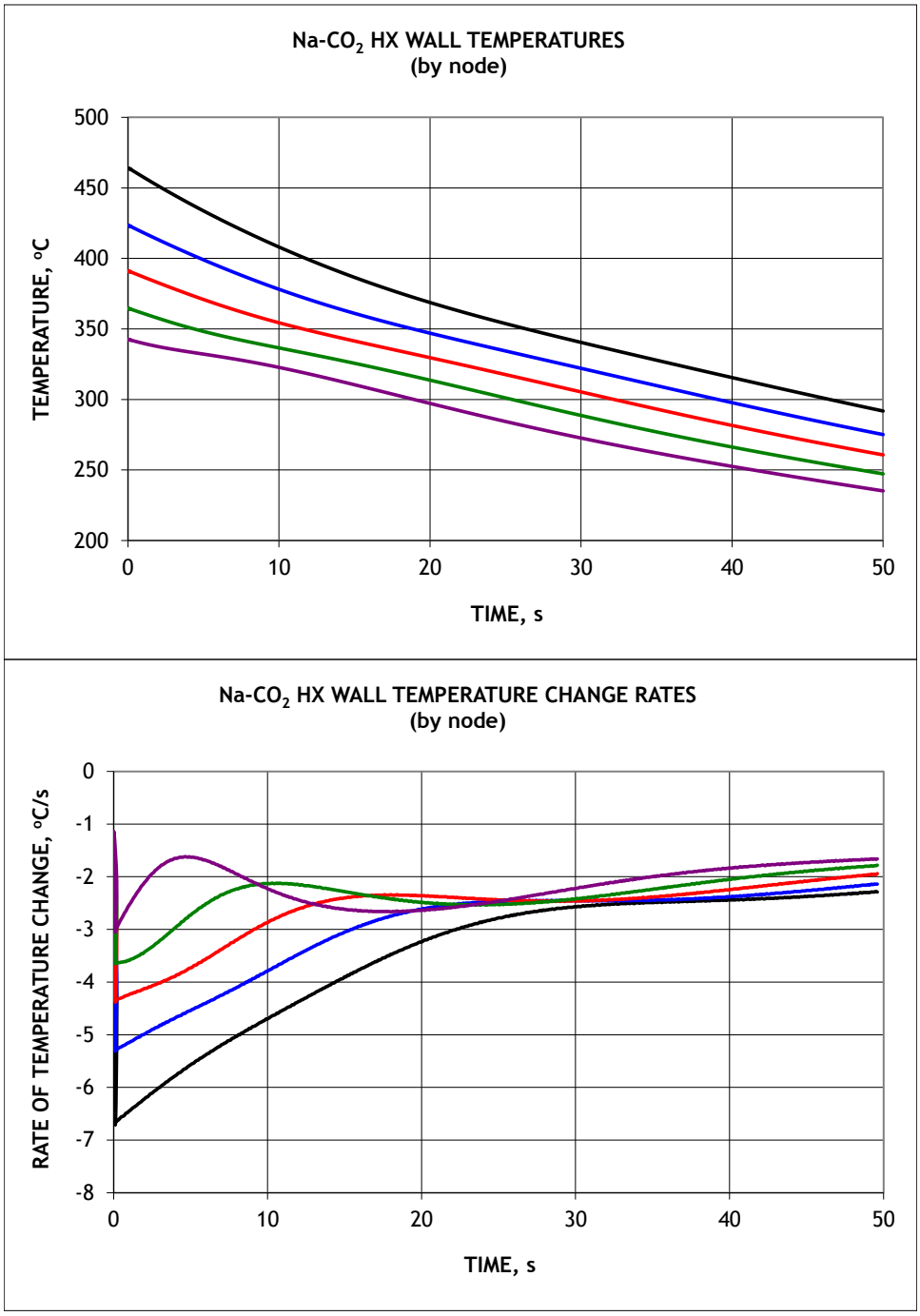

Figure 3-8. Na-CO_2 HX Thermal Transient for Loss of Intermediate Sodium Pump.

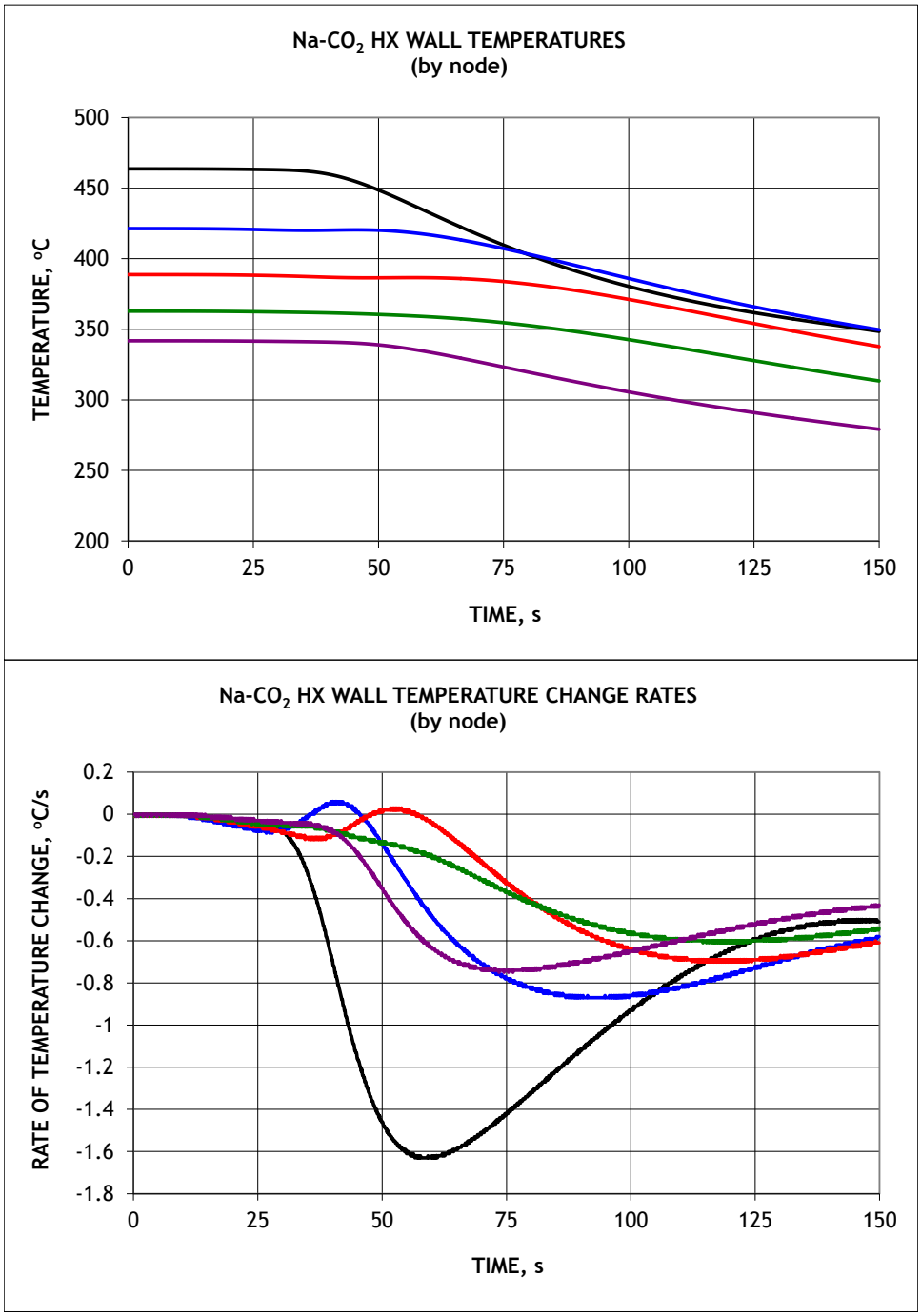

Figure 3-9. Na-CO_2 HX Thermal Transient for Reactor Scram with Primary Sodium Pump Trip.

4 Modeling of the Sandia S-CO_2 Loop with the Plant Dynamics Code

To validate the ANL Plant Dynamics Code (PDC), the modeling of the small-scale S-CO_2 loop assembled by Barber-Nichols, Inc. for Sandia National Laboratories (referred to as the "SNL S-CO_2 Loop" further in this document) has been initiated. The SNL S-CO_2 Loop is under ongoing phased construction during which additional components are incrementally installed. The ultimate future layout of the loop is shown in Figure 4-1 along with the design point conditions [6].

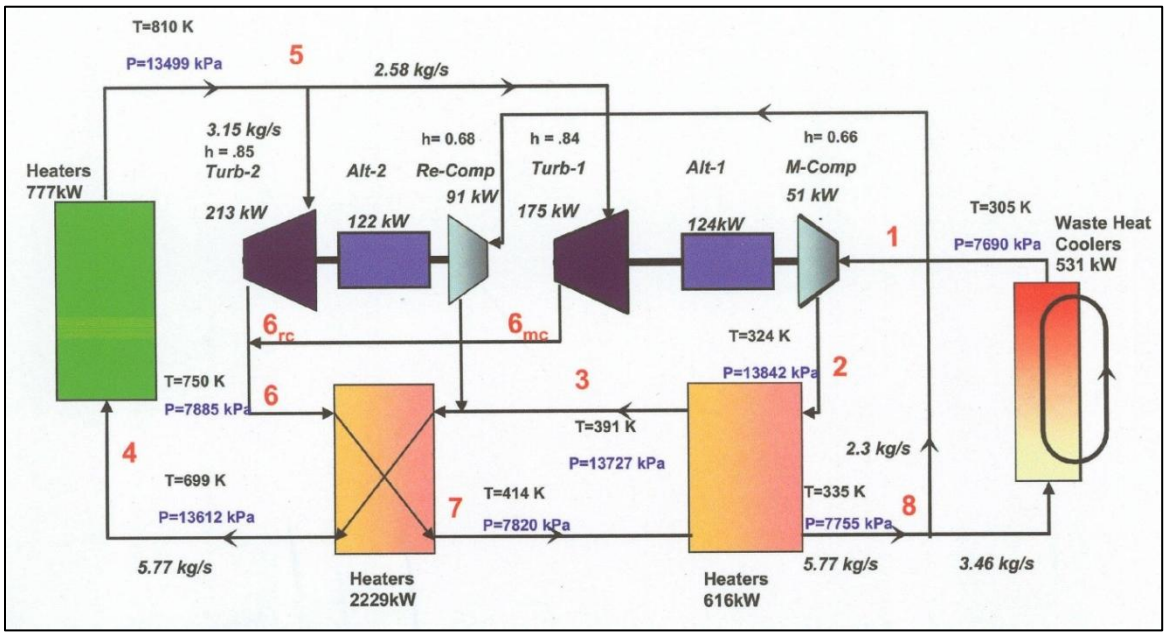

Figure 4-1. Projected Layout of the SNL S-CO_2 Loop.

Because the ultimate configuration of the loop is yet to be assembled following its future relocation from Barber-Nichols Inc. to SNL, experimental data for the entire recuperated S-CO_2 cycle with the ultimate heating capability shown in Figure 4-1 is not available yet. For the current loop modeling activity, only experimental data for an earlier phase of development of the loop was available. That partial loop configuration does not include the second Turbine-Alternator-Compressor (TAC) unit as well as the high temperature recuperator (Turb-2, Alt-2, Re-Comp, and Heaters 2229 kW in Figure 4-1).

4.1 Experimental Data

The configuration of the SNL S-CO_2 Loop modeled with the PDC is shown in Figure 4-2. That figure also shows the conditions (pressures and temperatures) at time 3200 s into the run 1041 of 12/01/2010. These particular conditions are selected for modeling for two reasons. First, as demonstrated in the example of experimental data in Figure 4-3,

they are achieved at the end of relatively steady operation at constant external, i.e. control, conditions. Such operation helps to achieve conditions close to steady-state (although true steady-state conditions were never achieved as shown in Figure 4-3). Second, unlike other quasi-static conditions, such as at 4500 s and 6100 s, the temperatures at 3200 s are maintained at supercritical level throughout the entire loop, which assures single-phase conditions everywhere and eliminates possible convergence problems with the analysis if the conditions are too close to the critical point.

During the analysis of the experimental data, some concerns were noted regarding the as-recorded experimental conditions (temperatures and pressures) in Figure 4-2. First, the pressure sensors around the low-temperature recuperator (LTR) do not show meaningful data. Similarly, the water pressure at the cooler inlet is too low, even below the outlet pressure. Those readings were ignored in the modeling. Second, there are some non-trivial changes in the conditions in pipes. Most of such changes can probably be attributed to not reaching the true steady-state conditions, such that the heat transfer between the CO_2 and pipes is significant. However, at the low-temperature side of the loop (around the compressor and cooler), the specific heat of CO_2 is large due to the proximity to the critical point such that even a small temperature change requires a significant amount of heat transfer. Thus, it is more likely that the difference in measured temperatures and pressures are caused by the measurement uncertainty, which is ±0.02 MPa for pressure and ±0.2 °C for temperature [7]. Still, in some instances, the difference cannot be explained by the experimental error alone. For example, the pressure in the pipe between the cooler and the compressor *increases* from 7.702 MPa to 7.763 MPa. Even without consideration of the pressure drop, the pressure rise (0.06 MPa) exceeds the measurement uncertainty by about three times. Consequently, in the current modeling, the pressure at the compressor inlet was ignored (see compressor modeling section below for more details).

The second significant concern is the non-conservation of energy in or around the turbine. According to the conditions in Figure 4-2, the entropy is *decreasing* in the turbine, as demonstrated in Table 4-1. Thus, if the conditions in Figure 4-2 really reflect the turbine inlet and outlet conditions, the turbine isotropic efficiency would greater than 100%, which is impossible. That discrepancy can only be explained by heat loss either in turbine itself or in the pipes between the turbine and the temperature sensor locations. Unfortunately, no measurements were taken to differentiate between the head transfer in the turbine and the heat loss (calculating the heat balance in the turbine based on measured TAC power involves the windage loss in all of the turbine, compressor, and alternator components which introduces another uncertainty because windage loss is significant and comparable to the net TAC power). Because of that heat loss, the validation of the turbine model cannot be effectively performed with the experimental data; only outlet pressure can be compared meaningfully with the experimental data. In addition, special provisions were taken in the steady-state cycle modeling to account for this heat loss in order to satisfy the energy conservation law, as described in the cycle modeling section below.

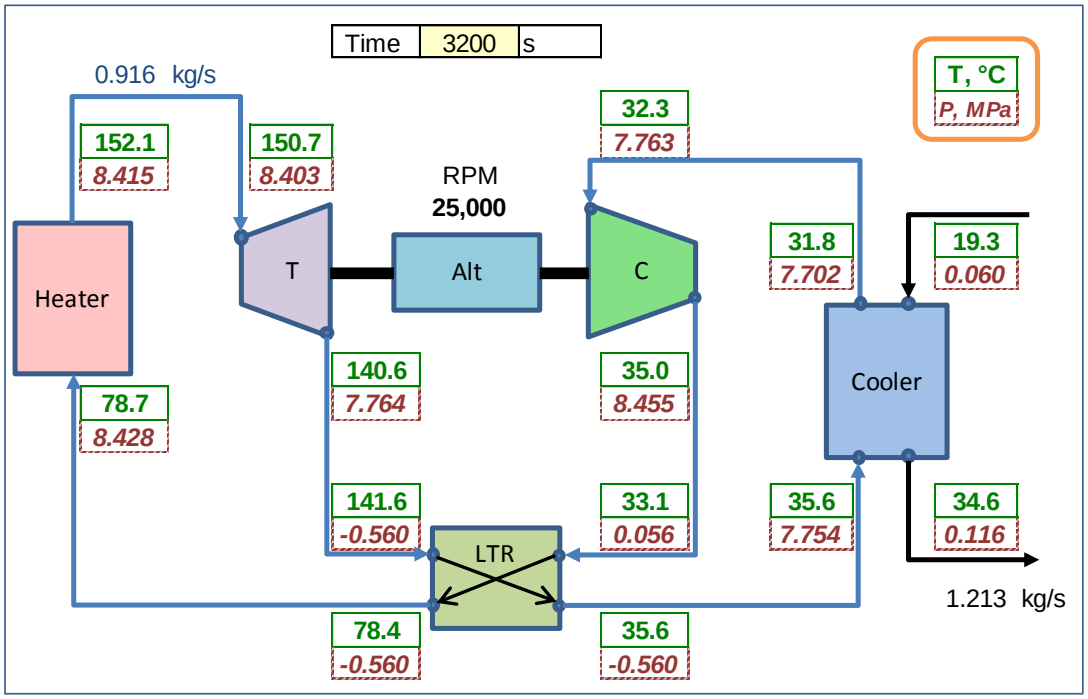

Figure 4-2. Modeled SNL S-CO_2 Loop Configuration and Experimental Data at 3200 s.

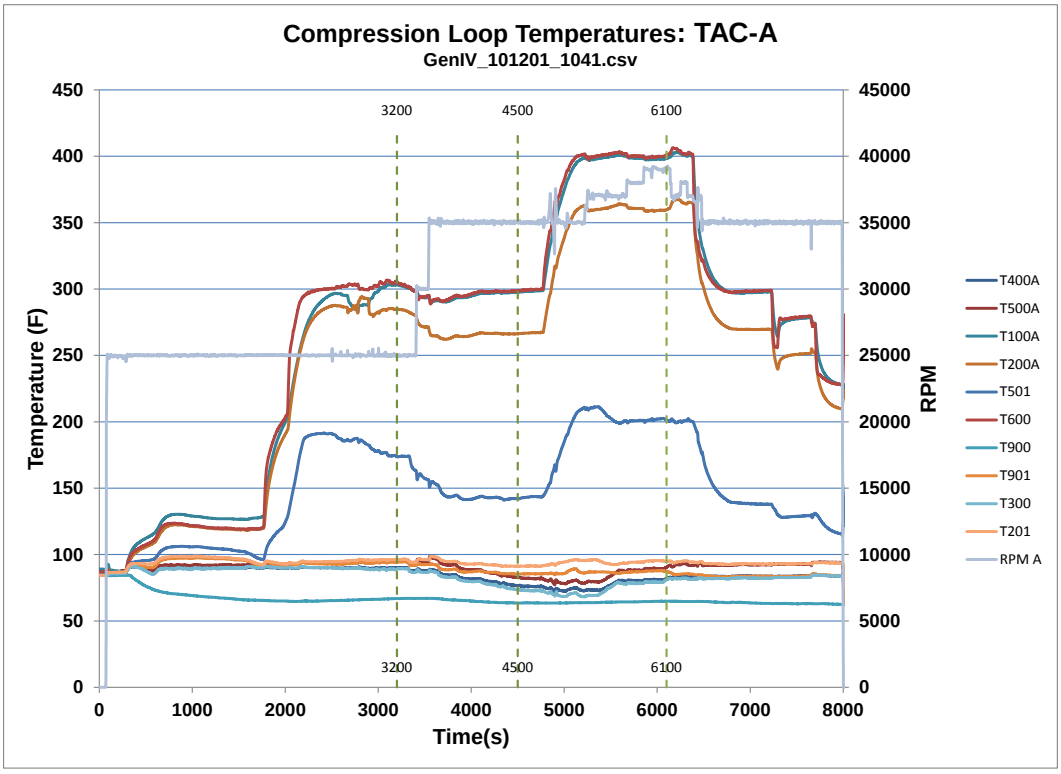

Figure 4-3. Example of Experimental Data for Run 1041.

Table 4-1. CO_2 Properties for Experimental Conditions around the Turbine

	Turbine Inlet	Turbine Outlet
Temperature, °C	150.7	140.6
Pressure, MPa	8.403	7.764
Enthalpy, kJ/kg	74.00	65.25
Entropy, kJ/kg-K	-588.46	-596.21

Even though the heat loss cannot be measured due to the lack of suitable instrumentation, it can be estimated based on an assumed value of the turbine efficiency. The isentropic expansion from the turbine inlet conditions in Table 4-1 to 7.764 MPa results in outlet temperature of 143.3 °C and enthalpy of 68.46 kJ/kg. Further calculations have shown that the turbine efficiency is around 90% based on static conditions (see turbine modeling section below). With this efficiency, the outlet enthalpy becomes:

$$\varepsilon_{S-S} = \frac{h_{in} - h_{out}}{h_{in} - h_{s,out}}$$

$$h_{out} = h_{in} - \varepsilon_{S-S}\left(h_{in} - h_{s,out}\right) = 69.01 \text{ kJ/kg}$$

Those enthalpy and outlet pressure correspond to turbine outlet temperature of 143.8 °C. The heat balance then is following:

$$Q_{Turbine} = \dot{m}(h_{in} - h_{out}) = 4.57 \text{ kW}$$

$$Q_{Heat\ Loss} = \dot{m}\left(h_{out} - h_{out,exp}\right) = 3.44 \text{ kW}$$

where $h_{out,exp}$ is the experimental value of turbine outlet enthalpy in Table 4-1 (65.25 kJ/kg).

This quick estimate demonstrates that the heat loss in the turbine and/or surrounding pipes is significant and is comparable to the heat (work) transfer in the turbine itself.

Although the experimental conditions at 3200 s (Figure 4-2) are selected for the analysis with the PDC for the reasons described above, the conditions at other quasi-static points in Figure 4-3 are still useful for some component model validation. For example, those conditions were used for the turbine model validation since the pressures and temperatures around the turbine remain well above the critical point. The experimental conditions at 4500 and 6100 s are shown in Figure 4-4.

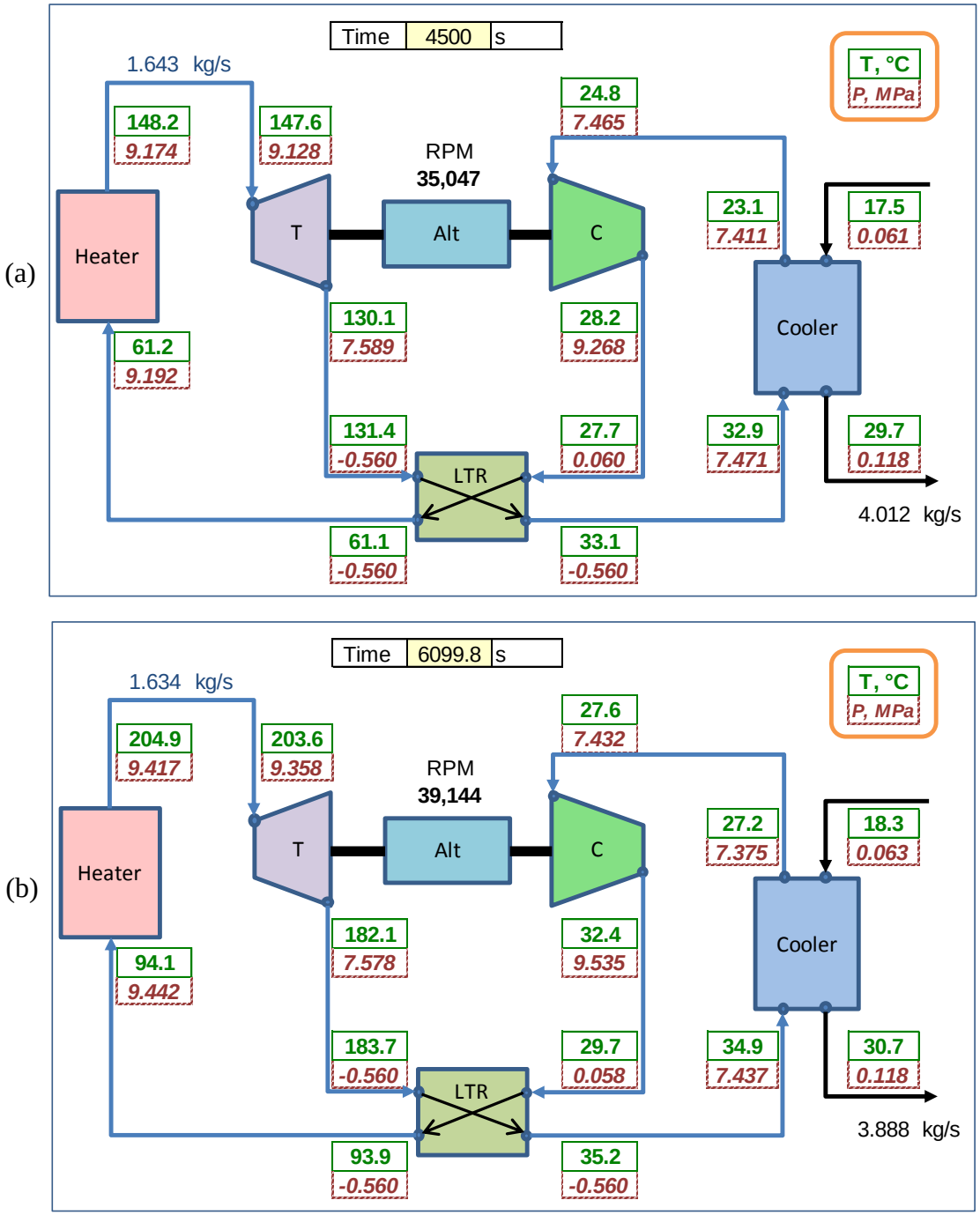

Figure 4-4. Experimental Conditions at 4500 s (a) and 6100 s (b).

4.2 Individual Component Models

In order to simulate the performance of the entire loop, the models for each component should first be developed. The description of those models is provided below along with the comparison of the predicted performance of each component with the experimental data.

4.2.1 Recuperator

The (low-temperature) recuperator (LTR) in SNL S-CO_2 Loop is a Printed Circuit Heat Exchanger™ (PCHE™) manufactured by Heatric. The internal configuration of this PCHE is Heatric's proprietary information and is not available for modeling. The only available parameters of the LTR are:

- External dimensions: 0.53 m length (including internal headers), 0.345 m width, and 0.221 m height
- HX configuration: platelet
- Heat transfer area: 41.88 m^2 [8]
- Hydraulic diameter: 0.5 mm [8]
- Flow area: 0.0018 m^2 [8].

The rest of the LTR design parameters and dimensions, including the channel diameter and pitch, channel zigzag angle, internal header length, plate thickness, etc., had to be guessed either on the available information or predicted performance.

The modeling of the LTR is carried out with the same heat exchanger performance model in PDC used in previous analysis of PCHEs, including the ANL PCHE tests [9]. First, the predicted LTR performance was compared against the Heatric design specifications. The design specifications are available for two sets of the conditions – one for completed loop in Figure 4-1 with different flow rates on two sides (Design Condition 1) and one with the same flow rate (Design Condition 2).

The comparison of the PCHE model predictions with either the design conditions or experimental data is provided in Table 4-2. In this and other similar tables in this chapter, two lines are shown for each set of conditions. The first line refers to either design specifications (D) or experimental data (E). The second line shows the results obtained from the model (M). The input data for model calculations is shown in the first few columns and is exactly the same as the experimental or design conditions. In case of the LTR, those data include the inlet pressures, temperatures, and flow rates for both sides.

The first two lines in Table 4-2 show the comparison of model prediction with the Heatric's design calculations. Those two design conditions were used to implement minor adjustment of the unavailable design parameters, such as channel zigzag angle. Overall, very good agreement is achieved in both design cases.

The next two lines show the results of comparison of model predictions with the experimental data at two selected times in run 1041. Overall, good agreement is achieved on temperatures even though the experimental conditions were not truly steady-state (as assumed in the model). However, the model significantly underpredicts the pressure drop for all cases. Note that the pressure drop was not directly measured in the experiment. The values in Table 4-2 were obtained as a difference in the measured absolute pressures. With the stated accuracy of measuring the absolute pressure of ±0.02 MPa (±20 kPa), the uncertainty of such difference becomes ±28 kPa, which in some cases, such as at 3200 s case, exceed the measured value. Moreover, as pointed out above for Figure 4-2, the pressure readings immediately adjacent to the LTR were not available such that the pressures at neighboring components had to be used for Table 4-2. As such, the resulting pressure drop in Table 4-2 on the experimental side will include two pipes on each side. For these reasons, no conclusion can be drawn on the model's ability to predict pressure drops for the experimental conditions. The adequacy of such predictions will be evaluated below in the cycle analysis section when pipe pressure drops are evaluated. Still, based on the fact that much better agreement is achieved for the design conditions, it is judged that the model predictions have adequate accuracy.

Table 4-2. Heat Exchanger Model Performance Prediction for LTR

	Input						Output				
	T_{hot_in}, °C	m_{hot}, kg/s	p_{hot_in}, MPa	T_{cold_in}, °C	m_{cold}, kg/s	p_{cold_in}, MPa		T_{hot_out}, °C	T_{cold_out}, °C	Δp_{hot}, kPa	Δp_{cold}, kPa
Design Condition 1	139.7	5.761	7.798	51.8	3.447	13.741	**D**	**61.8**	**116.6**	**128.9**	**97.2**
							M	**60.6**	**119.3**	**115.7**	**92.1**
Design Condition 2	447.8	3.447	7.798	49.7	3.447	13.741	**D**	**57.2**	**339.3**	**75.8**	**128.9**
							M	**57.5**	**338.8**	**74.0**	**125**
Test at 3200 s	141.6	0.915	7.763	35.0	0.915	8.455	**E**	**35.6**	**78.7**	**9.653**	**26.89**
							M	**35.9**	**84.8**	**4.096**	**10.35**
Test at 7233.8 s	133.3	1.403	7.166	33.5	1.403	8.585	**E**	**34.0**	**58.6**	**82.7**	**60.7**
							M	**34.4**	**61.9**	**9.06**	**18.07**
Test at 3200 s, adjusted*	141.6	0.915	7.763	35	0.915	8.455	**E**	**35.6**	**78.7**	**9.653**	**26.89**
							M	**36.6**	**81.4**	**3.447**	**8.437**

*Header length and fin efficiency were adjusted to match the experimental performance

The last line in Table 4-2 shows the results of the model predictions for the same experimental conditions as in the third line. This time some minor adjustments to the model were made to better predict the outlet temperature on the cold side. Note that with these adjustments, the prediction of the outlet temperature on the cold side is worse than

before. However, as it will be discussed in the cycle modeling sections, predicting the cold side outlet temperature is much more important for the cycle analysis since this temperature is used to calculate the CO_2 flow rate through the heaters and, therefore, for the entire loop. Because of that, the slightly adjusted LTR design was used in the cycle analysis below.

Additional information on the LTR dimensions is provided in Appendix A. The results of the performance at simulated cycle conditions are given in Appendix B along with other components and results.

4.2.2 Cooler

The modeling of the cooler is very similar to that of LTR described above. There is only one significant difference. The cooler design has a Z/I configuration of the plates (rather than platelet) with headers located outside of the HX block. While improvements were made recently to the steady-state ANL PCHE model to allow the treatment of the cross-flow region in the Z/I configuration, those changes were not applied to the dynamics part of the code yet. Therefore, for the SNL S-CO_2 loop cooler analysis with the PDC, first a model of a Z/I PCHE was developed and later an equivalent platelet configuration was derived. That equivalent configuration is based on the same dimensions of the channels, but assumes that the headers are located inside the HX block. Also, some minor adjustments were made to account for the cross-flow region in the cooler, which is not modeled with the platelet model.

The results of the PCHE model predictions for the cooler are provided in Table 4-3. The model prediction results are shown for both the Z/I configuration, “M (Z/I)” line, and equivalent platelet configuration, “M (Pl)” line. Since the dynamics model currently only supports the platelet configuration, further results in this report are obtained using this configuration for the cooler model. Again, very good agreement is achieved on temperatures.

The cooler model results in Table 4-3 were obtained based on an assumption of water flow on the cold side. In reality, the SNL S-CO_2 Loop utilizes a water/glycol mixture for cooling. The properties for this mixture are not programmed in the PDC code, but its properties are close to those of pure water, as confirmed by the results in Table 4-3. The only significant difference is the overprediction of the pressure drop on the cooler side, which does not affect the results of the S-CO_2 cycle calculations. Also, as discussed above, the experimental value for the cooling side pressure drop is not available.

Additional information on the cooler dimensions is provided in Appendix A. The results of the performance at simulated cycle conditions are given in Appendix B along with other components and results.

Table 4-3. Heat Exchanger Model Performance Predictions for Cooler

	Input						Output				
	T_{hot_in}, °C	m_{hot}, kg/s	p_{hot_in}, MPa	T_{cold_in}, °C	m_{cold}, kg/s	p_{cold_in}, MPa		T_{hot_out}, °C	T_{cold_out}, °C	Δp_{hot}, kPa	Δp_{cold}, kPa
Design Condition	61.8	3.506	7.755	18.9	15.74	0.521	**D**	**32.2**	**27.9**	**76**	**207**
							M (Z/I)	31.6	27.8	35.8	466.9
							M (Pl)	**32.0**	**27.6**	**33.4**	**466.9**
Test at 3200 s	35.6	0.915	7.702	19.338	1.213	0.116	**E**	**31.79**	**34.58**	**51.71**	**N/A**
							M (Z/I)	32.15	34.18	3.514	6.874
							M (Pl)	**32.1**	**34.33**	**3.36**	**6.888**

4.2.3 Heaters

The SNL S-CO_2 Loop uses electrical heaters to deliver the heat to the cycle. Electrical heaters are not modeled in the ANL PDC code. Rather than introducing the electrical heater model to the code, an attempt was made to simulate the electrical heaters with a shell-and-tube heat exchanger (S&T HX) with CO_2 flowing on the shell side. The tube outer diameter is exactly equal to that of the heaters. Since the current SNL S-CO_2 Loop configuration analyzed here employs two heaters in series, the tube length of the S&T HX is assumed to be twice the electrical element heated length. The tube pitch-to-diameter ratio was selected to conserve the hydraulic diameter on the CO_2 side. The shell diameter is selected to conserve the number of heater elements (tubes). No fins on the CO_2 side of the tubes are modeled. Additional information on the heater dimensions (as modeled as RHX) is provided in Appendix A.

The tube wall thickness was arbitrary selected to be 0.5 mm. To simulate the electrical heating with S&T HX, hot sodium was assumed inside the tubes. The sodium inlet temperature is selected as described below. It is assumed that the sodium temperature change in the heater is 10 °C to simulate approximately the constant temperature of the heating elements. The sodium flow rate is calculated in the code from the input value for the amount of heat delivered to the cycle.

The sodium inlet temperature is selected to conserve CO_2 outlet temperature and flow rate given its inlet temperature. For given inlet temperatures on both sides, sodium flow rate, and its outlet temperature, the CO_2 outlet temperature and CO_2 flow rate are uniquely defined from the overall heat transfer coefficient of the heat exchanger and conservation of energy. That property is used in the PDC to calculate the CO_2 flow rate in the HX and in the entire cycle. This part of the code was used to select the sodium inlet temperature in order to match the measured experimental performance of the heaters at several experimental conditions. Table 4-4 shows the results of the calculation of the sodium side inlet temperature for several conditions. Again, the inlet temperature was

selected to preserve the CO_2 outlet temperature. The sodium temperature varies between the different conditions which is consistent with the experimental measurements of the heater temperature. Note that the sodium temperature represents the bulk fluid temperature inside the tube while the experimental heater temperature represents the surface temperature of heated elements.

The results of the heater RHX performance at simulated cycle conditions are given in Appendix B along with other components and results.

Table 4-4. Selection of Hot Side Temperatures for Heater

Experiment			Model	
Time	T_{heater}, °C	Q_{CO2}, kW	T_{Na_in}, °C	T_{Na_out}, °C
3200	170.3	88.85	**197**	**187**
4500	174.0	215.89	**217.5**	**207.5**
6099.8	240.2	229.4	**279**	**269**

4.2.4 Compressor

The compressor model of the PDC has been already verified against the BNI/SNL experimental data [10,11]. Since the SNL S-CO_2 Loop uses the same compressor as the BNI/SNL loop, no further compressor model development and/or model validation is needed at this time.

However, as it was discussed in Section 4.1 above, reviewing the experimental data for the entire loop highlighted some possible problems with the experimental data. In particular, Figure 4-2 demonstrates that the measured compressor-inlet pressure is higher than the cooler-outlet pressure, which is not realistic. Although it is not clear whether a similar measurement uncertainty was present in earlier BNI/SNL experimental setups, such pressure measurement inaccuracy will definitely affect the outcome of the compressor model performance when compared to the current experimental data. In order to evaluate the effect of this pressure measurement uncertainty on the compressor performance, an analysis was carried out in which various compressor-inlet conditions were applied to the compressor performance model. The results of such a sensitivity analysis are shown in Table 4-5. In that table, points 300 and 400A refer to the measured cooler outlet and compressor inlet conditions, respectively; P and T are the pressure and temperatures at those points. Note that the model predictions in Table 4-5 are shown in two lines for each case: one for total conditions (M - Total) and the other for static conditions (M - Static). The difference between those two cases is the dynamic head presented by the fluid velocity at the compressor outlet. If the measurements were done precisely at the compressor (diffuser) outlet, then the pressure and temperature sensors

would measure the total conditions. On the other hand, if the measurements were done far away from the compressor (assuming no external losses), the dynamic head from the compressor outlet would be lost and the sensors would indicate static conditions (assuming that the flow speed in the pipes is smaller than at the diffuser outlet). Since the actual measurements are done in the pipe close to, but not exactly at, the compressor-outlet, it is very difficult to predict what part of the dynamic head is lost by that point. So, the measured conditions would be somewhere between the total and static conditions at the compressor-outlet. For these reasons, Table 4-5 lists both total and static conditions obtained from the compressor model. Note, however, that the difference between the total and static pressures and temperatures is not great for these experimental conditions. Also note that the PDC cycle performance model conservatively assumes the complete loss of the unused dynamic head at the compressor outlet, such that static conditions are sued for the cycle analysis.

Table 4-5. Selection of the Compressor-Inlet Conditions

	Input				**Output**			
	T_{in}, °C	p_{in}, MPa	m, kg/s	RPM		**T_{out}, °C**	**p_{out}, MPa**	**Eff., %**
Test at 3200 s 400A input	32.3	7.763	0.916	25,000	**E**	**35.0**	**8.455**	
					M - Total	**35.1**	**8.542**	**78.3**
					M - Static	**35.0**	**8.508**	**74.9**
Test at 3200 s 300 input	***31.8***	***7.702***	0.916	25,000	**E**	**35.0**	**8.455**	
					M - Total	**34.6**	**8.504**	**78.1**
					M - Static	**34.5**	**8.471**	**74.9**
Test at 3200 s **T400A P300 input**	32.3	***7.702***	0.916	25,000	**E**	**35.0**	**8.455**	
					M - Total	**35.3**	**8.449**	**78.4**
					M - Static	**35.1**	**8.414**	**74.8**

As the results in Table 4-5 indicate, the best match between the model prediction and the experimental data for both temperature and pressure is obtained in "T400A P300" case, i.e. when the measured compressor-inlet temperature and cooler-outlet pressure are used as an input data for the compressor performance calculations. This result suggests that the measurements of the compressor-inlet pressure are not accurate, which is consistent with the fact that in Figure 4-2 the compressor-inlet temperature is only 0.001 MPa lower than the turbine-outlet pressure, which is not realistic.

Appendix A has an input file for the compressor performance calculations which lists the assumed design input data. The results of the performance at simulated cycle conditions are given in Appendix B along with other components and results. Also, Appendix B contains a detailed output file from the compressor performance subroutine.

4.2.5 Turbine

The small power level of the SNL S-CO_2 Loop dictated the use of a radial turbine design. However, all previous analysis of the S-CO_2 cycle with the PDC relied on the axial turbine design. As indicated in the S-CO_2 cycle scale studies [12], the axial turbine design is beneficial for all cycles with electrical output greater than 30 MWe, i.e. for all commercial-scale plants for which the PDC was developed. For these reasons, the radial turbine model was not developed for the PDC at the time of this analysis. Moreover, validation of the radial turbine model with the SNL S-CO_2 Loop data will not necessarily apply to the axial turbine model used in all analyses with the PDC. Thus, development of a radial turbine model for PDC is needed only as a necessary component in simulating the entire SNL S-CO_2 Loop. It is unlikely that the radial turbine model will be used for the analyses of commercial-size S-CO_2 cycles with the PDC.

It was originally assumed that the radial turbine model from the G-PASS code [13] will be used in the PDC for SNL S-CO_2 Loop simulation. However, integration of a G-PASS subroutine into the PDC has proven to be problematic. For example, the radial turbine module uses structures which had to be introduced into the PDC requiring significant modifications to the PDC data storage structure. Also, the G-PASS radial turbine module uses pre-defined G-PASS tables for S-CO_2 properties (instead of the properties subroutines used in PDC); integrating those tables into the PDC would mean adopting a significant portion of the G-PASS code into the PDC. In addition, due to several delays and improvements, the G-PASS radial turbine module was not available in time for integration into the PDC for the present analysis, threatening further delays in the current analysis. Therefore, it was decided to develop a distinct radial turbine model specifically for PDC, as described below, rather than adopting the G-PASS model.

Even though the G-PASS radial turbine model was not integrated into the PDC, the development of the two radial turbine models was not completely independent. The authors of this report exchanged notes with R. Vilim on the radial turbine model equations and performance prediction. Also, the radial turbine model developed for the PDC uses the turbine design input data as compiled by R. Vilim. That usage of the turbine design parameters alone helped the model development significantly since the tables listing various design parameters were not provided to ANL and many necessary parameters had to be found from drawings or estimated.

The PDC radial turbine performance model is based on the model development started in FY06 [14]. For this work, the model was resurrected, some equations were updated, and the model was applied to the SNL S-CO_2 Loop turbine design and conditions. The model was developed following the approach in Reference [15]. The radial turbine model is similar to the centrifugal (radial) compressor model in the PDC, except that the flow is in the reverse direction – from the volute to the diffuser to the

impeller. The most important difference between the compressor and turbine models is the loss model and correlations.

The loss model for the developed radial turbine model was adopted completely from the same Reference [15] as the rest of the approach. The current radial turbine loss model includes incidence and profile losses for the diffuser and profile, incidence, blade loading, hub-to-shroud loading, and clearance flow losses for the impeller. In addition, a consideration of aerodynamic passage blockage due to the boundary layer is included for both diffuser and impeller.

The energy (head) and mass (continuity) conservation equations are very similar to those for the centrifugal compressors. In the diffuser, the total enthalpy is conserved while the total pressure is calculated based on the diffuser loss coefficient. The total enthalpy and total pressure define the outlet conditions. The inlet and outlet velocities are calculated from the continuity equations. Total conditions and the velocity at the outlet define the diffuser-outlet static conditions. Iterations are implemented on the outlet density (for the continuity equation) and the loss coefficients. A similar approach is taken for the impeller. For this rotating component with changing radius, the conservation of energy is expressed in terms of constant rothalpy (rather than enthalpy), which in the case of a radial turbine is calculated as [15]:

$$I = H_1 - \omega r_1 C_{\theta 1} + \frac{\Delta H_{DF}}{2}$$

where ΔH_{DF} = additional work due to disk friction.

Although the radial turbine model includes consideration of the volute at the inlet, the SNL S-CO_2 Loop turbine does not include a volute. Therefore, in the current treatment, the volute model is setup in a way that there is no total properties change in the volute.

Table 4-6 shows the results of the application of the radial turbine model to the BNI design conditions (Figure 4-1) and several experimental points. Similar to the compressor model above, two lines are shown for the model results – total and static outlet conditions. Overall, the model shows good agreement with either the design calculations or experimental conditions. Compared to the design conditions, the model overpredicts the turbine's performance. It could be due to some conservative assumptions taken during the turbine design to assure the required performance. More experimental data close to the design conditions is needed to find out the source of the discrepancy of the PDC turbine model with the design calculations performed by BNI.

For all experimental points in Table 4-6, the PDC radial turbine model predicts the outlet pressure very accurately – within or very close to the stated measurement uncertainty of 0.02 MPa, even if no uncertainty of the inlet pressure, temperature, and flow rate is considered. As discussed above in Section 4.1, the measured turbine-outlet temperature cannot be directly compared to that predicted by the analytical model,

possibly due to heat losses in or around the turbine. Therefore, it is expected that the predicted turbine outlet temperature would be higher than the experimental "turbine-outlet" value, which is confirmed by the results in Table 4-6.

Considering that the experimental value of the outlet temperature cannot be used for the turbine model verification, the accuracy of the model can only be assessed based on the prediction of the outlet pressure. As demonstrated above, that pressure prediction is very accurate with the current model. Therefore, the developed radial turbine model is judged to be adequate for cycle performance calculations. Again, validation of radial turbine model itself is not very important for the PDC, since all the cycle configurations analyzed so far employ axial turbine designs.

Appendix A has an input file for the turbine performance calculations which lists the assumed design input data. The results of the performance at simulated cycle conditions are given in Appendix B along with other components and results. Also, Appendix B contains a detailed output file from the radial turbine performance subroutine.

Table 4-6. Comparison of the PDC Radial Turbine Model Prediction with Experimental Data and Design Conditions

	Input				**Output**			
	T_{in}, °C	p_{in}, MPa	m, kg/s	RPM		**T_{out}, °C**	**p_{out}, MPa**	**Eff., %**
Design Conditions	536.9	13.499	2.58	75,000	**D**	**475.7**	**7.885**	**84**
					M - Total	**468.4**	**7.848**	**95.8**
					M - Static	**464.9**	**7.631**	**91.3**
Test at 3200 s	150.7	8.403	0.916	25,000	**E**	**140.6**	**7.764**	
					M - Total	**144.1**	**7.797**	**92.4**
					M - Static	**143.9**	**7.784**	**90.2**
Test at 4500 s	147.6	9.128	1.643	35,047	**E**	**130.1**	**7.589**	
					M - Total	**130.9**	**7.582**	**95.1**
					M - Static	**130.5**	**7.548**	**92.9**
Test at 6099.8 s	203.6	9.358	1.634	39,144	**E**	**182.1**	**7.578**	
					M - Total	**184**	**7.613**	**95.5**
					M - Static	**183.5**	**7.572**	**93.1**

4.2.6 Piping

The dimensions for the SNL S-CO_2 Loop pipes, including the inner diameter and length, were provided by SNL. Those dimensions, as implemented in the modeling are shown in the input file for the cycle calculations (Cycle_dat.txt) in Appendix A. The input file also lists the assumed number of bends and bend radius for each pipe. The number of bends was estimated from the available three-dimensional drawings and pictures of the SNL S-CO_2 Loop. It is assumed that all bends are 90° and the bend radius is equal to the pipe diameter ($r_B/D=1$).

The piping calculations in the PDC are set up in such a way that only the effects on the pressure drop are calculated. No heat transfer between the pipe wall surface and the fluid inside is accounted for, either in steady state or in transients. So, in the pipe calculations, the enthalpy of the fluid is conserved and the temperature change is evaluated from the pressure drop. There is, however, one special case with heat loss at the turbine outlet as discussed in Section 4.1. That special case is described in details in Section 4.3.2 below.

The results of the loop piping pressure drop analysis are presented in the cycle result output file (Cycle_res.txt) in Appendix B.

This section completes the description of the individual models for the SNL S-CO_2 Loop components. The modeling and the performance calculations for the entire loop are described in the following section.

4.3 Modeling of the Entire Loop

4.3.1 Structure

The current structure of the modeled SNL S-CO_2 Loop is shown in Figure 4-5. The figure is presented here for informational purposes only – the structure is created automatically by the code from the input file. The input file corresponding to the layout in Figure 4-5 is presented in Appendix A. Figure 4-5 also shows the nodes used in the modeling as they are referred to in the input file in Appendix A and the output files in Appendix B. Temperature and pressure nodes, located at each end of the pipes connecting the components, are shown in squares. The flow rate nodes are shown in circles and correspond to the pipes between the temperature nodes.

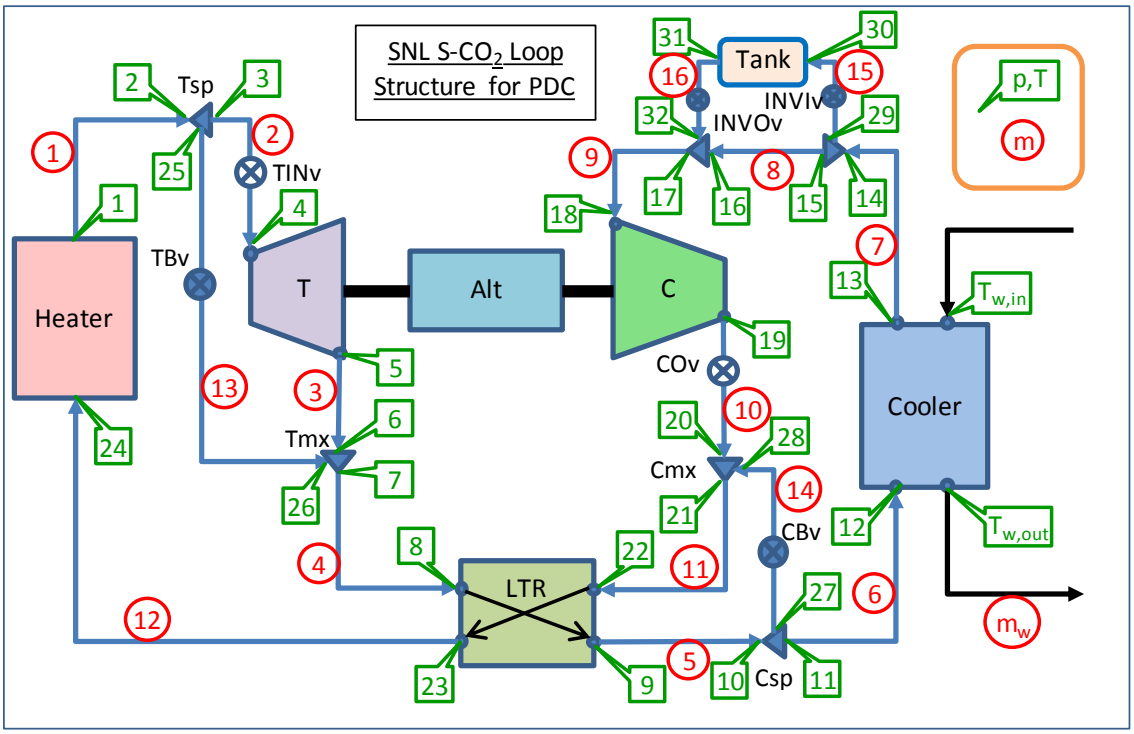

Figure 4-5. Modeled Structure of the SNL S-CO_2 Loop in the PDC.

The configuration of the main loop in Figure 4-5 is the same as in Figure 4-2 for the experimental setup. In addition to the main loop, a few other elements were added to the modeled structure for future modeling needs. In particular, both the turbine and compressor have bypass loops which are intended for addition of the second turbine and compressor for modeling the split-flow loop configuration. Those bypass loops have a splitter (e.g., Tsp), a mixer (Tmx), and a corresponding valve (TBv). Similarly, an inventory control tank (Tank) with corresponding splitter, mixer, and valves has been added to the model. In the current modeling, the valves for all those bypass loops are fully closed at the steady-state conditions such that there is no flow through the bypass loops. In addition to those components, the regulating valves are added at the turbine inlet (TINv) and at the compressor outlet (COv). Those valves are reserved for future control capabilities – at the current steady-state configuration the valves are assumed to be fully opened (as indicated by clear background in Figure 4-5 as opposed to dark background for fully closed bypass valves).

4.3.2 Additional Code Development and Solution Algorithm

During the simulation of the SNL S-CO_2 Loop with the steady-state part of the PDC it became clear that significant code modifications were needed for this particular task.

Those code modifications, described below in this section, were not necessary compatible with the usual analyses carried out with the PDC. For these reason, a replica of the PDC was created specifically for the analysis of the SNL S-CO_2 Loop. The code still uses the same subroutines as the main PDC code, but some aspects, such as an algorithm for finding a steady-state solution for example, required additional code development. It might be possible in the future to combine that special treatment into the main PDC code (by introducing special input flags for example); for this work, however, it was decided to work with a separate copy of the PDC.

The most significant code modification required for simulation of the SNL S-CO_2 Loop with the PDC was the treatment of the turbomachinery for steady-state initialization. The steady-state part of the PDC was originally developed to integrate the turbomachinery design into the overall cycle design. The required conditions, such as compressor inlet and outlet pressures, were provided through the input files, and the compressor or turbine design subroutine was called to develop a compressor or turbine design which would satisfy those boundary conditions. In the SNL S-CO_2 Loop, however, the designs of the turbine and compressor are already defined. That means that the outlet conditions, including the outlet pressure, have to be calculated using the turbomachinery performance subroutines and therefore cannot be selected arbitrarily. Moreover, the flow rate in the system is established based on the head-flow characteristics of both the turbine and compressor and the pressure drops in other components and piping. At the same time, as discussed in Section 4.2.3, the CO_2 flow rate should be consistent with the heat transfer from the heaters. Those additional limitations required the modification of the solution algorithm for the steady-state conditions. The new algorithm is described below.

The calculations for the cycle conditions start with calculating the CO_2 flow rate from the heater (RHX) performance. Those calculations assume that the CO_2 temperature and pressure at the RHX inlet are given, either from the first guess from the input file or from previous iterations. The flow rate is first guessed and the RHX heat transfer calculations are carried out. The results of such calculations are the outlet temperatures on both sides. The iterations on the CO_2 flow rate are then carried out in order to match the required temperature on the RHX hot side outlet. Those iterations will also yield the CO_2 temperature at the RHX outlet. The CO_2 flow rate is supplied to the rest of the cycle calculations. That part is exactly the same as it was in the PDC before.

The iterations within the cycle start with filling the pressure array. It is assumed that the pressure and temperature at the compressor impeller inlet are given in the input file. To obtain those conditions, the stand-alone compressor performance calculations, such as those described in Section 4.2.4, are carried out and the conditions at the impeller inlet are obtained from the output file. For example, the compressor performance output file in Appendix B shows that the impeller inlet (point 1-1) conditions are 7.690 MPa and 32.248 °C. Those values are supplied as input for the cycle calculations (see CompA_dat.txt in Appendix A). The compressor impeller-inlet conditions are selected since they usually provide the closest proximity to the critical point, such that fixing these

conditions above the critical point guarantees convergence of the properties calculations everywhere else in the cycle. With the compressor-inlet pressure, the compressor-outlet pressure is calculated from the compressor pressure ratio, which is updated every time the compressor performance subroutine is called. Then, the code fills the pressure array downstream of the compressor up to the turbine inlet based on the values of the pressure drop in each component and piping. Similarly, the pressures upstream of the compressor are filled up to the turbine with the reverse of the pressure drops. Then the rest of the pressures in the loop, such as after the splits and mixers, is filled. This part is similar to the approach that previously existed in the PDC, except for the fact that the compressor-outlet pressure is now calculated from its pressure ratio obtained on the previous iteration (rather than keeping the compressor-outlet pressure fixed at a given value). The pressure calculations are completed by calculating the pressure at the turbine outlet based on the turbine pressure ratio. The turbine pressure ratio is also recalculated every time the turbine performance subroutine is called. Notice that in this approach the turbine-outlet pressure is defined twice: first from the calculations upstream of the compressor and them from the pressure ratio obtained from the turbine performance subroutine. The resolution of that double-definition is described further in this section.

When all of the pressures are known, the code proceeds with calculating the temperatures in the cycle. Again, the calculations start at the compressor inlet. The temperature at the compressor impeller inlet is known. The temperature at the compressor outlet is calculated based on the known outlet pressure and compressor efficiency. The efficiency is again updated during the performance subroutine calculations[1]. The calculations of the temperatures then proceed downstream starting at the compressor outlet. Those calculations include the calculations of various components, such as heat exchangers and piping. When the turbine inlet conditions are calculated, the turbine efficiency is used to calculate the temperature at the turbine outlet. Usually, several iterations on the temperatures are needed to obtain a convergence on the inlet conditions for various components. For example, the inlet temperature on the hot side LTR inlet is defined by the turbine outlet temperature and the pressure drop in the pipes connecting the turbine with the LTR. In some cases, the first guess for the inlet temperature needs to be provided to start the iterations.

The temperature at the compressor inlet defines the conditions at the cooler outlet. Thus, the temperature calculations continue upstream of the compressor inlet. The compressor-inlet conditions are obtained from the performance subroutine for the given impeller-inlet conditions (or simply guessed to be just above the impeller-inlet conditions

[1] The approach to calculate the compressor outlet pressure and temperature based on the pressure ratio and efficiency is implemented to increase the speed of the calculations. Although the performance subroutines could be used directly to calculate the outlet conditions, those subroutines are relatively slow to be used inside of the cycle iterations. Once the iterations on cycle conditions are completed to obtain the flow rate and the compressor-inlet conditions, the performance subroutines are used to update the pressure ratio and efficiency. The cycle iterations are then repeated, and so on until convergence on the pressure ratio and efficiency is achieved. The same approach is used for turbine calculations.

for the first iteration). Then, the pressure drops in the pipes upstream of the compressor are used to calculate the required temperature at the cooler outlet. Similarly, cooler-inlet conditions on the CO_2 side are defined by the LTR cold side outlet temperature and pressure drops in the pipes between the LTR and the cooler. With the given inlet and outlet conditions and the fixed cooler design, the calculations for the cooler are carried out such that the cooling water flow rate is determined in order to meet the outlet conditions on the CO_2 side. This part is different from the previous design approach where the cooling water flow rate was fixed by the input and the required cooler length was calculated in the design calculations. In addition to the cooling water flow rate, the cooler calculations give the outlet temperature on the water side and the pressure drops on both sides. The CO_2 side pressure drop is then used in the cycle calculations to obtain the pressures as described above.

The iterations on the pressure and temperature for a given flow rate proceed until convergence is achieved. Those calculations will provide the conditions at the RHX (heaters) inlet. Then, the RHX calculations are repeated as described above to obtain the flow rate and the CO_2 temperature at the RHX outlet. Then, the cycle calculations are repeated. When the required convergence on the flow rate and RHX-inlet temperature is achieved, the turbomachinery performance subroutines are used to update the efficiency and the pressure ratio in the turbine and compressor for the current flow rate and inlet conditions. In the case of the compressor, the impeller-inlet conditions are fixed, so the performance subroutine also calculates the compressor-inlet conditions based on the current flow rate. When the turbomachinery performance parameters are obtained, the cycle iterations, including the flow rate, pressures and temperatures are repeated until the overall convergence is achieved.

It is mentioned above that the current solution algorithm double-defines the turbine-outlet pressure, first from the compressor-inlet conditions and pressure drops upstream of the compressor, and then from the turbine performance calculations. This happens because the PDC steady-state calculations are set up in a way that the CO_2 flow rate is calculated based on the conservation of energy and the performance of the RHX (heaters). In reality, when the designs of all components are defined, the flow rate in the system is found at the conditions in which the pressure ratio delivered by the compressor matches that of the rest of the cycle including the turbine. Those equilibrium conditions are schematically illustrated in Figure 4-6. The compressor pressure ratio decreases with increasing flow rate. For the turbine and the rest of the cycle, the pressure ratio is increasing with the flow rate. For example, the pressure drop in pipes and heat exchangers is roughly proportional to the square of the flow rate. The closed system will eventually find an equilibrium solution with the flow rate and pressure ratio matching both the compressor and system curves, as shown in Figure 4-6.

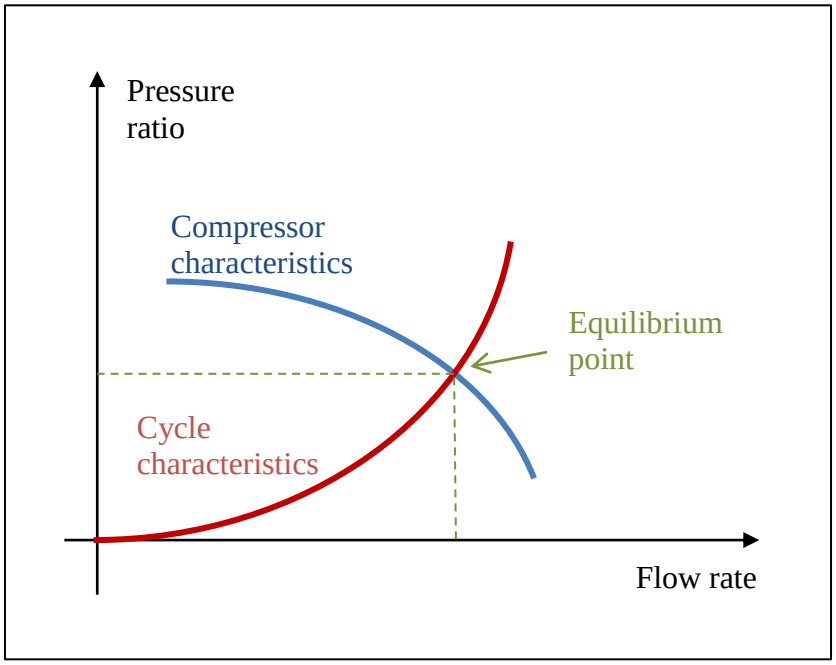

Figure 4-6. Equilibrium Flow Rate and Pressure Ratio in a Loop.

The approach to finding the steady-state flow rate based on the pressure-flow characteristics of the system was previously implemented in the PDC for quasi-static load following analysis of S-CO_2 cycles. Those calculations were applied to the off-design (rather than design) conditions. In the off-design mode, the heat removal by the cycle in the RHX was allowed to vary with changing flow rate. In the current simulation, however, the heat addition to the cycle is considered to be fixed, such that a similar approach could not be applied here.

There is another specific feature of the experimental conditions discussed above in Section 4.1 which has not been taking into account in the solution algorithm yet. It deals with the apparent heat loss in or around the turbine. As shown in Section 4.1, that heat loss is estimated to be significant (i.e., comparable to the turbine work), such that it is expected to have significant impact on the heat and flow balance in the system and should not be ignored in the current calculations. Similar observations were made by the experimentalists in their own analysis of the measured and predicted values for the turbine work [8]. That heat loss mechanism was discovered in this work due to apparent violation of conservation laws in the turbine which resulted in the turbine efficiency exceeding 100%. It is quite possible that there are other losses in the system which are much more difficult to discover based on the available data. Moreover, as discussed in the same Section 4.1, true steady state conditions were not obtained in the experiment. Therefore, it is expected that there would be some continuous heat transfer between the working fluid and the structures, such as the heat exchanger walls and the pipe walls.

Those non-steady-state mechanisms could not be simulated with the steady-state code by definition.

Following the analysis outlined above, an attempt was made to find the balance in the system by artificially introducing a heat loss mechanism to the system. Because it was apparent that some heat is being lost in or around the turbine, it was decided to apply the heat loss to the turbine-outlet pipe (Flow Node 3 in Figure 4-5). In this approach, the heat loss in this single pipe would simulate all the heat losses in the entire system, including those caused by the continuing heat exchange between the fluid and the structures. The applied correction works in the following way. Introduction of the heat loss in the turbine outlet pipe would reduce the fluid temperature at the LTR hot side inlet, resulting in a lower temperature at the cold side outlet. Consequently, the fluid temperature at the heater (RHX) inlet would be reduced. With a lower CO_2 temperature at the RHX inlet, the heat transfer characteristics of the RHX would improve, requiring less CO_2 flow to remove the same amount of heat from the RHX. As the flow rate decreases, the pressure ratio in the turbine also decreases while the pressure ratio in the compressor increases, as demonstrated in Figure 4-6. Thus, the amount of heat loss can theoretically be adjusted such that the system works at the flow equilibrium point in Figure 4-6. Practically, this means that the heat loss was adjusted until the turbine-outlet pressure calculated from the turbine performance matches the pressure calculated at the turbine outlet from the compressor-inlet pressure and all the pressure drops upstream of the compressor. At this point, no automatic iteration on the heat and flow balance is implemented; the heat loss is adjusted manually directly in the code to achieve the pressure agreement in the following way:

```
! Enthalpy = constant

h_CO2(o1)=h_CO2(i1)

if (im==3) then
   h_CO2(o1)=h_CO2(i1)+add_sub*7D3
end if
```

where `h_CO2` = enthalpy in the cycle,
`im` = pipe index,
`o1`, `i1` = outlet and inlet nodes for pipe `im`,
`add_sub` = -1 for normal direction (`i1`=5, `o1`=6) and =1 for reverse direction,
`7D3` = manual adjustment of the enthalpy.

Note that for all other pipes in the cycle, `h_CO2(o1)=h_CO2(i1)`, i.e. the enthalpy is still conserved everywhere else.

The above correction was proven to be effective and sufficient to achieve the heat, flow, and pressure balance in the cycle as demonstrated in the results section below.

However, to investigate whether that correction is realistic, additional analysis and, possibly, experiments are needed. Since the correction allows achieving the balance in the system, it is not anymore a question whether this correction is needed or not. It is more a question of whether it is appropriate to apply this correction in one place only or should a more detailed correction be applied in more places. However, without additional experimental data, that question cannot be answered at this time. Therefore, the current correction method was judged to be adequate.

To facilitate the calculations described above, several modifications to the input files were needed. To use the turbomachinery performance subroutines instead of design subroutines, a special flag was introduced in the input files for the turbine(s) and compressor(s). The input files require a value of the turbine or compressor efficiency for the first guess for the cycle iterations. That input parameter is now allowed to be less than zero. If the input value is negative (such as the case in the input files in Appendix A) then the performance subroutines will be used in steady-state calculations. The first guess for the turbomachinery efficiency in this case is the absolute value of the input parameter. Also, if the input efficiency is negative, then the design parameters have to be provided at the end of the turbine and compressor input files.

Two modifications were introduced in the input file for the cooler(s). First, the cooler length is now an input parameter. Previously, it was calculated as part of the cooler design calculations to match the required CO_2 outlet temperature. That capability is still retained if the input value for the cooler length is negative. In addition, the cooling fluid flow rate is now allowed to be negative in the input file. In this case, the design calculations will iterate on that flow rate, instead of cooler length, to match the CO_2 outlet temperature. Therefore, the cooler length should be provided in the input in this mode, i.e., cooling fluid flow rate and the cooler length are not allowed to be negative at the same time.

A line for the first guess for the CO_2 inlet temperatures was added for the recuperator and RHX input files. In the case of the recuperators, two values have to be provided for the hot and cold sides. Those values are used for the first guess only if no other information is available. For example, the capability to use the latest cycle output file as a starting point for pressure and temperature arrays is still retained in the PDC (see the first input parameter in the Cycle_dat.txt file). If this option is used, then there is no need for the first guess on the CO_2 side inlet temperatures for the recuperator(s) and RHX.

4.3.3 Results for Entire Loop Simulation

The detailed results of the calculations of the steady-state SNL S-CO_2 Loop analysis with the PDC for the conditions at 3200 s (Figure 4-2) are presented in Appendix B in the form of the output files exactly as they are obtained from the code. The results for the entire cycle include pressures, temperatures, enthalpies, and other properties for each

node in the cycle. It also shows the results of the pressure drop calculations for each pipe, including frictional, form loss, and valve components of the total pressure loss. In addition, the file shows the calculated flow rate in the system, heat balances in various components, and the calculated CO_2 inventory.

Appendix B also shows the results for the calculated conditions in each component, as well as the detailed results for the turbine and compressor performance calculations.

The graphical representation of the main results in Appendix B is shown in Figure 4-7 in comparison with the experimental data (repeated from Figure 4-2). The code result graph also shows the calculated heat balance for each component. In addition, it shows the simulated heat loss amount in the turbine-outlet pipe.

Given all the uncertainties and deficiencies of the experimental data discussed above, including uncertainties and unknowns in the design of each component, surprisingly good agreement is achieved between the code predictions and the experimental data. All the temperatures are very close – within 2 °C on the hot side and within 1 °C on the cold side.

Except for the compressor-inlet pressure, all the pressures in the loop also agree very well – within 0.05 MPa at most. This is despite the fact that the pressure drops in the stand-alone heat exchanger calculations (Section 4.2) were significantly different from those obtained from the available experimental data. Much better agreement on the cycle level suggests that the disagreement on the component level is most likely caused by the measurement uncertainly, in particular by calculating the pressure drop as a difference of two absolute pressures measured with an uncertainty comparable to that calculated difference. The experimental value for the compressor inlet pressure again seems unrealistic as discussed in Section 4.1, which is indirectly confirmed by much better agreement for all other pressures in the cycle.

The calculated CO_2 flow rate is again very close to the measured value. The importance of this agreement is strengthened by the fact that the flow rate was not provided as an input but rather was calculated from the heat balance in the system. Good agreement on the flow rate also indirectly confirms the accuracy of the correction for the heat loss as discussed below and in Section 4.3.2. The water flow rate, which again was calculated in the code based on the required performance of the cooler, is also very close to the measured value. It is noted, however, that the experimental setup uses a water/glycol mixture which was simulated with pure water in the code.

As the results in Figure 4-7 show, the heat loss in the turbine outlet pipe is estimated to be around 6.5 kW in order to provide the flow and pressure balance in the system. That value is about twice as high as the value of 3.4 kW estimated in Section 4.1. However, as discussed in the previous section, the modeled heat loss in this single pipe represents all the heat losses and the corrections for unsteady results in the entire loop. The results of the calculations show a much smaller, compared to the experimental data, variation in

temperature inside the pipes when only the pressure drop is taken into account. For example, the calculated temperature change in the pipe connecting the heater with the turbine is only 0.1 °C, while the experimental data shows a much larger temperature change of 1.4 °C. Taking into account that result and similar variations in the rest of the cycle, it seems that the estimated heat loss is a reasonable and a real correction for the loop.

The turbomachinery power, including the alternator power, calculated by the code could not be directly compared to the experimental data. The current cycle calculations do not account for the parasitic losses, such as windage, in the turbomachinery. Those losses have been shown to be a significant contribution to the overall power balance. For some reason, however, the provided experimental data did not include the readings from pressure and temperature sensors in the drain line. Those conditions are essential in estimating the windage losses. On the other hand, except for the value of the net electrical output, the windage losses do not affect the performance of the cycle components, provided that the turbomachinery rotational speed is measured and modeled correctly. Even in dynamics calculations, the experimental loop is set up in a way that the rotational speed is actively controlled all the time, such that the power balance on the TAC shaft does not play an important role for the cycle dynamics performance. Very good agreement on the turbomachinery inlet and outlet conditions and the flow rate provides the assurance that the power balance on the CO_2 side (i.e., excluding external losses) is predicted very well with the code.

Overall, very good agreement between the experimental data and the steady-state model predictions is obtained for the selected experimental conditions. Thus, the developed steady-state models, including those of individual components, are considered to be adequate for predicting the performance of the entire loop at steady-state conditions. It would be useful to verify the model predictions at other experimental conditions. However, at this point such experimental data is not available. A few other more or less steady-state points in the same experimental run, such as those in Figure 4-4, were obtained at cooler-outlet temperatures below the CO_2 critical point. Those conditions are expected to cause convergence problems in finding the steady-state solution for the temperatures inside the cooler.

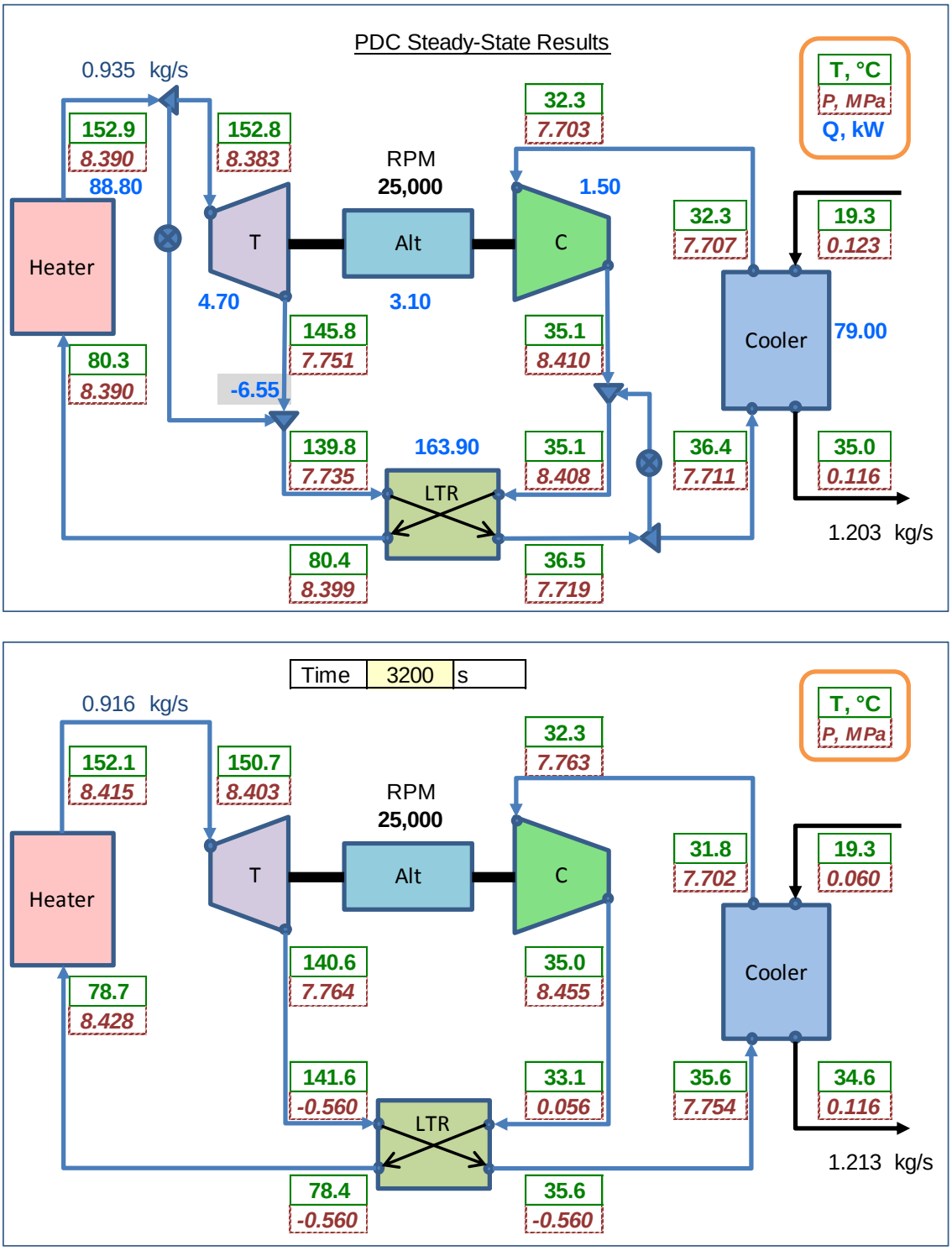

Figure 4-7. PDC Results (Top) of the Simulated SNL S-CO_2 Loop Experimental Conditions (Bottom).

4.4 Dynamic Simulation

It was originally planned that after the modeling of the steady-state part is complete, dynamic simulations of the SNL S-CO_2 Loop with the PDC can be carried out. However, several potential problems were discovered during the work with the experimental data which prevented or at least delayed the dynamic simulation.

First, the experimental data weren't made available to the authors until late in the FY. When the data was finally made available all the effort was directed to obtain very good agreement between the model and the experimental data for the steady-state performance. Without such agreement, the results of the dynamic simulation would not make much sense anyway.

Second, the available experimental data was focused on the operation on the cycle below the critical temperature at the compressor inlet. The PDC code however was designed for supercritical (at least in terms of the temperature) operation of the cycle. This limitation mostly comes from the CO_2 properties routines used in the PDC. Some CO_2 properties, such as specific heat, have singularities at the critical point. Because of that singularity behavior, calculating the properties very close to the critical point often requires some form of iterations, and may experience numerical and/or convergence problems. Also, simulating the conditions very close to the critical point usually requires a treatment of two-phase conditions, at least inside the iterations. Even though the provisions for the CO_2 properties in the two-phase region are included in the PDC, the code was never tested or applied to two-phase conditions. Those issues are most likely to present problems for finding the steady-state solution; the dynamics equations include much less iterations on properties. In any case, it would be beneficial to test the PDC first at the conditions it was designed for, i.e., at supercritical conditions, before subcritical calculations are attempted with the code.

Third, the dynamic simulation of the experimental loop requires detailed knowledge and accurate simulation of all control mechanisms implemented in the loop. The control system currently implemented in the PDC is designed for full-scale commercial power plants and cannot necessary be applied to the small-scale experiments. For example, the generator (alternator) output is controlled in the PDC by means of the turbine bypass valve. Not only turbine bypass is not implemented in the SNL S-CO_2 Loop, but also the alternator output is mostly irrelevant to the SNL S-CO_2 Loop setup where the TAC rotational speed is actively controlled. Similarly, all the previous dynamic simulations with the PDC assumed that the compressor-inlet temperature will be controlled to stay above the critical point. Obviously, this is not the case for the experimental run for which the experimental data is available. Therefore, the knowledge of how the compressor-inlet temperature is controlled in the SNL SCO_2 Loop experiments is required. That temperature control has been shown to be very important for the cycle performance.

However, no information has been made available to ANL so far on that or any other controls in the loop.

Lastly, the steady-state simulation described in previous sections of this report demonstrated the importance of the correct modeling of the heat losses in the system. Those heat losses were added to the steady-state code. Similar considerations need to be included into the dynamic equations. However, it is not clear at this point how it can best be implemented in the code. For steady-state calculations, the amount of the heat loss was adjusted manually to satisfy the conservation laws. The same approach would not work in the dynamic calculations. Therefore, some sort of the time history tables of the heat loss would need to be provided as an input for the dynamic part of the PDC code. At this point, the available experimental data does not seem to be sufficient to provide such an input.

The issues discussed above need to be resolved before any meaningful results of the dynamics simulation of the SNL S-CO_2 Loop with the PDC can be carried out. Therefore, working on these issues will have the highest priority for PDC development in the near future.

5 Summary and Future Work

A new approach was developed to couple the Plant Dynamics Code for S-CO_2 cycle calculations with SAS4A/SASSYS-1 calculations for the reactor side. The coupling was achieved using an executable file for the SAS4A/SASSYS-1 code, avoiding the need for modification of the SAS4A/SASSYS-1 source code. The new code system allows use of the full capabilities of both codes such that whole-plant transients can now be simulated without additional user interaction.

An automatic compressor surge control option was introduced into the PDC. The surge control uses flow recirculation around the compressor to keep the compressor flow from falling below the surge/stall limit. The implementation of surge control allows the dynamic calculation of some specific transients for which unstable compressor behavior close to surge limit would otherwise be expected. Transient analyses were carried out to confirm the effectiveness of compressor surge control. The S-CO_2 cycle control logic in the PDC was updated to include compressor surge control, but this control is used only when necessary. Since surge control works by recirculating part of the compressor flow, implementing it artificially increases the compressor work without changing the flow rate in the rest of the cycle. Thus, compressor surge control was designed only to avoid surge conditions and is not used in normal cycle control.

A new approach was developed to define the time step size for the numerical solution of the transient equations in the PDC. This new approach uses a relative contribution from each term in a Taylor series expansion to find the largest time step which still satisfies the convergence criteria. This approach defines the time step sized based on the already-calculated terms in the Taylor series, such that no additional calculations are needed, compared to the previous solution approach, where the time step was continuously divided in half to satisfy the convergence criteria. As a result of implementing the new time step solution algorithm, the calculational time with the PDC has been reduced by as much as 50%.

Several other code modifications, such as an updated treatment of S-CO_2 cycle flow mergers and splits, a modified enthalpy equation to improve the treatment of negative flow, and a revised solution of the RHX equations, were introduced. All of these modifications improved to code computational stability, while not significantly affecting the results of transient calculations.

The improved PDC was used to continue the investigation of the S-CO_2 cycle control and transient behavior. The coupled PDC-SAS4A/SASSYS-1 code capability was used to study the dynamic characteristics of a S-CO_2 cycle coupled to a SFR plant. The cycle control was investigated in a response to a linear reduction in the electrical grid demand

from 100% to 0% at a 5%/min rate. It was assumed in the calculations that the reactor operates in an autonomous regime. Previous analysis has demonstrated that such reactor operation is feasible due to the favorable reactivity feedbacks of the SFR cores with metallic fuel. Confirmatory calculations proved that the results obtained with the coupled PDC-SAS4A/SASSYS-1 code system are very close to those obtained in earlier analyses. The calculations also confirmed that the recent PDC modifications did not alter the results of transient calculations. Next, the coupled codes were used to improve S-CO_2 cycle control at lower grid loads. In previous analyses, turbine bypass control was assumed for grid loads below 50% since it was the simplest and fastest acting control mechanism. However, analysis of the results has shown that under this control approach, the cycle still needs a heat supply of about 60% of the nominal level to maintain operation with zero grid output. To improve cycle efficiency at low loads, other control mechanisms were investigated. It has been shown that utilization of turbine throttling control below 50% load significantly improved the cycle efficiency. As a result, the heat input for cycle operation with zero generator output now requires a heat input of 25% of the nominal value (compared to 60% with turbine bypass control). Consequently, the cycle control strategy was updated. The new control strategy still relies on inventory control in the 50%-90% load range and turbine bypass for fine and fast generator output adjustments, but it now also includes turbine throttling control in the 0%-50% load range.

In an attempt to investigate the feasibility of using the S-CO_2 cycle for normal decay heat removal from the reactor, the cycle control study was extended beyond the investigation of normal load following. The goals of this study were to find the combination of control mechanisms which would allow operation of the cycle with a heat input of about 6%, i.e. with the initial reactor decay heat generation rate following scram. It was shown that such operation is possible with the extension of inventory and turbine throttling controls. However, the cycle operation in this range is so inefficient that energy would need to be supplied from the electrical grid to the generator which would need to be capable of operating in a motoring mode. An electrical power input from the electrical grid having a magnitude of about 20% of the nominal plant output electrical power level would be needed to maintain the circulation of the CO_2 in the cycle. The work on finding a more efficient operating regime for the S-CO_2 cycle in the decay heat removal mode will be continued in the future. One possibility is to investigate turbomachinery operation at reduced rotational speed.

The coupled PDC-SAS4A/SASSYS-1 code system was also used to simulate thermal transients in the Na-CO_2 heat exchanger. The goal of this study was to find the maximum possible rate of the temperature change for the heat exchanger under normal operating or accident conditions. That temperature change information is required to properly design the heat exchanges for a S-CO_2 cycle accounting for thermal shocking loads. Before the PDC-SAS4A/SASSYS-1 code system was developed, thermal shock transients could only be approximated; now the results of the calculations based on the two codes are more realistic. Several possible conditions with the potential to introduce significant increases or reductions in the heat exchanger temperatures were identified and simulated. The conditions range from reactor scram and primary sodium pump failure or

intermediate sodium pump failure on the reactor side to pipe breaks and valve malfunctions on the S-CO_2 side. It was found that the maximum possible rate of the heat exchanger interstitial wall temperature change for the particular heat exchanger design assumed is limited to ±7 °C/s for less than 10 seconds. Similar analysis should be applied to other S-CO_2 cycle heat exchangers in the future. In the case of the recuperators, though, it is expected that the transients would be slower since it is difficult to introduce a flow disturbance on one side of a recuperator without affecting the flow on the other side.

Validation of the Plant Dynamics Code with available experimental data from the Sandia National Laboratories (SNL) small-scale S-CO_2 Brayton cycle demonstration has been started. The available data was obtained at Barber-Nichols Inc. using an earlier configuration of the S-CO_2 loop involving only a single-turbo-alternator-compressor (TAC) instead of two TACs, a single low temperature recuperator (LTR) instead of both a LTR and a high temperature recuperator, and fewer than the later to be installed full set of electric heaters.

The analysis of the available experimental data has highlighted several issues which complicated the modeling and/or validation of the models against the experimental data. Due to the absence of the full heating capability as well as the lack of a high temperature recuperator providing additional recuperation, the temperature conditions obtained with the loop are too low for the loop conditions to be prototypical of the S-CO_2 cycle. In particular, the data includes conditions in which subcritical flow is present whereas the complete demonstration to be assembled in the future would nominally operate in the supercritical regime. The experiments attempted to simulate steady-state conditions but in reality were not held in an unvarying state long enough to achieve a true steady state. In addition, differential pressure sensors were not installed for the heat exchangers such that pressure drop predictions from the model could not be directly compared to the experimental data due to the large uncertainties associated with small differences in the absolute pressures measured by the pressure transducers upstream and downstream of the heat exchangers. The difference in absolute pressure readings introduced significant uncertainty, sometimes even larger than the value itself, of the experimental data for the pressure drop. Also, simple heat balance calculations showed that there should be significant heat loss from the system, especially around the turbine. However, the experimental data was not sufficient to distinguish between the useful work and the heat loss in the turbine. To account for these shortcomings, some specific assumptions had to be made in the modeling of the SNL loop with the PDC.

The PDC code validation was started by predicting the steady-state performance of each individual component. Good agreement is obtained between the Printed Circuit Heat Exchanger model in the code and the temperature data for the low temperature recuperator and cooler which are both PCHEs. The development of a radial flow turbine model needed for the radial flow turbine component of the TAC initiated several years ago at ANL was completed and the model was implemented in the Plant Dynamics Code. The radial turbine model prediction for the turbine outlet pressure agrees well with the

measured value but the outlet temperatures disagree due to the presence of significant heat losses in the experiment loop. Comparison of the radial compressor model with the compressor data is difficult due to significant inaccuracies in the measured pressures particularly at the compressor inlet as well as significant windage and other parasitic losses in the compressor. Nonetheless, reasonably good agreement is obtained for the compressor when a parametric study on the compressor-inlet conditions was carried out.

Despite the issues identified with the experimental data which complicated the model development and/or model comparison, reasonably good agreement is obtained for conditions around the loop, including temperatures, pressures, and flow rates. However, an assumption and manual code modifications had to be made in order to account for the heat loss from the system. The resulting heat loss is a steady state value and it is not currently known how the heat loss would vary under various transient scenarios.

Consequently, it was not possible to attempt to model the transient behavior of the loop and compare with transient data. Development of a Plant Dynamics Code capability to calculate transients for various configurations of the loop during its phased assembly is a high priority for future work. The transient simulation of the loop would also require detailed information on the implemented control mechanisms and logic in the experimental loop. That information is crucial for transient simulation but is not available at this time.

In summary, future work will continue focusing on the PDC development and the analysis of the control and transient behavior of the S-CO_2 cycle. One of the highest priorities in this regard will be continuation of the PDC validation with the experimental data obtained from SNL S-CO_2 loop, or any other experimental data which might be available in the future. On the S-CO_2 cycle control analysis side, work will be continued in studying the cycle operation at low power.

Acknowledgements

The authors are grateful to Gary Rochau (SNL), the Technical Area Lead, Bob Hill (ANL/NE), the National Technical Director, Matt Hutmaker (U.S. DOE), the DOE Technical Manager, and Brian Robinson (U.S. DOE), the Headquarters Program Manager for the Advanced Reactor Concepts Program. The authors appreciate the efforts of Steve Wright (SNL) in transferring selected data to ANL. The authors are also indebted to Tom Fanning (ANL/NE) for his support with SAS4A/SASSYS-1 code.

References

1. Moisseytsev, A. and Sienicki, J. J., "Development of a Plant Dynamics Computer Code for Analysis of a Supercritical Carbon Dioxide Brayton Cycle Energy Converter Coupled to a Natural Circulation Lead-Cooled Fast Reactor," ANL-06/27, Argonne National Laboratory, July 2006.

2. Moisseytsev, A. and Sienicki, J. J., "Transient Accident Analysis of a Supercritical Carbon Dioxide Brayton Cycle Energy Converter Coupled to an Autonomous Lead-Cooled Fast Reactor," Nuclear Engineering and Design 238 (2008), pp. 2094-2105.

3. Moisseytsev, A. and Sienicki, J. J., "Analysis of Supercritical CO_2 Cycle Control Strategies and Dynamic Response for Generation IV Reactors," ANL-GenIV-124, Argonne National Laboratory, September 15, 2009.

4. Cahalan, J. E., Tentner, A. M., and Morris, E. E., "Advanced LMR Safety Analysis Capabilities in the SASSYS-1 and SAS4A Computer Codes," Proc. of the International Topical Meeting on Advanced Reactor Safety, 1994, Vol. 2, p. 1038, American Nuclear Society, Pittsburgh, April 17-21 (1994).

5. Moisseytsev, A. and Sienicki, J. J., "Autonomous Load Following Behavior of a Sodium-Cooled Fast Reactor with a Supercritical Carbon Dioxide Brayton Cycle," Paper 11192, 2011 International Congress on Advances in Nuclear Power Plants (ICAPP 11), Nice, France, May 2-5, 2011.

6. Rochau, G. E., "Supercritical CO_2 Brayton Cycle: The Doe Program," Presentation at SCO_2 Power Cycle Symposium, Boulder, Colorado, May 24-25, 2011.

7. Vilim, R.B., "Development and Validation of G-PASS Compressor Model for Split-Flow Loop Simulation," ANL-GenIV-144, Argonne National Laboratory, August 2010.

8. Wright, S. A., Conboy, T. M., and Rochau, G. E., "Break-even Power Transients for two Simple Recuperated S-CO_2 Brayton Cycle Test Configurations," SCO_2 Power Cycle Symposium, Boulder, Colorado, May 24-25, 2011.

9. Moisseytsev, A. Sienicki, J. J., Cho, D. H., and Thomas, M. R., "Comparison of Heat Exchanger Modeling with Data from CO_2-to-CO_2 Printed Circuit Heat Exchanger Performance Tests," Paper 10123, 2010 International Congress on Advances in Nuclear Power Plants (ICAPP 10), San Diego, CA, June 13-17, 2010.

10. Moisseytsev, A. and Sienicki, J. J., "Analysis of SNL Compressor Tests," ANL-GenIV-136, Argonne National Laboratory, June 9, 2010.

11. Moisseytsev, A., and Sienicki, J. J., "Validation of the ANL Plant Dynamics Code Compressor Model with SNL/BNI Compressor Test Data," 2011 Supercritical CO_2 Power Cycle Symposium, Boulder, CO, May 24-25, 2011.

12. Sienicki, J. J., Moisseytsev, A., Fuller, R.L., Wright, S. A., and Pickard, P. S., "Scale Dependencies of Supercritical Carbon Dioxide Brayton Cycle Technologies and the Optimal Size for a Next-Step Supercritical CO_2 Cycle Demonstration," 2011 Supercritical CO_2 Power Cycle Symposium, Boulder, CO, May 24-25, 2011.

13. Vilim, R.B., "Development and Validation of a Radial Inflow Turbine Model for Simulation of the SNL S-CO_2 Split-Flow Loop," ANL-ARC-195, Argonne National Laboratory, August 2011.

14. Moisseytsev, A., Kulesza, K. P., and Sienicki, J. J., "Control System Options and Strategies for Supercritical CO_2 Cycles," ANL-GenIV-081, Argonne National Laboratory, August 31, 2006.

15. Aungier, R.H., Turbine Aerodynamics: Axial-Flow and Radial Inflow Turbine Design and Analysis, ASME Press, New York, 2006.

Appendix A
Input Files for SNL S-CO_2 Loop Modeling with the Plant Dynamics Code

Cycle modeling (Cycle_dat.txt)

```
****************  Input data file for CO2 cycle efficiency calculations ****************
Recalculate (1) or use output files (0) for the first iteration
0
Working fluid
CO2
Maximum pressure in cycle (MPa) (p_min and T_min are set in Comp input)
8.455
Generator efficiency,%
98.5
Mechanical losses,%
1.0
Maximum number of iterations
20
--------------------------- Components ------------------------------------------
+++++++++++++++++++++++++++++++++++++++++++++++++++++++++++++++++++++++++++++++++++++++++++++++++
+ Types:       HX     Turb    Comp    Cool    Rec            Mixer          Split    Valve Tank    +
+ Req. conn:C  I,CO   I,O     I,O     HI,HO   HI,HO,CI,CO    I1,I2,O        I,O1,O2  -     I,O     +
+                     (I=inlet, O=outlet, H=hot, C=cold, I1,I2,O1,O2=I/O with port number)        +
+ Each component should have unique name                                                          +
+ Name should correspond to input file (Turb -> Turb_dat.txt)                                     +
+++++++++++++++++++++++++++++++++++++++++++++++++++++++++++++++++++++++++++++++++++++++++++++++++
------------- HX(s) ------------------------
RHX
------------- Turbine(s) -------------------
TurbA
------------- Compressor(s) ----------------
CompA
------------- Cooler(s) -------------------
Cool
------------- Recuperator(s) ---------------
LTR
------------- Mixer(s) ---------------------
Tmx
Cmx
INVmx
------------- Splitter(s) ------------------
Tsp
Csp
INVsp
------------- Valve(s) ---------------------
TINv
COv
TBv
CBv
INVIv
INVOv
------------- Tank(s) ----------------------
Tank
------------------------ Pipes and connections ---------------------------------
++++++++++++++++++++++++++++++++++++++++++++++++++++++++++++++++++++++++++++++++++
+ For each pipe inlet and outlet should be specified as:                         +
+      component name + connection                                               +
+ See above for component names and connections types (case sensitive)           +
+ Pipe count, length, diameter and number of bends and curvature should also     +
+ be given                                                                       +
++++++++++++++++++++++++++++++++++++++++++++++++++++++++++++++++++++++++++++++++++
No.     Input          -      Output         Count   L,m     D,m            N_bends        r_b/D
1       RHX     CO     -      Tsp     I      1       3.4967  0.04285        3              1
2       Tsp     O1     -      TurbA   I      1       3.4967  0.04285        4              1
3       TurbA   O      -      Tmx     I1     1       5.4102  0.03399        2              1
4       Tmx     O      -      LTR     HI     1       2.0828  0.04285        3              1
5       LTR     HO     -      Csp     I      1       3.302   0.03399        3              1
```

```
6       Csp     O1      -       Cool    HI      1       3.302   0.03399         3               1
7       Cool    HO      -       INVsp   I       1       2.6551  0.03399         4               1
8       INVsp   O1      -       INVmx   I1      1       0.1     0.03399         4               1
9       INVmx   O       -       CompA   I       1       2.6551  0.03399         4               1
10      CompA   O       -       Cmx     I1      1       2.5527  0.03399         1               1
11      Cmx     O       -       LTR     CI      1       2.5527  0.03399         1               1
12      LTR     CO      -       RHX     CI      1       5.0292  0.03399         3               1
13      Tsp     O2      -       Tmx     I2      1       10      0.05            1               1
14      Csp     O2      -       Cmx     I2      1       10      0.05            1               1
15      INVsp   O2      -       Tank    I       1       3       0.01            2               1
16      Tank    O       -       INVmx   I2      1       3       0.01            2               1
----------------------- Flow splits -------------------------------------------
+++++++++++++++++++++++++++++++++++++++++++++++++++++++++++++++++++++++++++++++
+ For each Split (list by Name) specify primary (O1) outlet flow fraction       +
+++++++++++++++++++++++++++++++++++++++++++++++++++++++++++++++++++++++++++++++
Split   Primary_fraction
Tsp     1
Csp     1
INVsp   1
----------------------- Valves ------------------------------------------------
++++++++++++++++++++++++++++++++++++++++++++++++++++++++++++++++++++++++++++++++
+ For each valve (list by Name) specify the location (pipe #) and resistance      +
+                                                                                 +
+ Resistance>=0 corresponds to pressure drop across the vale in MPa               +
+                   (0 - no effect from valve)                                    +
+ Resistance=-1 corresponds that dP should be calculated in cycle                 +
+                 (includes closed valves)                                        +
++++++++++++++++++++++++++++++++++++++++++++++++++++++++++++++++++++++++++++++++
Valve   Pipe#   Resistance
TINv    2       0
COv     10      0
TBv     13      -1
CBv     14      -1
INVIv   15      -1
INVOv   16      -1
-------------------------------------------------------------------------------
```

Compressor Input (CompA_dat.txt)

```
************************** Compressor #1 ******************************
Efficiency (for first guess, static-to-static, <0 = use given design at EOF), %
-77.6
Shaft revolution speed (rev/s)
416.667
Desired pressure ratio
1.1
Min. temperature control flag and value, C (used only if flag=1)
1 32.248D0
Min. pressure control flag and value, MPa (used only if flag=1)
1 7.690D0
Outlet pressure control flag and value, MPa (used only if flag=1)
0 20D0
Accuracy on exit pressure
1.D-8
Inlet nozzle efficiency, %
90
Compressor type (1-axial, 2-centrigugal)
2
--------------------- Axial compressor data ---------------------------
        .
        .
        . Data for the compressor design is not used and is omitted from this report
        .
        .
====================== (Centrifugal) compressor data ================================
Number of stages (imp. and diff. parameters below should be given as arrays for each stage)
1
IGV angle, deg
0
Return channel loss coefficient
0.4
Blade surface roughness, mkm
4.1
Number of labyrinth seals on impeller tip (0-unshrouded)
0
---------- Impeller ------------------------
Impeller hub radius at inlet, mm
2.537485
Impeller tip radius at inlet, mm
9.372047
Impeller inlet blade angle (with respect to axial direction), deg
-65 -45
Impeller discharge blade angle (with respect to radial direction), deg
-40
Impeller discharge radius, mm
18.6817
Blade height at discharge, mm
1.712036
Number of full blades
6
Number of splitter blades
6
Splitter blade length, fraction of full blade length
0.51
Blade thickness, mm
0.762
Blade length, mm
25.908
Tip (shroud) clearance-to-radius ratio
0.022
-------- Diffuser (nozzle) -------------------
Number of diffuser blades (0-vaneless diffuser)
17
```

```
Diffuser inner radius, mm
19.228
Diffuser outer radius, mm
33.621
Diffuser inlet blade angle (with respect to radial direction), deg
77.8
Diffuser discharge blade angle (with respect to radial direction), deg
33.99
Blade height at inlet, mm
1.905
Blade height at discharge, mm
1.905
Diffuser blade thickness at inlet, mm
0
Diffuser blade thickness at discharge, mm
6.591
Blade length, mm
23.812
-------------------- Shaft windage loss data --------------------------
Shaft cavity temperature (T-drain), K (<0, -F)
-40.36
Shaft cavity pressure (P-drain), MPa (<0, -psia)
3.802
CO2 vapor quality (0=liquid, 1=gas, for first guess on density)
1
Shaft radius, mm
25.4
Gap thickness, mm
3.175
Length of rotor, mm
168
```

Turbine Input (TurbA_dat.txt)

```
****************************** Turbine ******************************
Efficiency (for first guess, static-to-static), %
-92.3
Shaft revolution speed (rev/s)
416.667
Desired pressure ratio
1.08
        .
        .
        . Data for the turbine design is not used and is omitted from this report
        .
        .
**************************** Radial Turbine Design Data ***************************
Number of stages
1
Surface Roughness, m
1.7D-6
----------------------------- VOLUTE ---------------------------------------------
Inlet radius, m
0.159385D0
Outlet radius, m
0.083185D0
Inlet height, m
0.006096D0
Outlet height, m
0.006096D0
----------------------------NOZZLE (each entry is array for N_st)---------------------
Blade Height at Inlet, m
0.0038D0
Blade Height at Throat, m
0.0038D0
Blade Height at Outlet, m
0.0038D0
Radius at Inlet, m
0.0477D0
Radius at Throat, m
0.0366D0
Radius at Outlet, m
0.0349D0
Blade Number
10
Distance between blades at throat, m
0.0033D0
Chord Length, m
0.0303D0
Meridional distance to throat, m
0.0150D0
Meridional distance to trailing edge, m
0.0303D0
Blade Thickness at Inlet, m
0.0000D0
Blade Thickness at Throat, m
0.009D0
Blade Thickness at Outlet, m
0.0000D0
Blade angle at Inlet, degree
39.0D0
Blade angle at throat, degree
17.0D0
Blade angle at Outlet, degree
13.0D0
----------------------------ROTOR (each entry is array for N_st)---------------------
Blade Height at Inlet, m
0.0044D0
```

```
Blade Height at Throat, m
0.0096D0
Blade Thickness at Inlet, m
7.1D-4
Blade Thickness at Throat, m
7.1D-4
Blade Thickness at Outlet, m
7.1D-4
Radius at Inlet, m
0.0338D0
Tip Radius at Outlet, m
0.0064D0
Hub Radius at Outlet, m
0.01595D0
Radius at Throat, m
0.011175D0
Blade angle at Inlet, degree
90D0
Blade angle at Outlet, degree
-30D0
Passage curvature angle at inlet, degree
-90D0
Passage curvature angle at outlet, degree
0D0
Number of full blades
11
Number of splitter blades
0
Splitter blade fractional length
0.D0
Distance between blades at throat, m
0.00338D0
Chord Length, m
0.0366D0
Blade-shroud clearance gap, m
0.13D-3
```

Heater Input (RHX_dat.txt)

```
************* Reactor Heat Exchanger parameters ******************************
Type (0 - General, 1 - Shell-and-tube, 2 - Platelet PCHE, 3 - Z/I PCHE)
1
Given target efficiency on COLD SIDE (for general only), %
90.1
Given pressure drops for hot and cold sides (for general only), Pa
2.2D3 51.5D3
Hot side inlet and outlet plena volumes, m3
0 0
Cold side inlet and outlet plena volumes, m3
0 0
First guess for cold side inlet and outlet temperatures, if needed, C
78.7 152.1
----------------------- Shell-and-tube HX data -----------------------------
Outer diameter, m
0.0945  (for 12 tubes)
Length, m
4.546  =2.273x2
Inner and outer tube diameters, m
0.0135 0.0155
Tube pitch-to-diameter ratio
1.679
Tube material (5 characters)
SS316
Number of points for temperature calculations
21
Required accuracy (in secondary outlet temperature), C
1D-6
Tube side (1 - Primary, 2 - Secondary)
1
Heat transfer correlations for hot and cold sides
DB
DB
Number of fins on inner surface per tube
0
Width of fins on inner surface ,m
0.001
Length of fins on inner surface , m
0.0015
Number of fins on outer surface per tube
0
Width of fins on outer surface ,m
0.001
Length of fins on outer surface , m
0.0025
--------------------- PCHE data ---------------------------------------
        .
        .
        . PCHE Type data is not used and is omitted from this report
        .
        .
```

Heater (RHX) Hot Side Input (RHX_HS_dat.txt)

```
************* Input data for RHX hot side *******************
RHX primary fluid (RPF)
Na
RPF inlet temperature, C
197
RPF outlet temperature, C
187
RPF inlet pressure, MPa
0.1
RHX total power, MW
88.85D-3
```

LTR Input (LTR_dat.txt)

```
************* High Temperature Recuperator parameters ******************************
Type (0 - General, 1 - Shell-and-tube, 2 - Platelet PCHE, 3 - Z/I PCHE)
2
Given efficiency (for general only), %
95.1
Given pressure drops for hot and cold sides (for general only), Pa
36.1D3 13.1D3
Hot side inlet and outlet plena volumes, m3
0 0
Cold side inlet and outlet plena volumes, m3
0 0
First guess for inlet temperatures, hot and cold side, if needed, C
141.6 35.0
------------------------ Shell-and-tube HX data -----------------------------
        .
        .
        . Shell-and-tube Type data is not used and is omitted from this report
        .
        .
---------------------- PCHE data ---------------------------------------
Number of units (<0 - find N_unit to match hot outlet temperature)
1
Unit length, m
0.53
Unit width, m
0.345
Unit height, m
0.201
Headers length (each side), cm
10
Pressure boundary thickness, mm
14
Zigzag channel angles (hot and cold sides), deg
25 65
Fin efficiency
0.7
HT region pressure drop / total pressure drop ratio
0.7
Channel diameter (width) (hot and cold sides), mm
0.89 0.81
Channel depth (hot and cold sides, input 0 for PCHE), mm
0 0
Pitch-to-diameter ratio (hot and cold sides)
1.938 1.927
Layer thickness (hot and cold sides), mm
0.755 0.715
Material
SS316
Number of points for temperature calculations
21
Required accuracy (in secondary outlet temperature), C
1D-6
Heat transfer correlation (hot and cold sides) (DB, PG, MN, WF, PC)
PC
PC
```

Cooler Input (Cool_dat.txt)

```
************* Cooler parameters ******************************
Cooling fluid (3 characters)
H2O
Inlet temperature of cooling fluid, C
19.3
Outlet pressure of cooling fluid, Pa
0.116D6
Cooling fluid flow rate, kg/s
-1.213
Cooling fluid inlet and outlet pipe diameters, m
1.0 1.0
CO2 side inlet and outlet plena volumes, m3
0 0
Cooling fluid pump efficiency, %
90
Accuracy on outlet temperature
1.D-6
Cooler type (1 - Shell-and-tube, 2 - PCHE)
2
----------------------- Shell-and-tube HX data -----------------------------
        .
        .
        . Shell-and-tube Type data is not used and is omitted from this report
        .
        .
--------------------- PCHE HX data ---------------------------------------
Number of units
1
Unit length, m (<0 - find L to match hot outlet temperature)
0.496
Unit width, m
0.196
Unit height, m
0.199
Headers length (each side), cm
5  0
Pressure boundary thickness, mm
12
Zigzag channel angles (hot and cold sides), deg
60 60
Fin efficiency
1.0   0.7
HT region pressure drop / total pressure drop ratio
0.8 0.8
Channel diameter (width) (hot and cold sides), mm
1.611 1.611
Channel depth (hot and cold sides, input 0 for PCHE), mm
0 0
Pitch-to-diameter ratio (hot and cold sides)
1.285 1.285
Layer thickness (hot and cold sides), mm
1.265 1.265
Material
SS316
Number of points for temperature calculations
21 101
Required accuracy (in secondary outlet temperature), C
1D-6
Heat transfer correlation (hot and cold sides) (DB, PG, MN, WF, PC)
PC
PC
```

Appendix B
Output Files from the Plant Dynamics Code for SNL S-CO_2 Loop Modeling

Cycle results (Cycle_res.txt)

```
*****************  Input data file for CO2 cycle efficiency calculations *****************
*Recalculate (1) or use output files (0) for the first iteration                         *
*0                                                                                        *
*Working fluid                                                                            *
*CO2                                                                                      *
*Maximum pressure in cycle (MPa) (p_min and T_min are set in Comp input)                  *
*8.455                                                                                    *
*Generator efficiency,%                                                                   *
*98.5                                                                                     *
*Mechanical losses,%                                                                      *
*1.0                                                                                      *
*Maximum number of iterations                                                             *
*20                                                                                       *
*---------------------------- Components ------------------------------------------       *
*+++++++++++++++++++++++++++++++++++++++++++++++++++++++++++++++++++++++++++++++++++++++++*
*+ Types:        HX      Turb    Comp    Cool    Rec             Mixer           Split   *
*+ Req. conn:    CI,CO   I,O     I,O     HI,HO   HI,HO,CI,CO     I1,I2,O         I,O1,O2 *
*+                       (I=inlet, O=outlet, H=hot, C=cold, I1,I2,O1,O2=I/O with port num*
*+ Each component should have unique name                                                 *
*+ Name should correspond to input file (Turb -> Turb_dat.txt)                            *
*+++++++++++++++++++++++++++++++++++++++++++++++++++++++++++++++++++++++++++++++++++++++++*
*------------- HX(s) ------------------------                                            *
*RHX                                                                                      *
*------------- Turbine(s) -------------------                                            *
*TurbA                                                                                    *
*------------- Compressor(s) ----------------                                            *
*CompA                                                                                    *
*------------- Cooler(s) -------------------                                             *
*Cool                                                                                     *
*------------- Recuperator(s) ---------------                                            *
*LTR                                                                                      *
*------------- Mixer(s) ---------------------                                            *
*Tmx                                                                                      *
*Cmx                                                                                      *
*INVmx                                                                                    *
*------------- Splitter(s) ------------------                                            *
*Tsp                                                                                      *
*Csp                                                                                      *
*INVsp                                                                                    *
*------------- Valve(s) ---------------------                                            *
*TINv                                                                                     *
*COv                                                                                      *
*TBv                                                                                      *
*CBv                                                                                      *
```

```
*INVIv                                                                          *
*INVOv                                                                          *
*------------- Tank(s) ----------------------                                   *
*Tank                                                                            *
*------------------------ Pipes and connections ----------------------------------*
*++++++++++++++++++++++++++++++++++++++++++++++++++++++++++++++++++++++++++++++++*
*+ For each pipe inlet and outlet should be specified as:                       +*
*+       component name + connection                                            +*
*+ See above for component names and connections types (case sensitive)          +*
*+ Pipe count, length, diameter and number of bends and curvature should also    +*
*+ be given                                                                      +*
*++++++++++++++++++++++++++++++++++++++++++++++++++++++++++++++++++++++++++++++++*
*No.     Input          -       Output         Count   L,m     D,m     N_bends r_b/D   *
*1       RHX     CO     -       Tsp     I      1       3.4967  0.04285 3       1       *
*2       Tsp     O1     -       TurbA   I      1       3.4967  0.04285 4       1       *
*3       TurbA   O      -       Tmx     I1     1       5.4102  0.03399 2       1       *
*4       Tmx     O      -       LTR     HI     1       2.0828  0.04285 3       1       *
*5       LTR     HO     -       Csp     I      1       3.302   0.03399 3       1       *
*6       Csp     O1     -       Cool    HI     1       3.302   0.03399 3       1       *
*7       Cool    HO     -       INVsp   I      1       2.6551  0.03399 4       1       *
*8       INVsp   O1     -       INVmx   I1     1       0.1     0.03399 4       1       *
*9       INVmx   O      -       CompA   I      1       2.6551  0.03399 4       1       *
*10      CompA   O      -       Cmx     I1     1       2.5527  0.03399 1       1       *
*11      Cmx     O      -       LTR     CI     1       2.5527  0.03399 1       1       *
*12      LTR     CO     -       RHX     CI     1       5.0292  0.03399 3       1       *
*13      Tsp     O2     -       Tmx     I2     1       10      0.05    1       1       *
*14      Csp     O2     -       Cmx     I2     1       10      0.05    1       1       *
*15      INVsp   O2     -       Tank    I      1       3       0.01    2       1       *
*16      Tank    O      -       INVmx   I2     1       3       0.01    2       1       *
*----------------------- Flow splits -------------------------------------------*
*++++++++++++++++++++++++++++++++++++++++++++++++++++++++++++++++++++++++++++++++*
*+ For each Split (list by Name) specify primary (O1) outlet flow fraction       +*
*++++++++++++++++++++++++++++++++++++++++++++++++++++++++++++++++++++++++++++++++*
*Split   Primary_fraction                                                        *
*Tsp     1                                                                       *
*Csp     1                                                                       *
*INVsp   1                                                                       *
*----------------------- Valves ------------------------------------------------*
*++++++++++++++++++++++++++++++++++++++++++++++++++++++++++++++++++++++++++++++++*
*+ For each valve (list by Name) specify the location (pipe #) and resistance    +*
*+                                                                               +*
*+ Resistance>=0 corresponds to pressure drop across the vale in MPa             +*
*+                   (0 - no effect from valve)                                  +*
*+ Resistance=-1 corresponds that dP should be calculated in cycle               +*
*+                 (includes closed valves)                                      +*
*++++++++++++++++++++++++++++++++++++++++++++++++++++++++++++++++++++++++++++++++*
*Valve   Pipe#   Resistance                                                      *
```

```
*TINv    2       0                                                          *
*COv     10      0                                                          *
*TBv     13      -1                                                         *
*CBv     14      -1                                                         *
*INVIv   15      -1                                                         *
*INVOv   16      -1                                                         *
*-----------------------------------------------------------------------     *
********************************** End of Input Data ************************************
 ******** Results ************
 -------- Cycle nodes ----------
```

Point#	Component	Conn.	p MPa	T C	s kJ/kg-K	h kJ/kg	rho kg/m3	w m/s	cp kJ/kg-K
1	RHX	CO	8.390	152.861	-5.820E-01	7.664E+01	1.179E+02	3.030E+02	1.189E+00
2	Tsp	I	8.387	152.848	-5.819E-01	7.664E+01	1.179E+02	3.030E+02	1.189E+00
3	Tsp	O1	8.387	152.848	-5.819E-01	7.664E+01	1.179E+02	3.030E+02	1.189E+00
4	TurbA	I	8.383	152.833	-5.819E-01	7.664E+01	1.178E+02	3.030E+02	1.189E+00
5	TurbA	O	7.751	145.829	-5.809E-01	7.150E+01	1.107E+02	2.999E+02	1.178E+00
6	Tmx	I1	7.738	139.850	-5.975E-01	6.450E+01	1.131E+02	2.967E+02	1.187E+00
7	Tmx	O	7.738	139.850	-5.975E-01	6.450E+01	1.131E+02	2.967E+02	1.187E+00
8	LTR	HI	7.735	139.839	-5.974E-01	6.450E+01	1.130E+02	2.967E+02	1.187E+00
9	LTR	HO	7.719	36.501	-1.100E+00	-1.109E+02	2.841E+02	1.997E+02	6.288E+00
10	Csp	I	7.715	36.470	-1.100E+00	-1.109E+02	2.839E+02	1.997E+02	6.291E+00
11	Csp	O1	7.715	36.470	-1.100E+00	-1.109E+02	2.839E+02	1.997E+02	6.291E+00
12	Cool	HI	7.711	36.440	-1.100E+00	-1.109E+02	2.838E+02	1.997E+02	6.294E+00
13	Cool	HO	7.707	32.320	-1.376E+00	-1.954E+02	5.786E+02	1.943E+02	1.978E+01
14	INVsp	I	7.706	32.313	-1.376E+00	-1.954E+02	5.785E+02	1.941E+02	1.983E+01
15	INVsp	O1	7.706	32.313	-1.376E+00	-1.954E+02	5.785E+02	1.941E+02	1.983E+01
16	INVmx	I1	7.705	32.309	-1.376E+00	-1.954E+02	5.785E+02	1.941E+02	1.986E+01
17	INVmx	O	7.705	32.309	-1.376E+00	-1.954E+02	5.785E+02	1.941E+02	1.986E+01
18	CompA	I	7.703	32.302	-1.376E+00	-1.954E+02	5.784E+02	1.940E+02	1.992E+01
19	CompA	O	8.410	35.109	-1.375E+00	-1.939E+02	5.927E+02	2.201E+02	1.053E+01
20	Cmx	I1	8.409	35.105	-1.375E+00	-1.939E+02	5.926E+02	2.200E+02	1.054E+01
21	Cmx	O	8.409	35.105	-1.375E+00	-1.939E+02	5.926E+02	2.200E+02	1.054E+01
22	LTR	CI	8.408	35.100	-1.375E+00	-1.939E+02	5.926E+02	2.200E+02	1.055E+01
23	LTR	CO	8.399	80.396	-8.277E-01	-1.842E+01	1.710E+02	2.559E+02	1.560E+00
24	RHX	CI	8.390	80.340	-8.276E-01	-1.842E+01	1.709E+02	2.558E+02	1.559E+00
25	Tsp	O2	8.387	152.848	-5.819E-01	7.664E+01	1.179E+02	3.030E+02	1.189E+00
26	Tmx	I2	7.738	139.850	-5.975E-01	6.450E+01	1.131E+02	2.967E+02	1.187E+00
27	Csp	O2	7.715	36.470	-1.100E+00	-1.109E+02	2.839E+02	1.997E+02	6.291E+00
28	Cmx	I2	8.409	35.105	-1.375E+00	-1.939E+02	5.926E+02	2.200E+02	1.054E+01
29	INVsp	O2	7.706	32.313	-1.376E+00	-1.954E+02	5.785E+02	1.941E+02	1.983E+01
30	Tank	O2	8.000	40.000	-1.081E+00	-1.039E+02	2.779E+02	2.058E+02	4.961E+00
31	Tank	O2	8.000	40.000	-1.081E+00	-1.039E+02	2.779E+02	2.058E+02	4.961E+00
32	INVmx	I2	7.705	0.000	-1.768E+00	-3.101E+02	9.600E+02	6.109E+02	2.267E+00

```
 -------- Pipe flows ----------
  Pipe# Start  End      m          A         u          M#     dp_f/dL     dp_f       dp_b       dp_v       dp_tot
```

	Node	Node	kg/s	m2	m/s	-	kPa/m	kPa	kPa	kPa	kPa
1	1	2	9.347E-01	1.442E-03	5.497E+00	0.018	6.186E-01	2.163E+00	1.021E+00	0.000E+00	3.184E+00
2	3	4	9.347E-01	1.442E-03	5.499E+00	0.018	6.188E-01	2.164E+00	1.362E+00	0.000E+00	3.526E+00
3	5	6	9.347E-01	9.074E-04	9.206E+00	0.031	2.141E+00	1.158E+01	1.735E+00	0.000E+00	1.332E+01
4	7	8	9.347E-01	1.442E-03	5.733E+00	0.019	6.443E-01	1.342E+00	1.060E+00	0.000E+00	2.402E+00
5	9	10	9.347E-01	9.074E-04	3.627E+00	0.018	8.442E-01	2.787E+00	1.030E+00	0.000E+00	3.818E+00
6	11	12	9.347E-01	9.074E-04	3.628E+00	0.018	8.445E-01	2.789E+00	1.031E+00	0.000E+00	3.820E+00
7	13	14	9.347E-01	9.074E-04	1.780E+00	0.009	4.249E-01	1.128E+00	7.516E-01	0.000E+00	1.880E+00
8	15	16	9.347E-01	9.074E-04	1.781E+00	0.009	4.249E-01	4.249E-02	7.516E-01	0.000E+00	7.941E-01
9	17	18	9.347E-01	9.074E-04	1.781E+00	0.009	4.250E-01	1.128E+00	7.517E-01	0.000E+00	1.880E+00
10	19	20	9.347E-01	9.074E-04	1.738E+00	0.008	4.155E-01	1.061E+00	1.845E-01	0.000E+00	1.245E+00
11	21	22	9.347E-01	9.074E-04	1.738E+00	0.008	4.155E-01	1.061E+00	1.845E-01	0.000E+00	1.245E+00
12	23	24	9.347E-01	9.074E-04	6.025E+00	0.024	1.398E+00	7.033E+00	1.684E+00	0.000E+00	8.717E+00
13	25	26	0.000E+00	1.963E-03	0.000E+00	0.000	0.000E+00	0.000E+00	0.000E+00	6.489E+02	6.489E+02
14	27	28	0.000E+00	1.963E-03	0.000E+00	0.000	0.000E+00	0.000E+00	0.000E+00	-6.941E+02	-6.941E+02
15	29	30	0.000E+00	7.854E-05	0.000E+00	0.000	0.000E+00	0.000E+00	0.000E+00	-2.945E+02	-2.945E+02
16	31	32	0.000E+00	7.854E-05	0.000E+00	0.000	0.000E+00	0.000E+00	0.000E+00	2.953E+02	2.953E+02

```
 --------- Mass flow rate -------------
m =    0.9347 kg/s
 --------- Turbine/compressor efficiencies -------------
TurbA   92.9545 %
CompA   77.6120 %
 --------- Turbine/compressor axial speeds -------------
TurbA   60.0000 m/s
CompA   40.0000 m/s
 --------- Turbine/compressor exit speeds -------------
TurbA   15.6112 m/s
CompA   11.0894 m/s
 --------- Recuperator efficiencies -------------
LTR     98.6627 %
 --------- Recuperators pressure drops -------------
LTR  : LP     0.0464 %
LTR  : HP     0.1045 %
 --------- Cooler(s) parameters -------------
 ---Cool ---
L_cooler=    0.4960 m
PD_cooler=    0.0465 %
PD2_cooler=    0.0068 MPa
m_w=    1.2028 kg/s
Tw_out=   35.0134 C
pw_in=    0.1228 MPa
Effectiveness =   91.6795 %
 --------- Works -------------
W_TurbA  =    0.0047 MW
W_CompA  =    0.0015 MW
W_Cool _pump  =    0.0000 MW
Q_RHX     =    0.0888 MW
```

```
Q_RHX    =    0.0889 MW
Q_LTR    =    0.1639 MW
Q_Cool   =    0.0790 MW
W_gen (gross)  =    0.0031 MW
 -------------------- Working Fluid Inventory --------------------
 ----- Inside components -----------
M_TurbA  =    0.0000 kg
M_CompA  =    0.0000 kg
M_RHX    =    9.1963 kg
M_LTR    =    1.3776 kg
M_Cool   =    0.8096 kg
 ----- Inside pipes ---------------
Pipe       1         0.6 kg
Pipe       2         0.6 kg
Pipe       3         0.5 kg
Pipe       4         0.3 kg
Pipe       5         0.9 kg
Pipe       6         0.9 kg
Pipe       7         1.4 kg
Pipe       8         0.1 kg
Pipe       9         1.4 kg
Pipe      10         1.4 kg
Pipe      11         1.4 kg
Pipe      12         0.8 kg
Pipe      13         2.3 kg
Pipe      14         8.6 kg
Pipe      15         0.1 kg
Pipe      16         0.1 kg
 -----------------------------------------------------
TOTAL               32.6 kg
 =========== Brayton cycle efficiency ==========
E=    3.4558 %
```

Equipment Design and Performance Results (BC_des.txt)

Division	Items	Spec. (SI)	Unit	Remarks
RHX	Type	S&T		
	Quantity	1		All parameters below are per unit
	Heat transfer capacity	0.09	MWt	
	Hot side fluid	Na		
	Hot side temperature inlet	197.0	C	
	Hot side temperature outlet	187.0	C	
	Hot side pressure inlet	0.100	MPa	
	Hot side pressure outlet	0.032	MPa	
	Hot side flow rate	6.6	kg/s	
	Hot side pressure drop	68.1	kPa	
	Cold side fluid	CO2		
	Cold side temperature inlet	80.3	C	
	Cold side temperature outlet	152.9	C	
	Cold side pressure inlet	8.390	MPa	
	Cold side pressure outlet	8.390	MPa	
	Cold side flow rate	0.9	kg/s	
	Cold side pressure drop	0.4	kPa	
	Efficiency	62.2	%	
	Efficiency (CO2 side)	62.2	%	
	Properties			
	Hot side - inlet			
	Density	903.7	kg/m3	
	Spec. heat	1344.5	J/kg-K	
	Viscosity	456.6	mkPa*s	
	Thermal cond.	82138.8	mW/m-K	
	Hot side - outlet			
	Density	905.9	kg/m3	
	Spec. heat	1348.2	J/kg-K	
	Viscosity	472.6	mkPa*s	
	Thermal cond.	82840.0	mW/m-K	
	Cold side - inlet			
	Density	170.9	kg/m3	
	Spec. heat	1559.0	J/kg-K	
	Viscosity	20.4	mkPa*s	
	Thermal cond.	28.4	mW/m-K	
	Cold side - outlet			
	Density	117.9	kg/m3	
	Spec. heat	1189.3	J/kg-K	
	Viscosity	22.3	mkPa*s	
	Thermal cond.	31.3	mW/m-K	
LTR	Type	PCHE		
	Quantity	1		All parameters below are per unit
	Heat transfer capacity	0.16	MWt	
	Hot side temperature inlet	139.8	C	
	Hot side temperature outlet	36.5	C	
	Hot side pressure inlet	7.735	MPa	
	Hot side pressure outlet	7.719	MPa	
	Hot side flow rate	0.9	kg/s	
	Hot side pressure drop	16.7	kPa	
	Cold side temperature inlet	35.1	C	
	Cold side temperature outlet	80.4	C	
	Cold side pressure inlet	8.408	MPa	
	Cold side pressure outlet	8.399	MPa	
	Cold side flow rate	0.9	kg/s	
	Cold side pressure drop	8.8	kPa	
	Efficiency	98.7	%	
	Heat transfer area	16.3	m2	
	Unit width	0.345	m	
	Unit height	0.201	m	
	Unit length	0.530	m	
	Heat transfer length	0.330	m	

	Plate material	SS316		
	Number of plates	118		Each side
	Hot side channel diameter	0.9	mm	Semi-circular channel
	Hot side channel pitch	1.7	mm	
	Hot side plate thickness	0.8	mm	
	Hot side number of channels	179		Per plate
	Hot side channel length	0.338	m	Heat transfer region
	Hot side channel angle	25.0	deg	
	Cold side channel diameter	0.8	mm	Semi-circular channel
	Cold side channel pitch	1.6	mm	
	Cold side plate thickness	0.7	mm	
	Cold side number of channels	171		Per plate
	Cold side channel length	0.391	m	Heat transfer region
	Cold side channel angle	65.0	deg	
	Void fraction	21.5	%	From channels
	Metal mass	0.229	tonnes	Dry
	Cost	13.7	K$	
	CO2 mass	1.4	kg	Operating conditions
	Properties			
	Hot side - inlet			
	Density	113.0	kg/m3	
	Spec. heat	1187.2	J/kg-K	
	Viscosity	21.7	mkPa*s	
	Thermal cond.	30.0	mW/m-K	
	Hot side - outlet			
	Density	284.1	kg/m3	
	Spec. heat	6287.5	J/kg-K	
	Viscosity	22.5	mkPa*s	
	Thermal cond.	45.6	mW/m-K	
	Cold side - inlet			
	Density	592.6	kg/m3	
	Spec. heat	10546.5	J/kg-K	
	Viscosity	43.9	mkPa*s	
	Thermal cond.	75.4	mW/m-K	
	Cold side - outlet			
	Density	171.0	kg/m3	
	Spec. heat	1559.5	J/kg-K	
	Viscosity	20.4	mkPa*s	
	Thermal cond.	28.5	mW/m-K	
Cool	Type	PCHE		
	Quantity	1		All parameters below are per unit
	Heat transfer capacity	0.08	MWt	
	Heat transfer area	9.4	m2	
	Unit width	0.196	m	
	Unit hieght	0.199	m	
	Unit length	0.496	m	
	Heat transfer length	0.396	m	
	Number of plates	69		Each side
	Plate material	SS316		
	CO2 side channel diameter	1.6	mm	Semi-circular channel
	CO2 side channel pitch	2.1	mm	
	CO2 side plate thickness	1.26	mm	
	CO2 side number of channels	72		Per plate
	CO2 side channel length	0.457	m	Heat transfer region
	CO2 side channel angle	60.0	deg	
	H2O side channel diameter	1.6	mm	Semi-circular channel
	H2O side channel pitch	2.1	mm	
	H2O side plate thickness	1.26	mm	
	H2O side number of channels	72		Per plate
	H2O side channel length	0.457	m	Heat transfer region
	H2O side channel angle	60.0	deg	
	Void fraction	34.2	%	From channels
	CO2 temperature inlet	36.4	C	
	CO2 temperature outlet	32.32	C	
	CO2 pressure inlet	7.711	MPa	
	CO2 pressure outlet	7.707	MPa	

	CO2 flow rate	0.9	kg/s	
	CO2 side pressure drop	3.6	kPa	
	Water temperature inlet	19.3	C	
	Water temperature outlet	35.0	C	
	Water pressure inlet	0.123	MPa	
	Water pressure outlet	0.116	MPa	
	Water flow rate	1.2	kg/s	
	Water side pressure drop	6.8	kPa	
	Water pump power	0.000	MW	Total all units
	Efficiency	91.7	%	
	Metal mass	0.101	tonnes	Dry
	Cost	6.1	K$	
	CO2 mass	0.8	kg	Operating conditions
	Properties			
	CO2 side - inlet			
	Density	283.8	kg/m3	
	Spec. heat	6294.0	J/kg-K	
	Viscosity	22.4	mkPa*s	
	Thermal cond.	45.6	mW/m-K	
	CO2 side - outlet			
	Density	578.6	kg/m3	
	Spec. heat	19775.2	J/kg-K	
	Viscosity	42.4	mkPa*s	
	Thermal cond.	83.6	mW/m-K	
	H2O side - inlet			
	Density	998.3	kg/m3	
	Spec. heat	4184.6	J/kg-K	
	Viscosity	1.019	mPa*s	
	Thermal cond.	0.597	W/m-K	
	H2O side - outlet			
	Density	994.0	kg/m3	
	Spec. heat	4179.3	J/kg-K	
	Viscosity	0.719	mPa*s	
	Thermal cond.	0.623	W/m-K	
TurbA	Type	Axial		
	Power	0.00	MW	
	Number of stages	6		
	Rotational speed	416.7	rev/s	
	Max Mach number	0.00		
	CO2 temperature inlet	152.8	C	
	CO2 temperature outlet	145.8	C	
	CO2 pressure inlet	8.38	MPa	
	CO2 pressure outlet	7.751	MPa	
	CO2 flow rate	0.9	kg/s	
	Efficiency	0.0	%	Total-to-static
	CO2 mass	0.0	kg	Operating conditions
CompA	Type	Centr.		
	Power	0.00	MW	
	Number of stages	1		
	Rotational speed	416.7	rev/s	
	Axial length	0.00	m	Without casing, estimated
	Max diameter	0.07	m	Without casing and volute
	Hub radius min	0.3	cm	
	Hub radius max	0.3	cm	
	Impeller radius min	1.9	cm	
	Impeller radius max	1.9	cm	
	Blade height min	0.2	cm	
	Blade height max	0.7	cm	
	Blade length min	2.4	cm	
	Blade length max	2.6	cm	
	Max Mach number	0.00		
	CO2 temperature inlet	32.30	C	
	CO2 temperature outlet	35.1	C	
	CO2 pressure inlet	7.703	MPa	
	CO2 pressure outlet	8.41	MPa	
	CO2 flow rate	0.9	kg/s	

```
|               | Efficiency                    |      0.0 | %       | Total-to-static                   |
|               | CO2 mass                      |      0.0 | kg      | Operating conditions              |
|---------------|-------------------------------|----------|---------|-----------------------------------|
```

Turbine Performance Results (RadTurb_res.txt)

```
        ************ Results for Radial Turbine ***************
 ----------------Inlet parameters----------------
*-------------------------------------------*-------------*--------*
| Turbine inlet pressure                    |       8.3831| MPa    |
|-------------------------------------------|-------------|--------|
| Turbine inlet temperature                 |     152.8333| C      |
|-------------------------------------------|-------------|--------|
| Fluid mass flow rate                      |       0.9347| kg/s   |
|-------------------------------------------|-------------|--------|
| Shaft revolution speed                    |   25000.0200| RPM    |
*-------------------------------------------*-------------*--------*


         POSITION INDEX DESCRIPTION

 11 - Volute Inlet
 12 - Volute Outlet
 21 - Nozzle Inlet
 22 - Nozzle Throat
 23 - Nozzle Outlet
 31 - Rotor  Inlet
 32 - Rotor  Outlet


       PROPERTIES DISTRIBUTION BY LOCATION

Pos.            Pt,[MPa]       p,[MPa]     Tt, [C]     T,[C]  rhot,[kg/m3]  rho,[kg/m3]

  11         8.383052615         8.382952975    152.833302944502    152.832184464435      117.828240127522619
117.827154202053094
  12         8.383052419         8.382687093    152.833302138527    152.829197498699      117.828237375964406
117.824257495616948

  21         8.383052419         8.380126879    152.829197498699    152.800422243901      117.828237376085070
117.796367407307898
  22         8.367672089         8.117382854    152.770187791519    149.917093590598      117.612884694934479
114.874692999048492
  23         8.365307287         8.155953106    152.760483945522    150.378318364827      117.579785343477226
115.290961216568277

  31         8.365308002         8.143510506    152.760482876606    150.235157170969      117.579781231375179
115.154416573750169
  33         7.764532579         7.751030336    145.990731292464    145.828899881271      110.882534392284342
110.732450796763743


                                          s,[kJ/kg-K]  Ht,[kJ/kg]  h,[kJ/kg]

   11      -0.58185370713       76.6400465885       76.6392024122
   12      -0.58185369930       76.6400465885       76.6369473188

   21      -0.58185368759       76.6400465887       76.6152208525
   22      -0.58154697550       76.6400465887       74.4868394066
   23      -0.58149977774       76.6400465887       74.8419681752

   31      -0.58149977774       76.6400465887       74.7339857170
   33      -0.58092371866       71.6231495354       71.5012953730


                      FLOW / RELATIVE / BLADE ANGLES (DEG)

  N-IN ***** N-OUT ***** R-IN ****** R-OUT
```

```
    90.00000   9.44425   8.39822  65.12028
    90.00000   9.44425  18.21196 -31.97300
    39.00000  13.00000  90.00000 -30.00000


       VELOCITY PROFILES
 St  Pos    Cm                      Ct                      C                  M#         Vsd,[m/s]

   21       7.0463800928635       0.0000000000000       7.0463800928635         0.0233       302.9829
   23       9.8400126323621      59.1551432959776      59.9679650060988         0.1986       301.9008

   31       9.0176155574542      61.0803106813497      61.7423820667153         0.2046       301.8368
   33      14.1623355851551       6.5678440605720      15.6111602653531         0.0521       299.9057


  Wm       Wt      W          U
       9.0176155574542   -27.4079531853172    28.8533063642727       88.4882638667
      14.1623355851551   -22.6882609308482   -26.7456339108424       29.2561049914


        PARAMETER OUTPUTS
  C_out, h_out, p_out, T_out, rho_out, Mass
        15.6111602653531     71501.295372988   7751030.335716794    145.828899881271      110.732450796763743
0.9346504914

               LOSS COEFFICIENTS

 -------NOZZLE

             Yn          Y_p_n        Y_inc_n
         0.084761       0.075382       0.009379

 -------ROTOR

                  Yr                 Y_p               Y_inc                Y_bl                 Y_hs
Y_cl
              0.678215            0.011584            0.573533            0.056246            0.036754
0.000099



        USEFUL DATA


 Mass-----P ratio--------S to S---------T to S---T-T

    0.934650    1.081540   92.954516   90.949790   93.106464
```

Compressor Performance Results (Comp1_res.txt)

```
************ Results for compressor ***************
 ----------------Inlet parameters----------------
*-------------------------------------------*-------------*--------*
| Working fluid                             |        CO2  |        |
|-------------------------------------------|-------------|--------|
| Compressor inlet pressure                 |        7.703| MPa    |
|-------------------------------------------|-------------|--------|
| Compressor inlet temperature              |       32.302| C      |
|-------------------------------------------|-------------|--------|
| Mass flow rate                            |        0.935| kg/s   |
|-------------------------------------------|-------------|--------|
| Shaft revolution speed                    |      416.667| rev/s  |
*-------------------------------------------*-------------*--------*
 -----------             1  stages ------------
         Position index description
 1 - Impeller inlet (eye)
 2 - Impeller outlet (discharge)
 3 - Diffuser inlet
 4 - Diffuser outlet (discharge)


       Properties distribution by location
 St  Pos   p, MPa     T, C     C, m/s  rho,kg/m3 s,kJ/kg-K  h,kJ/kg   Vsd,m/s
  1  1     7.690    32.248     6.323   578.090  -1.37592   -195.44    193.24
  1  2     8.209    34.341    32.309   589.037  -1.37519   -194.33    214.03
  1  3     8.232    34.428    30.222   589.385  -1.37510   -194.26    214.69
  1  4     8.410    35.109    11.089   592.652  -1.37480   -193.87    220.07



       Static and total parameters by stage
 St  Pos   p, MPa    T, C    h,kJ/kg    C, m/s     p0,MPa    T0,C   h0,kJ/kg    W, m/s    p0r,MPa    T0r,C
h0r,kJ/kg
  1  1     7.690    32.248  -195.441     6.323     7.702    32.296  -195.421    19.054     7.795    32.685  -
195.259
  1  2     8.209    34.341  -194.328    32.309     8.518    35.496  -193.806    21.389     8.345    34.842  -
194.225
  1  3     8.232    34.428  -194.262    30.222     8.502    35.439  -193.806    30.222     8.502    35.439  -
193.806
  1  4     8.410    35.109  -193.867    11.089     8.447    35.244  -193.806    11.089     8.447    35.244  -
193.806



       Blade and flow angles (deg)
 St  Pos  alpha     beta     k       i       d
  1   1    0.00  -70.62  -65.00   -5.62   19.66
  1   2   70.46  -59.66  -40.00   -5.62   19.66
  1   3   76.82   76.82   77.80    0.98   -7.20
  1   4   41.19   41.19   33.99    0.98   -7.20



       Velocity triangles (m/s, deg)
 St  Pos    Cm      Ct       C      M#     alpha     u      Wm       Wt      W      beta    f_st
  1   1    6.32    0.00    6.32   0.183    0.00   17.97    6.32  -17.97   19.05 -70.620    1.21
  1   2   10.80   30.45   32.31   0.151   70.46   48.91   10.80  -18.46   21.39 -59.659    1.21
  1   3    6.89   29.43   30.22   0.141   76.82    0.00    6.89   29.43   30.22  76.821    1.21
  1   4    8.35    7.30   11.09   0.050   41.19    0.00    8.35    7.30   11.09  41.188    1.21



       Loss coefficients
 St  Part   Y_inc     Y_ch      Y_sf      Y_bl     Y_lam     Y_mix     Y_dif     Y_hs       Y_cl      Y_cr       Y
```

```
  1 Imp  0.099811  0.000000  0.067372  0.106437  0.022237  0.001951  0.112970  0.012601  0.116871  0.000000
0.540250
  1 Dif  0.003534  0.000000  0.140321  0.001127  0.059767  0.000000  0.000000  0.000000  0.000000  0.000000
0.204749

Flow coefficient =   0.030

---Work input---- <-------I------>  W,MW
Blade (B)           0.6226            0.00
Disk frict. (DF)            0.0234
Leakage     (L)             0.0293
Recirculat. (R)             0.0000
Parasitic (DF+L+R)  0.0527            0.00
======TOTAL=======                    0.00


Compressor isentropic static-to-static efficiency =  77.612 %
Compressor isentropic  total-to-total  efficiency =  78.464 %
Compressor isentropic  total-to-static efficiency =  74.658 %



 ---------Pressures------------
     Pnt   p,kPa  p,psia
    P400  7702.8  1117.2
    P100  8209.4  1190.7
    P500  8410.2  1219.8

Total pressure ratio =    1.092

 ---------Temperatures------------
     Pnt     T,C     T,K     T,F
    T400   32.30  305.45   90.14
    T500   35.11  308.26   95.20

 ---------Shaft windage power loss------------
 Properties
   Temperature=      4.64 C
   Pressure=        3.802 MPa
   Density=       106.584 kg/m3
   Viscosity=      15.187 mkPa*s
 Re = 1.482E+06
 Cd = 2.120E-03

Impeller power =      0. MW
Shaft windage power loss =      0. MW
Impeller + Shaft power consumption =      0. MW
```

Nuclear Engineering Division
Argonne National Laboratory
9700 South Case Avenue, Bldg. #208
Argonne, IL 60439

www.anl.gov

Argonne National Laboratory is a U.S. Department of Energy
laboratory managed by UChicago Argonne, LLC